THE ASTROPHYSICAL JOURNAL, 551:973–1015, 2001 April 20

CEPHEID CALIBRATION OF THE PEAK BRIGHTNESS OF TYPE Ia SUPERNOVAE. X. SN 1991T IN NGC 4527

A. SAHA
National Optical Astronomy Observatories, 950 North Cherry Avenue, Tucson, AZ 85726

ALLAN SANDAGE
The Observatories of the Carnegie Institution of Washington, 813 Santa Barbara Street, Pasadena, CA 91101

FRANK THIM, LUKAS LABHARDT, AND G. A. TAMMANN
Astronomisches Institut der Universität Basel, Venusstrasse 7, CH-4102 Binningen, Switzerland

J. CHRISTENSEN
National Optical Astronomy Observatories, 950 North Cherry Avenue, Tucson, AZ 85726

AND

N. PANAGIA[1] AND F. D. MACCHETTO[1]
Space Telescope Science Institute, 3700 San Martin Drive, Baltimore, MD 21218
Received 2000 July 19; accepted 2000 December 1

ABSTRACT

Repeated imaging observations have been made of NGC 4527 with the *Hubble Space Telescope* between 1999 April and June, over an interval of 69 days. Images were obtained on 12 epochs in the F555W band and on five epochs in the F814W band. The galaxy hosted the Type Ia supernova SN 1991T, which showed relatively unusual behavior by having both an abnormal spectrum near light maximum, and a slower declining light curve than the prototypical Branch-normal SNe Ia. A total of 86 variables that are putative Cepheids have been found, with periods ranging from 7.4 days to over 70 days. From photometry with the DoPHOT program, the dereddened distance modulus is determined to be $(m - M)_0 = 30.67 \pm 0.12$ (internal uncertainty) using a subset of the Cepheid data whose reddening and error parameters are secure. A parallel analysis of the Cepheids using photometry with ROMAFOT yields $(m - M)_0 = 30.82 \pm 0.11$. The final adopted modulus is $(m - M)_0 = 30.74 \pm 0.12 \pm 0.12$ ($d = 14.1 \pm 0.8 \pm 0.8$ Mpc). The photometric data for SN 1991T are used in combination with the Cepheid distance to NGC 4527 to obtain the absolute magnitude for this supernova of $M_V^0(\max) = -19.85 \pm 0.29$. The relatively large uncertainty is a result of the range in estimates of the reddening to the supernova. Thus, SN 1991T is seen to be only moderately brighter (by ~ 0.3 mag) than the mean for spectroscopically normal supernovae, although magnitude differences of up to 0.6 mag cannot be ruled out.

Subject headings: Cepheids — distance scale — galaxies: individual (NGC 4527) — supernovae: individual (SN 1991T)

1. INTRODUCTION

This is the tenth paper of a series whose purpose is to obtain Cepheid distances to galaxies that have produced supernovae of Type Ia (SNe Ia), thereby calibrating their absolute magnitudes at maximum light.

1.1. *Homogeneity and Diversity among SNe Ia*

From the tightness of the Hubble diagram, it was recognized early on that many Type I supernovae have nearly the same absolute magnitude at maximum, and that they would be useful in obtaining distances to the galaxies that produced them. If true, supernovae could play a major role in the calibration of the extragalactic distance scale (Kowal 1968), leading to the Hubble constant quite directly. The only intermediate step required would "simply" be to calibrate their mean absolute magnitude at maximum if that mean was strictly a constant, or to devise means to determine the second-parameter corrections if there is a range in absolute magnitude (i.e., a significant diversity).

Evidence for the spectral homogeneity of a subclass of supernovae eventually called Type I was progressively discovered. The evidence began with the exhaustive discussion of the spectra of SN 1937C in IC 4182 and SN 1937D in NGC 1003 by Minkowski (1939). His further discussion of supernovae spectra showed differences from the prototype spectra he had studied in 1939. As a result, he introduced the Type I and Type II classification that became standard (Minkowski 1941, 1964).

More subtle differences in the spectra, even within the Type I class, began to be recognized in 1964. Bertola (1964), Bertola & Sussi (1965), and Bertola, Mammano, & Perinotto (1965) had noticed the lack of certain spectral features (no λ6150 Å absorption and no P Cygni profiles) in a few SNe I, contrary to most of the class, but no further action was taken at that time. However, by 1985 the variations discovered by Bertola were shown to be general, and the SNe Ia class was divided into the subtypes Ia and Ib (Panagia 1985; Wheeler & Levreault 1985; Uomoto & Kirshner 1985; Branch 1986; Harkness et al. 1987). The class was formally named by Elias et al. (1985), and formally defined by Porter & Filippenko (1987).

Diversity was soon again noticed even in the new Ib class. Harkness et al. (1987) and Harkness & Wheeler (1990) showed that the Type Ib should again be divided into two separate groups on the basis of spectra. They introduced the new class of Ic.

[1] Affiliated with the Astrophysics Division, Space Sciences Department of ESA.

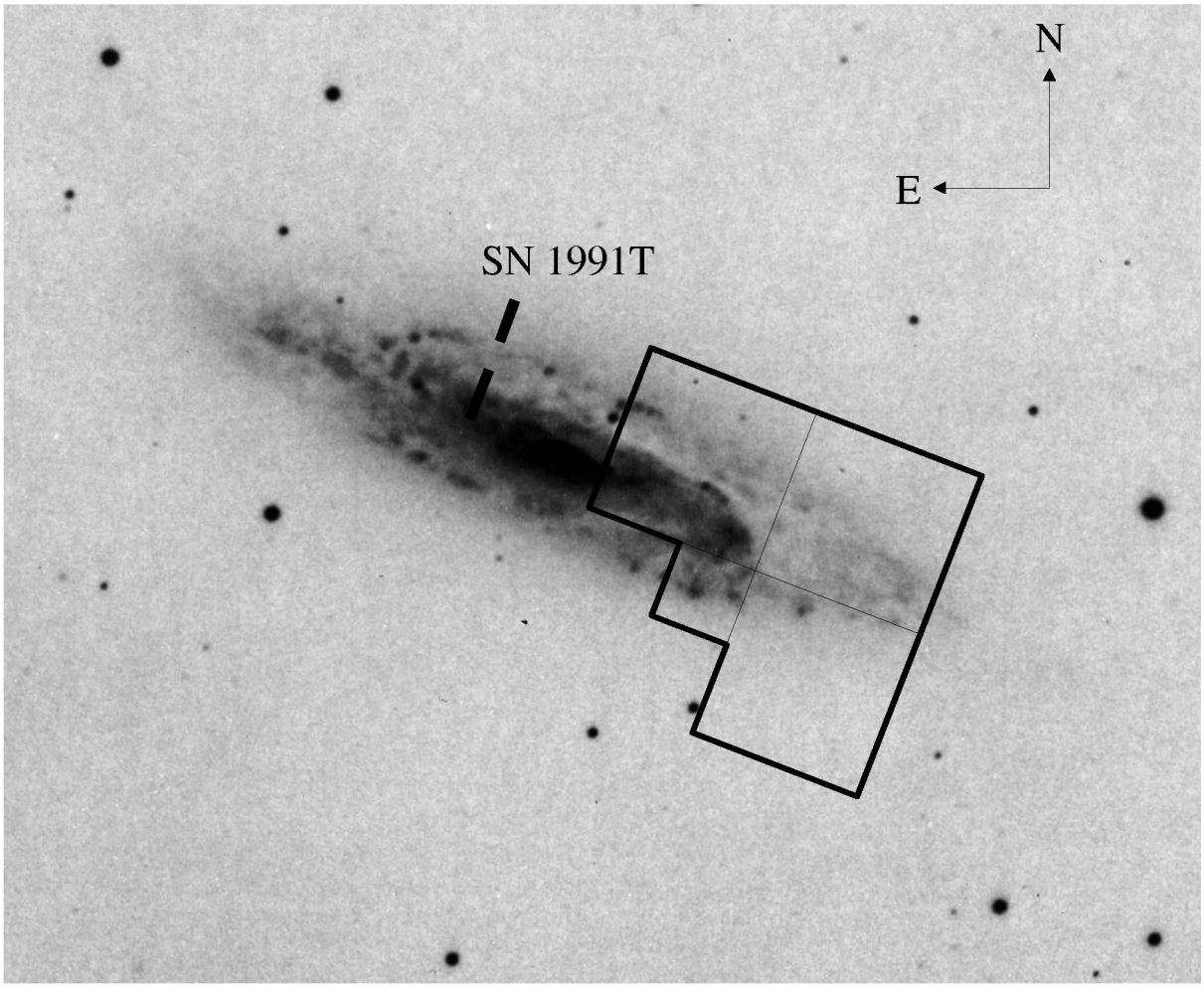

FIG. 1.—Ground-based image of NGC 4527. The field covered by the WFPC2 of the *HST* is superposed. North is up, and east is to the left. The position of SN 1991T is marked.

TABLE 1

JOURNAL OF OBSERVATIONS

Data Archive Designation	HJD at Midexposure	Filter	Exposure Time (s)
u42g0101r + ... 02r	2451279.84066	F555W	2500
u42g0103r + ... 04r	2451279.97330	F814W	2500
u42g0201r + ... 02r	2451288.17122	F555W	2500
u42g0301r + ... 02r	2451295.29066	F555W	2500
u42g0303r + ... 04r	2451295.42296	F814W	2500
u42g0401r + ... 02r	2451301.20074	F555W	2500
u42g0501r + ... 02r	2451341.83407	F555W	2500
u42g0503r + ... 04r	2451341.96740	F814W	2500
u42g0601r + ... 02r	2451311.00733	F555W	2500
u42g0603r + ... 04r	2451311.13928	F814W	2500
u42g0701r + ... 02r	2451315.03824	F555W	2500
u42g0801r + ... 02r	2451319.67260	F555W	2500
u42g0901r + ... 02r	2451325.18059	F555W	2500
u42g1001r + ... 02r	2451331.96185	F555W	2500
u42g1003r + ... 04r	2451332.09553	F814W	2500
u42g1101r + ... 02r	2451339.81879	F555W	2500
u42g1201r + ... 02m ...	2451348.81809	F555W	2500

The stability (constancy) of the mean absolute magnitude of the classical SN Ia type was also being questioned. Progressive improvements in the photometry of SNe since the pioneering work of Baade (1938) and Baade & Zwicky (1938) had shown the remarkable similarity of the shape of the light curves of SNe Ia. However, by 1973 it began to be noticed that small systematic differences in fact do exist in the details of the light curves, in particular in their decay rates after maximum light. Barbon, Ciatti, & Rosino (1973) gave an important summary, following earlier indications of a decay-rate absolute magnitude correlation by Pskovskii (1967, 1971, 1984). There were also indications that the expansion velocities of the SNe Ia are not all the same and that the differences are correlated with absolute magnitude and decay rate (Branch 1981, 1982).

However, at the same time as spectral diversities were being found that required division of the Minkowski broad class I into three groups, improvements in the photometry and the discovery of many more SNe Ia at relatively large redshifts ($v > 3000$ km s^{-1}) permitted major improvements in the formulation of the Hubble diagram (redshift versus apparent magnitude at maximum) of SNe Ia.

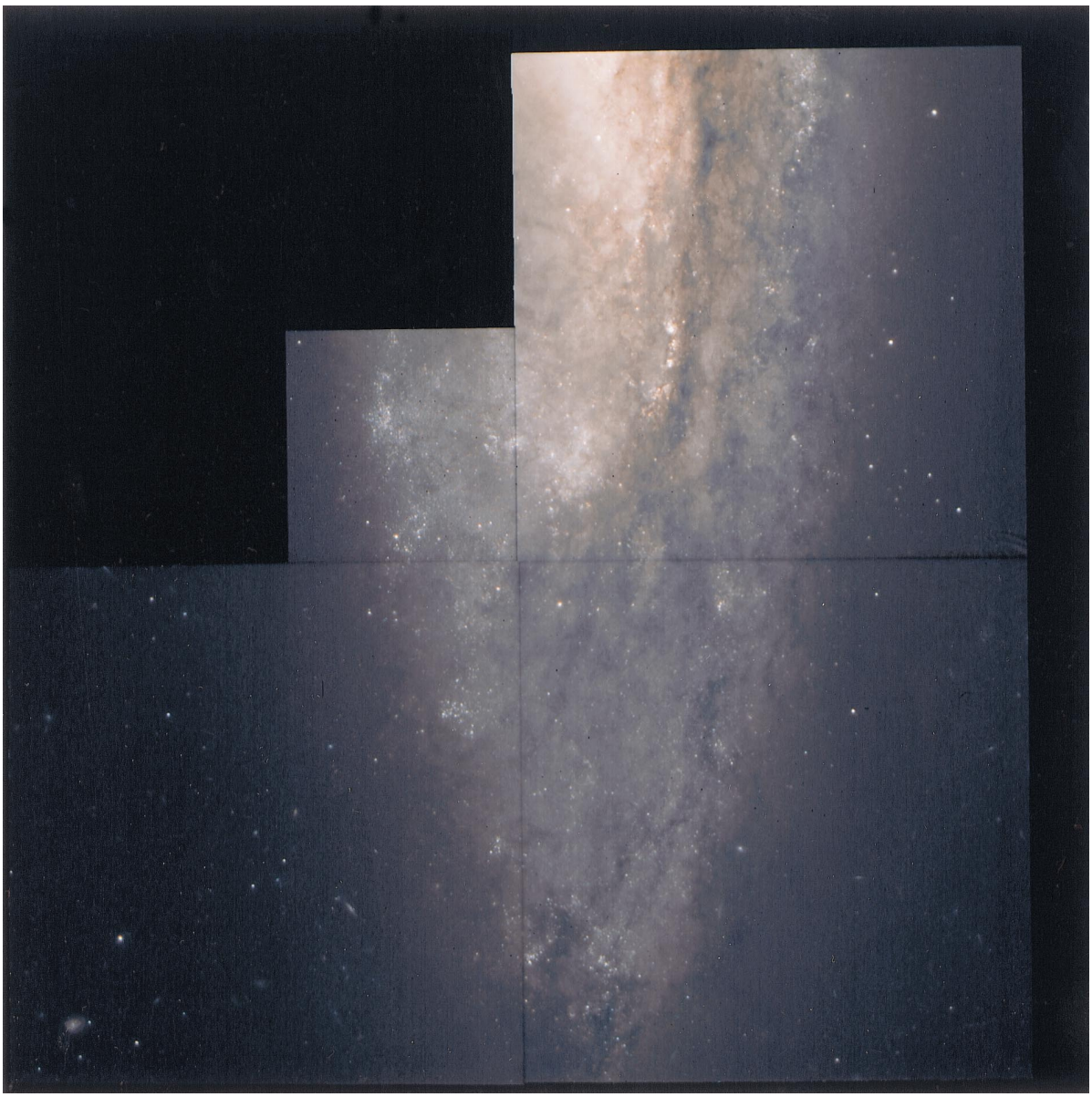

FIG. 2.—Color image of the *HST* field made by stacking several frames in both the *V* and *I* passbands and combining

The distribution of magnitude residuals about the linear regression of m versus 5 log v for a linear velocity-distance relation of course immediately gives the rms scatter of the mean absolute magnitude, $\langle M \rangle_{\rm SNe\ Ia}$. This Hubble diagram scatter became progressively smaller as the photometry improved (Sandage & Tammann 1982, 1993, 1997), showing that any systematic deviation in $\langle M \rangle_{\rm SNe\ Ia}$ must be smaller than $\sim$0.4 mag for Branch-normal (Branch, Fisher, & Nugent 1993) SNe Ia, to which the samples that defined the cited Hubble diagrams had been restricted.

A history of this early work and the pros and cons of believing $\langle M \rangle_{\rm SNe\ Ia}$ to be remarkably stable is given by Branch & Tammann (1992), again with the samples restricted to Branch-normal SNe Ia. It was because of this remarkable apparent constancy of $\langle M \rangle_{\rm SNe\ Ia}$ for samples so restricted that we also restricted the absolute-magnitude calibrations in the first nine papers of this series to such SNe Ia subtypes.

It is now known, primarily from the extensive new precise photometry by the supernova group at Cerro-Tololo lead by M. M. Phillips, that when the restriction on spectral normalcy is removed, an appreciable range of $\langle M \rangle_{\rm SNe\ Ia}$ is present. It is also now known that a small range in $M_{\rm max}$ exists even among the restricted Branch-normal SNe Ia. The range depends on both decay rate and color (Tripp 1998; Saha et al. 1999, hereafter Paper IX; Tripp & Branch 1999; Phillips et al. 1999; Parodi et al. 2000), confirming the decay-rate part of the correlation suggested by Pskovskii (1967, 1971, 1984) and by Barbon et al. (1973).

The early paper by Phillips (1993) began the modern discussions of the decay rate–absolute magnitude relation. Tammann & Sandage (1995), Paper IX, Parodi et al. (2000), and Sandage, Tammann, & Saha (2000) have argued that the steep slope in their initial formulation was overestimated. The magnitude of this dependence is now accepted to be milder (Hamuy et al. 1996) than in their initial formulation.

A more complete review of the many discovery paths from homogeneity to diversity from Kowal to the present, and of the amplitude of each second parameter as it is

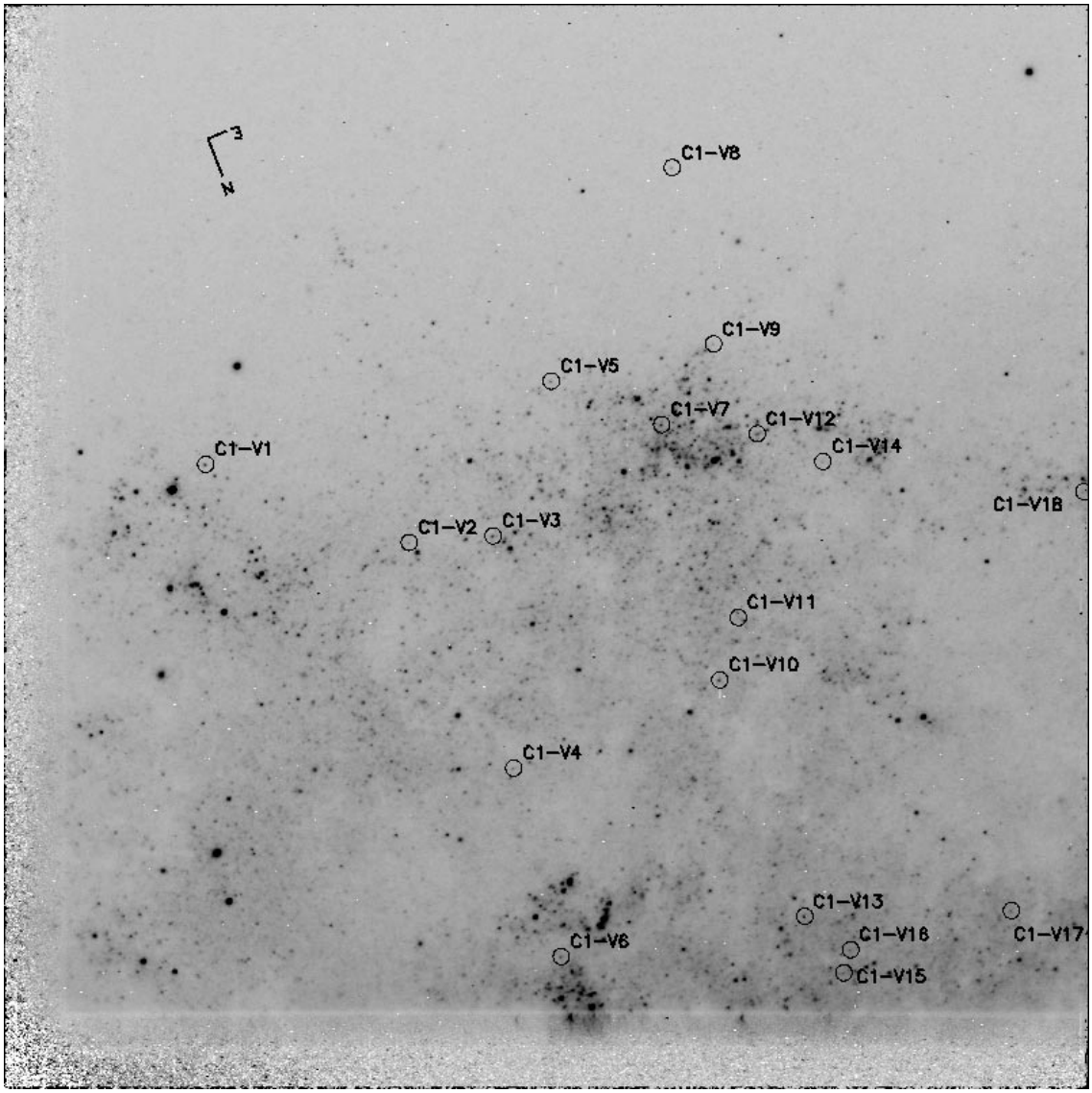

FIG. 3.—Identifications for all the variable stars found. The numbers are the same as in Tables 2, 3, 4, and 5. Each of the four WFPC2 chips are shown separately.

currently understood, or as it is now or has been controversial, is given in Sandage et al. (2000).

1.2. *The Abnormal Spectral Case of SN 1991T*

A new development was begun with the discovery of a different kind of spectral abnormality in the supernova 1991T that was discovered on 1991 April 13 in NGC 4527. The discovery was made 15 days before maximum light, which occurred on April 28. A detailed summary of the many discoveries and discussions by many different groups of the spectral diversity shown by SN 1991T is given in the Introduction of the paper by Fisher et al. (1999).

Briefly, Filippenko et al. (1992) obtained spectra from 12 days before maximum to 47 days after maximum (hereafter -12 to $+47$ days), showing that the premaximum spectra "did not resemble those of any other supernova [but] beginning near maximum light the usual SNe Ia lines of intermediate-mass elements slowly developed, and months after the explosion the iron-dominated spectrum appeared almost identical to that of a typical SN Ia" (Fisher et al. 1999). The same description of the abnormal spectra before maximum (-13 to -7 days) was given by Ruiz-Lapuente et al. (1992), and by Phillips et al. (1992) for before and after maximum light (-13 to $+66$ days). All independent data showed that the spectrum was not Branch-normal before maximum light but almost identically resembled Branch-normal prototypes after maximum light.

Was the absolute magnitude at maximum light also peculiar?

1.3. *Previous Estimates of the Absolute Magnitude at Maximum of SN 1991T*

A large literature has developed based on the premise that SN 1991T was very much brighter than the usual Branch-normal SNe Ia, which all have $\langle M \rangle_{\rm SNe\ Ia} = -19.48 \pm 0.07$ in both B and V, with an rms dispersion of only 0.2 mag (Paper IX, Table 5 and eqs. [10] and [11]). A number of special (nonstandard) supernova explosion models have been discussed, some using absolute magnitudes as bright as -20.2 (e.g., Fisher et al. 1999), fully 0.7 mag brighter than

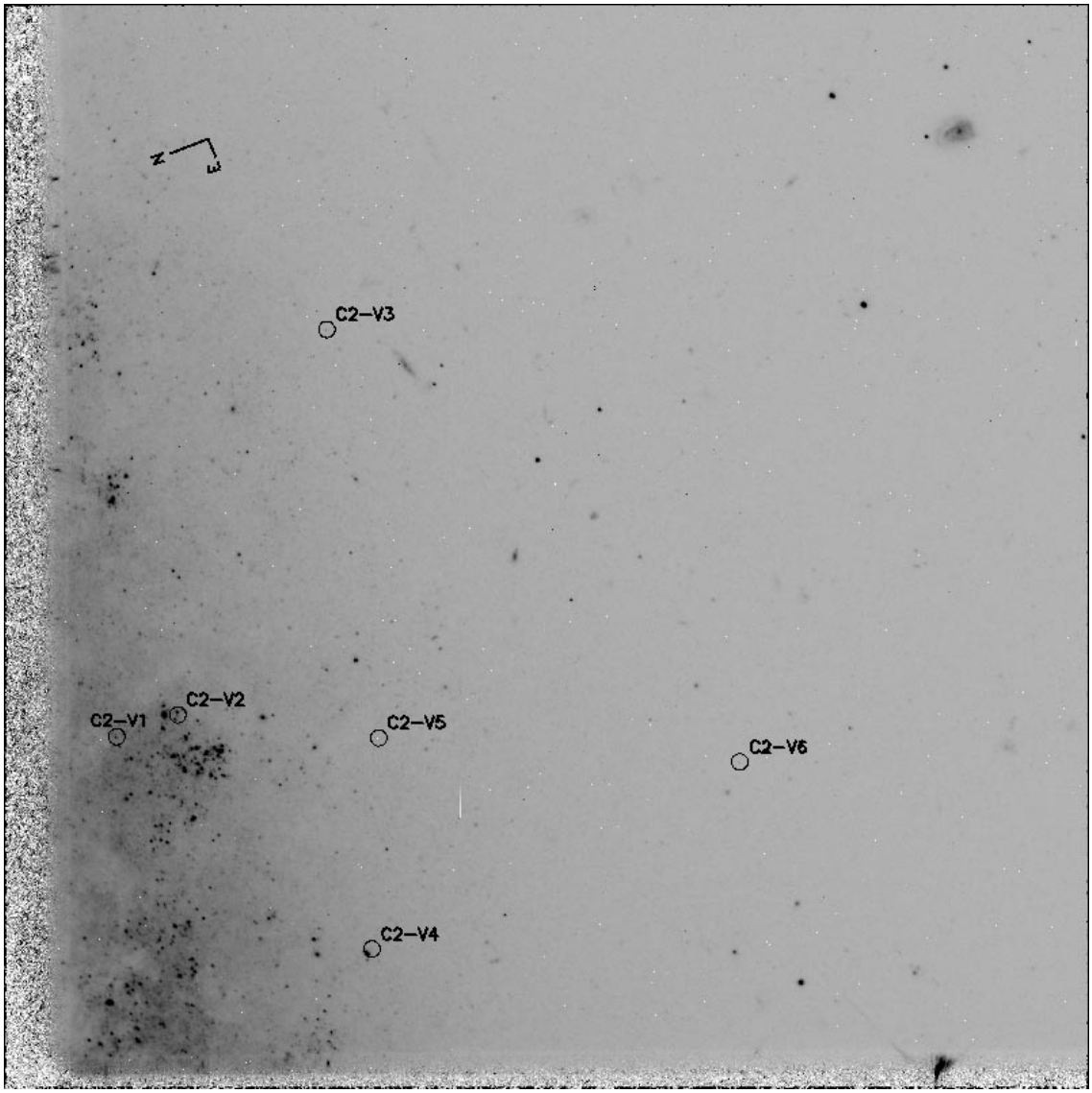

FIG. 3.—*Continued*

the present canonical Branch-normal mean absolute magnitude (see Livio et al. 2000).

However, we share the opinion of many of the authors we have cited that the evidence for such bright absolute magnitude rests on quite insecure grounds for at least some of the estimates of $M(\max)_{1991T}$ in the literature. Even before obtaining the Cepheid data presented in this paper, our opinion of a few of the methods used to obtain these bright estimates has led us to question whether $M(\max)_{1991T}$ was any more abnormal than ~ 0.3 mag from $\langle M(\max)\rangle = -19.5$, and therefore whether it deviates at all from the shallow decay-rate versus absolute magnitude relation that we derived in Paper IX of this series (Fig. 12).

Fisher et al. (1999, their § 5) give a good summary of some of the evidence used by others to infer an abnormally bright absolute magnitude for SN 1991T. Most unfortunately, the problem lies almost entirely with the value of the extinction suffered by SN 1991T itself. The different estimates of the extinction by different authors, plus a variety of assumptions regarding the distance of NGC 4527 relative either to the bulk of the main Virgo cluster spirals or to a proposed membership in the tight X group of de Vaucouleurs (1975), which is the group named 11-4 by Tully (1988) containing NGC 4496A, NGC 4536, and NGC 4527, also complicated the early estimates. One can obtain conclusions that range from the result that $M(\max)$ of SN 1991T is normal compared with Branch-normal SNe Ia (Phillips et al. 1992, in an early paper), to having an absolute magnitude of SN 1991T that is at least 0.6 mag brighter than the mean of normal SNe Ia (Filippenko et al. 1992), or having $M_V^0(1991T)$ 0.75 mag brighter than SN 1981B in NGC 4536 (Fisher et al. 1999, their Table 1).

Our purpose in this paper is to obtain the absorption-corrected distance to the parent galaxy NGC 4527, thereby circumventing all assumptions of relative distances by group associations to other galaxies for which Cepheid distances are also available.

Although we are confident that our absorption-corrected Cepheid modulus of NGC 4527 is systematically correct to within the external uncertainties quoted in §§ 4 and 5, the conclusion regarding $M(\max)$ for SN 1991T still depends on the uncertain assumptions we make concerning its

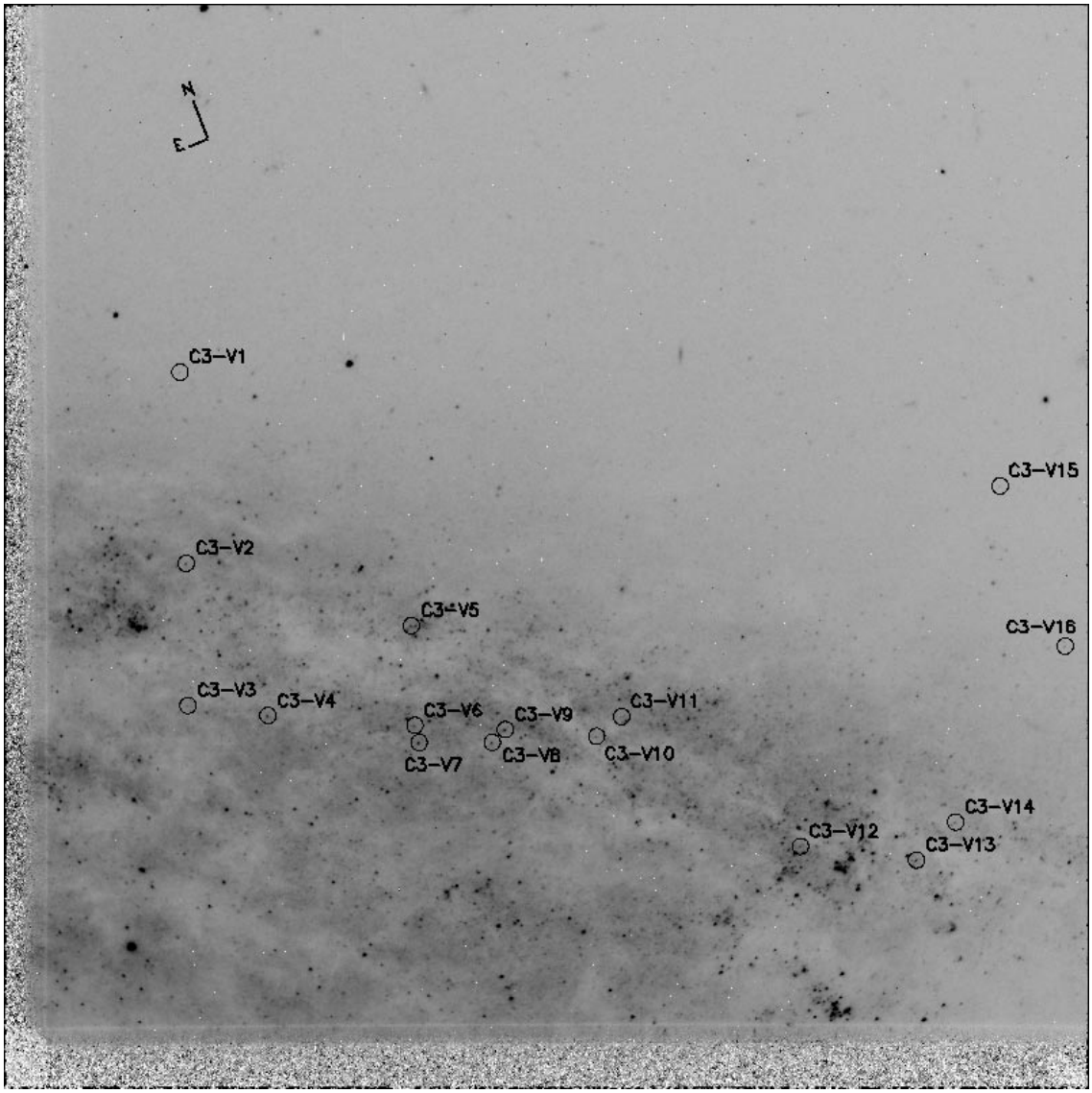

FIG. 3.—*Continued*

absorption. We discuss all the possibilities based on the various assumptions concerning the absorption.

2. OBSERVATIONS AND PHOTOMETRY

2.1. *The Data*

Repeated images of a field in NGC 4527 were obtained using the WFPC2 (Holtzman et al. 1995a) on the *Hubble Space Telescope* (*HST*). The field is shown in Figure 1, marked over a ground-based image of NGC 4527. The composite image of this field taken with the WFPC2 is shown in Figure 2. There are 12 discrete epochs in the F555W passband, and five epochs in the F814W passband, spanning a period of 69 days. The duration of this period is constrained by the time window during which this target can be observed with *HST* without altering the field orientation.

The epochs were spaced strategically over this period to provide maximum leverage on detecting and finding periods of Cepheid variables over the period range 10–65 days. Each epoch in each filter was made of two subexposures taken back-to-back on successive orbits of the spacecraft. This allows the removal of cosmic rays by an anticoincidence technique described by Saha et al. (1996a, hereafter Paper V). The images from various epochs are in common alignment to within 3–4 pixels on the scale of the PC chip, which is 1–2 pixels on the scale of the other three wide-field chips. The journal of observations is given in Table 1.

2.2. *Photometry*

2.2.1. *The Analysis Done in Tucson*

The details of processing the images, combining the subexposures for each epoch while removing cosmic rays and performing the photometry with a variant of DoPHOT (Schechter et al. 1993) optimized for WFPC2 data, have been given in Paper V and are not repeated here. The reduction procedure for the data is identical to that described in Paper V, with the one exception of a change in the definition of the "partial aperture," which is discussed in Paper IX.

In keeping with the precepts in Paper V, the measurements in any one passband are expressed in the magnitude system defined by Holtzman et al. (1995b) that is native to the WFPC2. These are the F555W and F814W "ground

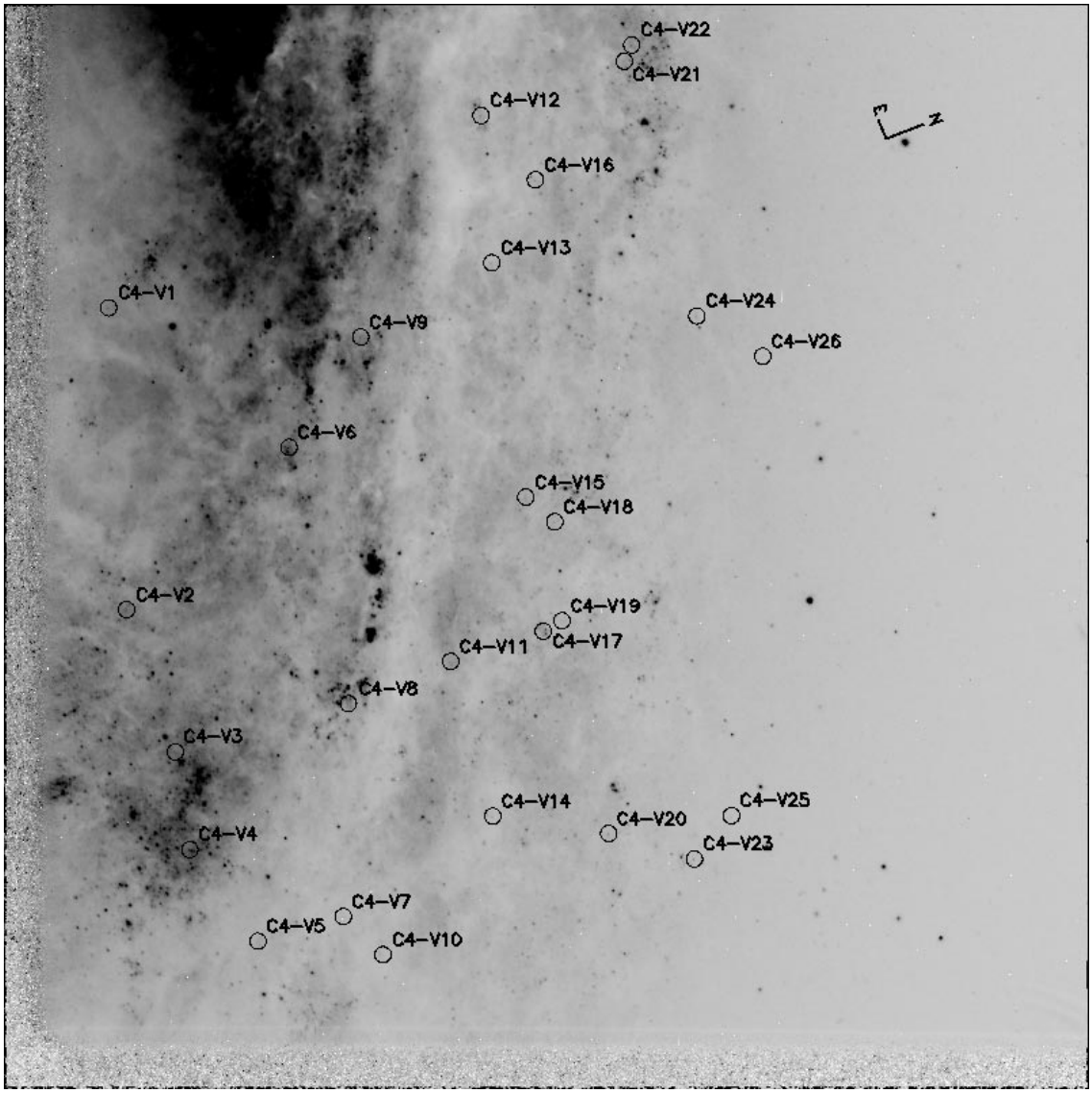

FIG. 3.—*Continued*

system" magnitudes calibrated with *HST* "short" exposure frames. The issue of the discrepancy of the photometric zero points for the "long" and "short" WFPC2 exposures, originally found by P. B. Stetson (1995, private communication) is described in some detail in Paper V. This phenomenon is attributed to charge-transfer problems in the WFPC2 CCDs, which are at their worst when the background level in the image is near zero. With increasing background levels, the problem is less present. Thus, "short" exposures of standard stars and/or fields that have near zero background yield photometry that is systematically different from "long" exposures that have higher levels of background. In previous papers of the series (except for IC 4182 and NGC 5253, which were done with WF/PC, not WFPC2) we *added* 0.05 mag in *both* passbands to the Holtzman et al. (1995b) calibration whenever the exposures are longer than several hundred seconds, and (consequently) the background level in electrons has been relatively high. Improved characterization of this problem as a function of background level and other parameters for the photometric procedures used in this series of papers is now available, and is given in Saha et al. (2000). However, the last word on this topic has perhaps not been said, particularly concerning secular trends due to continuing radiation damage of the CCDs. We opt to follow the procedure used in previous papers of nominally adding 0.05 mag at the final stage of the reductions, while (as before) presenting the light curves in the *uncorrected* system. In an eventual accounting, all the results can be treated at par, and corrected by a common prescription.

2.2.2. *The Analysis Done in Basel*

A parallel analysis was done independently at Basel and is described fully in § 5. As part of this analysis, photometry on the NGC 4527 images was performed independently using the ROMAFOT package. Discussion of the Basel procedures, and the comparison with DoPHOT-based analysis done in Tucson, is postponed to § 5.

3. IDENTIFICATION AND CLASSIFICATION OF THE VARIABLE STARS

Armed with measured magnitudes and their reported errors at all available epochs for each star in the object list, the method described by Saha & Hoessel (1990) was used to

TABLE 2

POSITION OF THE VARIABLE STARS ON U42G0101R AND 02R

Variable ID	*X* Position	*Y* Position	Variable ID	*X* Position	*Y* Position
C1-V1	148.36	460.08	C1-V2	298.30	402.49
C1-V3	360.12	407.32	C1-V4	375.35	236.14
C1-V5	403.07	521.44	C1-V6	410.44	97.22
C1-V7	484.49	489.44	C1-V8	492.13	678.84
C1-V9	522.73	548.80	C1-V10.....	527.21	301.16
C1-V11.....	540.98	347.19	C1-V12.....	554.97	482.63
C1-V13.....	589.86	126.94	C1-V14.....	603.22	462.17
C1-V15.....	618.72	85.29	C1-V16.....	623.71	102.30
C1-V17.....	742.17	131.15	C1-V18.....	795.62	439.90
C2-V1	82.70	259.27	C2-V2	127.69	275.40
C2-V3	237.64	559.45	C2-V4	270.90	102.82
C2-V5	275.83	258.40	C2-V6	542.05	240.74
C3-V1	129.36	528.00	C3-V2	134.03	387.03
C3-V3	135.17	282.31	C3-V4	194.25	274.95
C3-V5	300.00	341.11	C3-V6	302.60	267.74
C3-V7	305.61	255.01	C3-V8	359.56	255.11
C3-V9	369.25	264.58	C3-V10.....	436.53	259.57
C3-V11.....	454.94	274.09	C3-V12.....	586.75	178.44
C3-V13.....	672.26	168.40	C3-V14.....	701.09	196.39
C3-V15.....	733.89	444.13	C3-V16.....	782.02	326.09
C4-V1	76.79	575.46	C4-V2	90.05	352.98
C4-V3	125.86	248.07	C4-V4	136.55	176.03
C4-V5	186.83	108.56	C4-V6	209.69	472.61
C4-V7	249.80	126.75	C4-V8	253.50	283.67
C4-V9	262.62	553.92	C4-V10.....	279.05	98.59
C4-V11.....	328.98	314.79	C4-V12.....	351.20	717.17
C4-V13.....	359.12	608.59	C4-V14.....	359.96	200.73
C4-V15.....	384.24	435.91	C4-V16.....	391.35	669.77
C4-V17.....	397.16	337.02	C4-V18.....	405.67	417.76
C4-V19.....	410.94	344.78	C4-V20.....	445.35	187.90
C4-V21.....	456.87	757.15	C4-V22.....	462.33	769.18
C4-V23.....	508.54	169.13	C4-V24.....	510.38	569.40
C4-V25.....	535.82	201.03	C4-V26.....	558.990	539.71

identify variable stars. The details specific to WFPC2 data have been given in various degrees of detail in Papers V, VI (Saha et al. 1996b), and VIII (Saha et al. 1997). Again, parallel efforts were made by the Tucson and Basel groups, and the results for identified Cepheids were merged. More than 90% of the Cepheid candidates found by DoPHOT were also found by ROMAFOT.

All variable stars definitely identified are marked in Figure 3. However, some of the identified variables cannot be seen in Figure 3 because of their extreme faintness and/or because of the large variation in surface brightness over the field. Hence, to complement these charts, we set out in Table 2 the *X* and *Y* pixel positions for these objects as they appear in the images identified in the *HST* data archive as U42G0101R and U42G0102R.

The photometry on the Holtzman et al. (1995b) "short-exposure" calibration system for the final list of 66 variable stars is presented in Table 3 for each epoch and each filter. The periods were determined with the Lafler-Kinman (1965) algorithm, using only the F555W passband data. Aliasing is not a serious problem for periods between 10 and 65 days because the observing strategy incorporated an optimum timing scheme, as before in this series.

The resulting light curves in the F555W passband, together with periods and mean magnitudes (determined by integrating the light curves, converted to intensities, and then converting the average back to magnitudes, and called the "phase-weighted intensity average" in Saha & Hoessel 1990), are shown in Figure 4, plotted in order of descending period.

Most of the variable stars identified in this manner can be immediately recognized by their periods and light curves as Cepheids. In fact, none of the 66 objects are a priori inconsistent with being Cepheids, although there is a range in the quality of the light curves. The objects C3-V5 and C3-V7 are borderline detections, and their amplitudes, if real, are extremely small. C3-V13 and C4-C23 also have very low amplitudes, but are more convincing as variables. C1-V1 and C2-V6 have periods larger than the 69 day observing baseline, and so their period determinations cannot be very reliable. The best estimate for the periods of these stars is made from the existing data from a subjective assessment of the implied light curve based on an assumed period.

The available data for the variables in F814W were folded with the ephemerides derived above using the F555W data. The results are plotted in Figure 5. Note, however, that four of the variables discovered from the F555W photometry were not found by our procedure in the F814W images (C1-V12, C2-V4, C4-V7, and C4-V11). This is because they either are intrinsically faint or else appear faint due to high extinction and may not register clearly on the F814W frames, which do not reach as faint a limiting magnitude as those in F555W. Since photometry of such objects was obviously impossible in F814W, they are dropped from Figure 5 and also from further analysis.

The mean magnitudes in F814W (integrated as intensities

TABLE 3

PHOTOMETRY OF VARIABLE STARS: MAGNITUDES AND ERROR ESTIMATES

HJD	C1-V1	C1-V2	C1-V3	C1-V4	C1-V5	C1-V6	C1-V7	C1-V8
				F555W				
2451331.9619.....	25.27 0.06	26.42 0.14	25.26 0.06	26.66 0.15	25.43 0.06	26.43 0.17	24.84 0.05	25.94 0.07
2451339.8188.....	25.38 0.08	26.55 0.16	25.34 0.06	25.89 0.10	25.93 0.09	25.68 0.09	24.94 0.05	26.58 0.44
2451348.8181.....	25.26 0.06	26.06 0.10	25.31 0.05	26.61 0.15	26.08 0.16	25.66 0.08	25.22 0.05	25.72 0.07
2451279.8407.....	24.93 0.05	26.56 0.14	25.52 0.06	26.05 0.12	25.44 0.06	26.27 0.13	24.88 0.05	26.52 0.17
2451288.1712.....	24.86 0.05	26.14 0.09	25.38 0.06	26.31 0.11	25.81 0.08	25.73 0.08	24.96 0.05	25.93 0.08
2451295.2907.....	24.80 0.09	26.84 0.24	25.45 0.06	25.48 0.09	26.24 0.12	25.88 0.09	25.14 0.05	26.43 0.10
2451301.2007.....	24.85 0.05	26.18 0.09	24.95 0.08	26.08 0.15	25.11 0.07	25.55 0.07	25.30 0.06	26.23 0.12
2451341.8341.....	25.32 0.09	26.47 0.14	...	25.95 0.10	26.12 0.11	25.93 0.11	25.02 0.07	26.27 0.11
2451311.0073.....	24.94 0.05	26.39 0.15	25.21 0.06	26.51 0.13	25.64 0.09	25.51 0.09	25.49 0.07	25.98 0.07
2451315.0382.....	25.05 0.06	26.71 0.15	25.01 0.08	25.45 0.08	26.13 0.10	25.45 0.08	25.46 0.06	26.21 0.08
2451319.6726.....	25.06 0.05	26.66 0.16	25.47 0.06	25.94 0.10	26.36 0.13	25.97 0.11	25.15 0.05	26.38 0.13
2451325.1806.....	25.16 0.05	25.94 0.08	25.31 0.05	26.68 0.16	26.13 0.11	25.60 0.08	24.68 0.04	25.65 0.08
				F814W				
2451332.0955.....	23.78 0.05	25.31 0.12	24.86 0.11	25.55 0.20	23.96 0.06	25.99 0.23	23.76 0.05	24.90 0.08
2451279.9733.....	23.63 0.05	25.53 0.16	25.14 0.12	24.98 0.12	24.49 0.05	25.61 0.17	24.03 0.05	25.20 0.11
2451295.4230.....	23.47 0.05	25.63 0.14	25.01 0.13	24.92 0.12	25.05 0.13	25.86 0.43	23.88 0.06	24.92 0.12
2451341.9674.....	23.82 0.05	25.33 0.14	25.00 0.11	24.94 0.12	24.85 0.09	25.33 0.15	23.64 0.05	25.47 0.13
2451311.1393.....	23.55 0.05	25.17 0.12	25.17 0.11	25.71 0.19	24.62 0.08	25.23 0.14	24.38 0.06	25.11 0.13
HJD	C1-V9	C1-V10	C1-V11	C1-V12	C1-V13	C1-V14	C1-V15	C1-V16
				F555W				
2451331.9619.....	27.12 0.20	25.06 0.06	27.35 0.24	25.97 0.17	25.22 0.09	26.80 0.19	25.75 0.09	26.76 0.20
2451339.8188.....	26.25 0.12	25.34 0.08	26.44 0.15	26.28 0.21	25.55 0.14	26.18 0.09	26.83 0.26	25.85 0.18
2451348.8181.....	26.72 0.19	25.63 0.09	26.73 0.28	25.38 0.22	...	27.18 0.21	25.74 0.09	26.89 0.40
2451279.8407.....	26.13 0.12	24.98 0.06	26.48 0.13	24.97 0.22	25.82 0.16	27.20 0.28	26.63 0.20	26.82 0.23
2451288.1712.....	27.01 0.28	25.12 0.06	27.17 0.21	25.45 0.07	25.86 0.16	26.27 0.10	26.11 0.16	26.55 0.18
2451295.2907.....	27.01 0.20	25.27 0.11	27.58 0.39	25.83 0.10	25.73 0.37	26.97 0.19	26.38 0.19	26.12 0.12
2451301.2007.....	26.50 0.13	25.46 0.09	26.70 0.16	25.90 0.11	24.92 0.12	26.32 0.10	25.97 0.13	26.06 0.10
2451341.8341.....	26.32 0.16	25.41 0.09	26.33 0.14	25.94 0.11	25.05 0.09	26.52 0.15	26.35 0.19	26.23 0.18
2451311.0073.....	27.00 0.21	25.09 0.06	26.56 0.16	25.83 0.13	25.48 0.15	26.69 0.18	26.36 0.16	26.88 0.28
2451315.0382.....	26.38 0.14	24.82 0.05	26.76 0.15	25.56 0.11	25.02 0.09	26.44 0.12	25.64 0.09	25.83 0.10
2451319.6726.....	26.72 0.17	24.80 0.05	27.10 0.35	25.38 0.19	26.38 0.45	27.31 0.27	25.99 0.12	25.97 0.15
2451325.1806.....	26.80 0.19	24.96 0.05	27.82 0.39	25.22 0.09	25.62 0.12	26.95 0.21	26.91 0.25	26.15 0.13
				F814W				
2451332.0955.....	25.80 0.22	23.99 0.06	25.24 0.14	...	24.69 0.15	25.81 0.17	25.22 0.16	25.55 0.21
2451279.9733.....	...	23.95 0.05	24.97 0.13	24.35 0.09	...	26.07 0.22	25.75 0.22	25.22 0.15
2451295.4230.....	...	24.17 0.09	25.52 0.17	...	25.09 0.45	26.12 0.25	25.17 0.14	25.15 0.17
2451341.9674.....	25.64 0.16	24.20 0.07	24.72 0.09	...	25.88 0.28	25.71 0.18	25.64 0.20	25.53 0.22
2451311.1393.....	...	23.98 0.08	24.86 0.09	...	24.13 0.11	25.40 0.15	25.64 0.25	26.38 0.42
HJD	C1-V17	C1-V18	C2-V1	C2-V2	C2-V3	C2-V4	C2-V5	C2-V6
				F555W				
2451331.9619.....	27.14 0.31	26.57 0.17	25.74 0.09	26.07 0.12	25.80 0.06	27.51 0.35	27.07 0.21	26.49 0.12
2451339.8188.....	25.43 0.09	27.01 0.28	25.49 0.07	26.45 0.36	26.65 0.13	27.34 0.30	27.65 0.42	26.75 0.16
2451348.8181.....	26.07 0.14	26.17 0.13	25.05 0.06	25.36 0.09	25.73 0.07	26.63 0.17	...	26.75 0.16
2451279.8407.....	25.42 0.11	27.32 0.43	25.39 0.07	25.99 0.12	26.23 0.09	26.62 0.15	...	27.27 0.25
2451288.1712.....	25.77 0.12	26.52 0.12	25.71 0.08	26.22 0.13	26.34 0.11	27.06 0.21	26.01 0.09	27.39 0.26
2451295.2907.....	25.99 0.24	26.70 0.22	25.70 0.09	25.48 0.09	26.66 0.12	26.96 0.19	26.48 0.14	27.50 0.31
2451301.2007.....	26.81 0.31	27.42 0.45	25.30 0.07	25.80 0.10	26.07 0.27	27.55 0.33	26.62 0.14	27.64 0.38
2451341.8341.....	25.70 0.12	26.34 0.16	24.97 0.06	26.61 0.24	26.42 0.11	27.81 0.49	27.52 0.36	26.71 0.14
2451311.0073.....	25.36 0.08	25.77 0.18	25.24 0.06	...	25.73 0.06	27.45 0.27	26.58 0.13	26.49 0.09
2451315.0382.....	25.99 0.16	26.84 0.22	25.40 0.06	25.69 0.09	26.25 0.09	25.56 0.09	27.28 0.46	26.38 0.12
2451319.6726.....	26.12 0.14	26.40 0.12	25.55 0.08	25.56 0.10	26.71 0.13	27.73 0.44	27.14 0.26	26.42 0.11
2451325.1806.....	26.34 0.16	26.45 0.17	0.00 0.00	0.00 0.00	0.00 0.00	0.00 0.00	0.00 0.00	0.00 0.00
				F814W				
2451332.0955.....	25.63 0.24	26.28 0.33	24.68 0.09	24.98 0.12	25.08 0.10	...	26.12 0.22	25.13 0.10
2451279.9733.....	24.52 0.10	25.53 0.22	23.96 0.08	24.91 0.14	25.30 0.12	...	25.30 0.15	25.77 0.14
2451295.4230.....	24.76 0.14	25.63 0.19	24.81 0.12	24.67 0.13	25.41 0.14	...	25.66 0.20	26.28 0.32
2451341.9674.....	24.69 0.11	26.07 0.23	24.13 0.07	25.34 0.15	25.56 0.13	...	26.15 0.25	25.49 0.12
2451311.1393.....	24.56 0.09	26.22 0.40	24.09 0.07	25.26 0.14	25.39 0.11	...	25.69 0.16	25.71 0.16

TABLE 3—*Continued*

HJD	C3-V1	C3-V2	C3-V3	C3-V4	C3-V5	C3-V6	C3-V7	C3-V8
				F555W				
2451331.9619.....	26.15 0.13	25.62 0.09	27.56 0.43	...	25.11 0.05	26.26 0.17	24.80 0.04	24.98 0.04
2451339.8188.....	26.72 0.22	24.88 0.05	25.92 0.10	25.26 0.05	25.33 0.07	25.96 0.11	24.55 0.04	25.15 0.06
2451348.8181.....	25.81 0.11	25.14 0.07	27.05 0.27	25.39 0.08	25.31 0.07	25.66 0.11	24.72 0.04	25.25 0.07
2451279.8407.....	26.63 0.21	25.46 0.09	26.50 0.18	25.35 0.06	25.10 0.05	26.21 0.18	24.65 0.07	24.98 0.06
2451288.1712.....	25.58 0.09	26.02 0.17	26.91 0.22	25.47 0.07	25.21 0.06	25.63 0.10	24.80 0.06	25.21 0.06
2451295.2907.....	26.20 0.13	25.48 0.09	26.40 0.22	25.18 0.07	25.35 0.07	25.68 0.10	24.88 0.05	25.28 0.05
2451301.2007.....	26.60 0.17	24.84 0.05	26.76 0.22	24.93 0.05	25.43 0.06	25.69 0.10	24.92 0.05	25.42 0.07
2451341.8341.....	26.71 0.22	24.88 0.05	25.49 0.08	25.27 0.07	...	25.30 0.07	24.67 0.08	25.14 0.06
2451311.0073.....	25.99 0.11	25.25 0.07	26.42 0.15	24.93 0.06	25.20 0.08	26.35 0.16	24.95 0.05	25.13 0.06
2451315.0382.....	26.22 0.14	25.36 0.07	26.49 0.16	24.86 0.05	25.11 0.06	25.35 0.06	24.98 0.05	24.92 0.06
2451319.6726.....	26.95 0.22	25.68 0.10	26.80 0.25	24.93 0.05	25.45 0.07	25.53 0.09	24.90 0.05	24.95 0.06
2451325.1806.....	26.02 0.11	25.81 0.10	26.22 0.18	25.07 0.06	25.38 0.07	25.93 0.09	24.92 0.05	24.94 0.05
				F814W				
2451332.0950.....	25.05 0.12	25.13 0.30	26.11 0.29	23.76 0.05	23.53 0.07	24.43 0.09	24.26 0.06	23.77 0.05
2451279.9730.....	25.69 0.25	24.38 0.08	25.52 0.17	23.98 0.05	24.34 0.09	24.69 0.08	24.09 0.05	23.78 0.05
2451295.4220.....	25.10 0.14	24.61 0.09	25.83 0.26	23.85 0.06	24.58 0.10	24.34 0.08	24.41 0.08	24.07 0.05
2451341.9670.....	25.80 0.22	24.13 0.06	26.38 0.39	23.90 0.07	24.36 0.10	24.23 0.07	24.06 0.06	23.92 0.05
2451311.1390.....	25.05 0.11	24.09 0.06	25.75 0.20	23.28 0.05	24.40 0.08	24.64 0.09	24.49 0.08	23.91 0.05
HJD	C3-V9	C3-V10	C3-V11	C3-V12	C3-V13	C3-V14	C3-V15	C3-V16
				F555W				
2451331.9619.....	24.48 0.04	26.06 0.12	25.78 0.11	26.06 0.14	25.08 0.08	26.65 0.16	26.51 0.15	25.83 0.08
2451339.8188.....	24.60 0.05	25.66 0.09	26.63 0.23	25.75 0.08	25.00 0.06	25.62 0.18	26.80 0.18	26.36 0.16
2451348.8181.....	24.80 0.06	25.95 0.11	25.97 0.13	25.38 0.08	24.71 0.06	25.89 0.16	26.11 0.10	25.28 0.17
2451279.8407.....	24.32 0.05	25.99 0.12	26.83 0.27	25.67 0.11	24.77 0.06	26.10 0.14	25.84 0.10	25.21 0.08
2451288.1712.....	24.58 0.08	26.13 0.12	26.03 0.13	25.59 0.08	24.72 0.05	26.30 0.12	27.02 0.21	26.15 0.11
2451295.2907.....	24.86 0.05	25.94 0.10	27.05 0.30	25.30 0.08	24.74 0.06	25.57 0.08	26.40 0.15	26.43 0.16
2451301.2007.....	24.95 0.06	25.55 0.08	25.83 0.10	25.55 0.10	24.85 0.06	26.05 0.14	26.98 0.18	25.18 0.05
2451341.8341.....	24.76 0.05	25.75 0.11	27.44 0.38	25.43 0.08	24.84 0.04	25.34 0.06	26.97 0.23	26.39 0.19
2451311.0073.....	24.99 0.05	25.56 0.09	26.83 0.21	25.65 0.10	25.02 0.05	26.60 0.29	26.66 0.18	26.00 0.10
2451315.0382.....	24.71 0.05	25.80 0.08	26.77 0.19	25.74 0.10	25.08 0.06	25.80 0.08	27.00 0.22	26.12 0.09
2451319.6726.....	24.41 0.05	25.43 0.09	26.24 0.14	26.01 0.13	25.08 0.06	25.53 0.15	25.85 0.10	26.38 0.13
2451325.1806.....	24.42 0.04	25.65 0.09	26.89 0.23	25.91 0.12	25.12 0.06	26.02 0.11	26.64 0.16	25.41 0.06
				F814W				
2451332.0950.....	23.40 0.06	24.69 0.10	24.80 0.10	24.23 0.09	23.76 0.05	25.31 0.14	25.74 0.17	24.75 0.08
2451279.9730.....	23.52 0.05	24.99 0.11	26.11 0.31	24.39 0.09	23.67 0.05	25.11 0.11	25.44 0.13	24.63 0.07
2451295.4220.....	23.88 0.05	24.81 0.09	26.11 0.31	24.16 0.11	23.56 0.05	24.85 0.10	25.66 0.18	25.30 0.14
2451341.9670.....	23.30 0.06	25.32 0.25	25.88 0.21	24.17 0.08	23.66 0.05	24.78 0.16	26.09 0.22	25.57 0.23
2451311.1390.....	23.82 0.05	24.57 0.09	25.84 0.22	24.03 0.09	23.65 0.05	25.35 0.17	25.12 0.11	25.10 0.09
HJD	C4-V1	C4-V2	C4-V3	C4-V4	C4-V5	C4-V6	C4-V7	C4-V8
				F555W				
2451331.9619.....	25.44 0.10	25.30 0.10	26.05 0.22	24.77 0.10	26.42 0.19	24.19 0.06	26.52 0.16	24.74 0.13
2451339.8188.....	25.61 0.13	24.83 0.06	25.00 0.11	24.41 0.08	26.21 0.15	24.30 0.06	27.70 0.47	24.67 0.12
2451348.8181.....	25.05 0.08	25.03 0.08	25.35 0.12	24.62 0.09	25.60 0.07	25.24 0.18	26.36 0.18	24.95 0.13
2451279.8407.....	25.52 0.12	25.23 0.09	25.85 0.23	24.65 0.10	25.73 0.16	24.60 0.07	26.93 0.26	24.77 0.14
2451288.1712.....	24.76 0.06	25.41 0.15	25.45 0.15	24.57 0.10	26.16 0.16	24.53 0.06	26.78 0.30	25.33 0.19
2451295.2907.....	25.19 0.08	25.13 0.08	25.80 0.26	24.70 0.11	25.86 0.11	24.00 0.04	25.60 0.09	25.18 0.16
2451301.2007.....	25.52 0.10	24.86 0.06	25.85 0.21	24.82 0.12	26.25 0.13	24.31 0.06	27.36 0.42	24.67 0.12
2451341.8341.....	25.52 0.12	24.91 0.08	25.08 0.11	24.42 0.10	26.50 0.19	24.31 0.06	27.38 0.43	25.19 0.12
2451311.0073.....	25.56 0.12	24.99 0.08	25.18 0.14	25.03 0.12	26.12 0.16	24.11 0.05	26.36 0.16	25.47 0.22
2451315.0382.....	25.18 0.10	25.09 0.08	25.05 0.12	25.39 0.27	26.24 0.16	24.13 0.07	25.64 0.13	24.80 0.15
2451319.6726.....	25.05 0.08	25.23 0.09	25.61 0.17	25.18 0.15	25.77 0.09	24.26 0.05	27.01 0.25	24.55 0.13
2451325.1806.....	25.25 0.09	25.24 0.09	26.05 0.35	25.10 0.15	26.01 0.12	24.59 0.08	27.31 0.34	25.24 0.13
				F814W				
2451332.0950.....	24.14 0.11	24.02 0.11	24.74 0.23	23.43 0.09	24.94 0.13	23.13 0.15	...	23.68 0.32
2451279.9730.....	24.17 0.10	23.89 0.07	24.84 0.24	23.36 0.07	24.70 0.12	23.30 0.22	...	...
2451295.4220.....	23.75 0.11	24.08 0.10	24.49 0.14	23.31 0.06	24.94 0.14	23.02 0.14	...	23.65 0.31
2451341.9670.....	24.59 0.22	23.57 0.07	24.41 0.16	22.91 0.09	25.07 0.17	23.45 0.23	...	24.00 0.21
2451311.1390.....	24.64 0.16	23.45 0.10	24.25 0.15	23.68 0.10	25.02 0.17	23.18 0.16	...	...

TABLE 3—*Continued*

HJD	C4-V9	C4-V10	C4-V11	C4-V12	C4-V13	C4-V14	C4-V15	C4-V16
				F555W				
2451331.9619.....	25.38 0.16	26.42 0.15	26.19 0.20	25.47 0.10	26.23 0.21	26.26 0.13	26.05 0.16	25.80 0.11
2451339.8188.....	25.31 0.16	26.30 0.14	25.65 0.12	25.56 0.12	24.98 0.08	25.43 0.07	25.71 0.12	25.91 0.14
2451348.8181.....	24.89 0.12	25.99 0.11	26.07 0.19	24.88 0.07	25.28 0.09	25.69 0.09	26.14 0.16	24.99 0.07
2451279.8407.....	25.19 0.12	25.76 0.09	26.06 0.19	25.08 0.14	25.55 0.11	25.42 0.08	26.15 0.17	25.00 0.06
2451288.1712.....	24.92 0.11	26.99 0.29	25.75 0.14	25.35 0.10	25.83 0.14	25.99 0.11	25.40 0.08	25.35 0.08
2451295.2907.....	25.24 0.12	25.98 0.14	26.34 0.23	25.30 0.12	26.25 0.21	26.23 0.14	25.45 0.11	25.32 0.13
2451301.2007.....	25.41 0.14	...	25.53 0.10	25.40 0.12	25.05 0.08	26.22 0.16	25.97 0.14	25.94 0.14
2451341.8341.....	25.39 0.16	26.82 0.32	25.68 0.13	25.56 0.15	25.02 0.07	25.46 0.09	25.92 0.15	25.65 0.12
2451311.0073.....	25.32 0.14	26.28 0.14	26.08 0.18	24.83 0.06	25.38 0.11	25.60 0.08	25.50 0.09	25.26 0.13
2451315.0382.....	24.97 0.10	26.96 0.21	26.39 0.25	24.85 0.08	25.44 0.11	25.70 0.09	25.44 0.14	25.00 0.06
2451319.6726.....	24.66 0.09	26.13 0.10	25.65 0.11	25.20 0.12	25.63 0.13	25.94 0.13	25.84 0.12	25.26 0.07
2451325.1806.....	25.07 0.12	26.58 0.17	25.74 0.12	25.33 0.08	25.83 0.14	25.92 0.12	25.97 0.16	25.55 0.12
				F814W				
2451332.0950.....	23.84 0.13	25.26 0.19	...	24.24 0.11	24.17 0.12	24.51 0.12	24.99 0.18	24.26 0.11
2451279.9730.....	24.11 0.19	24.71 0.14	...	24.02 0.10	24.13 0.15	24.02 0.07	25.12 0.22	23.55 0.08
2451295.4220.....	23.81 0.19	24.90 0.17	...	24.07 0.12	24.38 0.17	24.52 0.13	24.88 0.17	24.74 0.16
2451341.9670.....	23.89 0.21	25.18 0.16	...	24.31 0.14	23.80 0.08	24.07 0.08	24.80 0.16	24.33 0.11
2451311.1390.....	23.94 0.16	24.78 0.14	...	23.90 0.09	24.05 0.12	24.01 0.08	24.55 0.16	24.03 0.10

HJD	C4-V17	C4-V18	C4-V19	C4-V20	C4-V21	C4-V22	C4-V23	C4-V24
				F555W				
2451331.9619.....	24.67 0.12	25.78 0.07	25.99 0.13	25.18 0.05	25.72 0.13	24.60 0.06	25.09 0.05	25.30 0.07
2451339.8188.....	26.01 0.19	26.12 0.17	26.67 0.26	25.30 0.06	25.86 0.14	24.74 0.07	25.22 0.05	25.80 0.09
2451348.8181.....	25.39 0.11	26.22 0.14	26.56 0.17	25.67 0.07	25.08 0.07	24.88 0.05	25.31 0.05	25.14 0.05
2451279.8407.....	25.49 0.11	25.89 0.09	26.06 0.12	25.09 0.06	25.62 0.11	24.95 0.07	25.26 0.05	25.32 0.07
2451288.1712.....	25.25 0.06	26.43 0.14	26.61 0.16	24.74 0.07	25.65 0.10	24.50 0.05	25.32 0.07	25.70 0.11
2451295.2907.....	25.80 0.16	25.66 0.08	26.56 0.21	25.45 0.07	25.15 0.09	24.65 0.06	25.30 0.06	25.23 0.06
2451301.2007.....	25.26 0.11	25.59 0.07	25.63 0.09	25.93 0.17	25.40 0.10	24.84 0.07	24.88 0.04	25.68 0.10
2451341.8341.....	25.86 0.14	26.23 0.12	27.08 0.32	25.31 0.06	26.03 0.15	24.82 0.07	25.30 0.05	25.76 0.10
2451311.0073.....	25.60 0.10	26.07 0.12	26.72 0.26	25.88 0.13	26.03 0.19	24.95 0.08	24.85 0.05	25.30 0.08
2451315.0382.....	25.26 0.11	26.09 0.10	27.16 0.36	25.12 0.05	26.13 0.18	25.14 0.08	24.85 0.04	25.31 0.08
2451319.6726.....	25.61 0.10	26.15 0.13	26.59 0.19	24.85 0.05	25.77 0.14	25.07 0.08	24.89 0.05	25.68 0.12
2451325.1806.....	26.30 0.39	25.10 0.07	26.14 0.15	24.94 0.05	25.38 0.10	24.73 0.06	25.08 0.04	25.80 0.10
				F814W				
2451332.0950.....	24.74 0.19	...	24.64 0.09	23.84 0.07	24.74 0.17	23.62 0.09	23.72 0.05	24.38 0.08
2451279.9730.....	24.53 0.17	24.49 0.10	24.64 0.10	23.88 0.06	24.64 0.13	23.73 0.09	23.83 0.05	24.41 0.09
2451295.4220.....	...	24.51 0.10	24.74 0.12	23.93 0.06	24.21 0.10	23.64 0.07	23.65 0.08	24.38 0.09
2451341.9670.....	...	24.74 0.12	24.63 0.14	23.90 0.08	24.77 0.16	23.74 0.07	23.77 0.05	24.61 0.09
2451311.1390.....	24.73 0.19	24.59 0.11	24.71 0.11	24.32 0.07	24.64 0.11	23.83 0.08	23.35 0.05	24.40 0.09

HJD	C4-V25	C4-V26
	F555W	
2451331.9619.....	26.08 0.11	25.67 0.08
2451339.8188.....	27.19 0.29	26.42 0.17
2451348.8181.....	26.71 0.28	26.43 0.14
2451279.8407.....	26.38 0.14	26.51 0.15
2451288.1712.....	25.99 0.12	25.66 0.08
2451295.2907.....	26.60 0.24	26.28 0.20
2451301.2007.....	26.44 0.16	26.86 0.22
2451341.8341.....	26.88 0.20	26.66 0.15
2451311.0073.....	26.12 0.11	25.69 0.10
2451315.0382.....	26.71 0.17	26.08 0.10
2451319.6726.....	26.26 0.12	26.76 0.21
2451325.1806.....	26.50 0.16	26.55 0.19
	F814W	
2451332.0950.....	25.21 0.17	24.83 0.12
2451279.9730.....	25.10 0.14	25.41 0.21
2451295.4220.....	25.33 0.19	24.98 0.17
2451341.9670.....	25.21 0.16	25.30 0.19
2451311.1390.....	25.19 0.14	24.92 0.14

TABLE 4

CHARACTERISTICS OF THE CEPHEIDS

Object (1)	Period (days) (2)	$\langle V \rangle$ (3)	$\sigma_{\langle V \rangle}$ (4)	$\langle I \rangle$ (5)	$\sigma_{\langle I \rangle}$ (6)	U_V (7)	U_I (8)	U_T (9)	σ_{U_T} (10)	Quality Index (11)
C1-V1	83.400	25.030	0.059	23.580	0.057	31.733	31.269	30.606	0.27	3
C1-V2	20.800	26.340	0.141	25.440	0.194	31.378	31.284	31.149	0.56	3
C1-V3	14.800	25.260	0.065	25.035	0.122	29.890	30.426	31.192	0.38	3
C1-V4	20.500	26.019	0.126	25.139	0.105	31.040	30.963	30.854	0.38	5
C1-V5	25.400	25.668	0.101	24.450	0.257	30.945	30.558	30.006	0.68	5
C1-V6	12.900	25.775	0.101	25.465	0.255	30.240	30.674	31.293	0.67	3
C1-V7	51.500	25.127	0.057	23.678	0.353	31.252	30.726	29.976	0.89	3
C1-V8	20.400	26.087	0.165	24.954	0.248	31.102	30.771	30.299	0.68	4
C1-V9	12.100	26.614	0.180	25.819	1.444	31.003	30.942	30.856	3.52	1
C1-V10.....	45.000	25.100	0.070	24.023	0.055	31.063	30.892	30.649	0.28	3
C1-V11.....	33.500	26.844	0.249	25.154	0.208	32.453	31.631	30.456	0.66	5
C1-V12.....	31.8:	25.69	...	...	...	...	...	...	...	0
C1-V13.....	14.200	25.491	0.243	25.384	0.777	30.071	30.720	31.647	1.93	3
C1-V14.....	13.200	26.654	0.181	25.757	0.173	31.147	30.996	30.781	0.54	4
C1-V15.....	15.400	26.066	0.170	25.299	0.315	30.743	30.743	30.743	0.83	3
C1-V16.....	23.000	26.257	0.189	25.260	0.258	31.415	31.237	30.982	0.72	2
C1-V17.....	28.400	25.940	0.203	24.843	0.231	31.351	31.101	30.742	0.67	2
C1-V18.....	7.400	26.536	0.254	25.767	0.628	30.335	30.237	30.098	1.58	3
C2-V1	38.900	25.340	0.072	24.208	0.267	31.128	30.884	30.534	0.69	3
C2-V2	27.800	25.871	0.169	24.904	0.149	31.256	31.133	30.956	0.49	5
C2-V3	16.700	26.226	0.137	25.166	0.195	31.001	30.718	30.313	0.56	3
C2-V4	13.9	26.83	...	...	...	...	...	...	...	0
C2-V5	66.200	26.702	0.264	26.132	0.908	33.127	33.514	34.066	2.25	4
C2-V6	90.000	26.851	0.221	25.519	0.280	33.645	33.309	32.830	0.78	5
C3-V1	19.500	26.224	0.159	25.145	0.228	31.184	30.903	30.501	0.64	5
C3-V2	39.200	25.416	0.097	24.325	0.323	31.214	31.010	30.720	0.83	5
C3-V3	13.900	26.533	0.210	26.066	0.424	31.219	31.518	31.946	1.09	1
C3-V4	62.900	25.171	0.059	23.787	0.056	31.535	31.101	30.481	0.27	2
C3-V5	21.200	25.314	0.062	24.082	0.279	30.493	30.081	29.493	0.72	1
C3-V6	26.100	25.866	0.126	24.414	0.151	31.176	30.558	29.677	0.46	2
C3-V7	58.000	24.902	0.052	24.187	0.150	31.169	31.393	31.713	0.43	3
C3-V8	56.100	25.179	0.060	23.861	0.058	31.315	30.922	30.359	0.27	3
C3-V9	48.500	24.715	0.053	23.601	0.242	30.768	30.570	30.286	0.63	3
C3-V10.....	8.800	25.785	0.098	24.721	0.439	29.792	29.421	28.892	1.10	1
C3-V11.....	15.200	26.510	0.220	25.212	0.528	31.172	30.639	29.877	1.34	4
C3-V12.....	54.400	25.772	0.107	24.156	0.167	31.963	31.277	30.297	0.49	2
C3-V13.....	66.600	24.988	0.061	23.631	0.053	31.421	31.021	30.450	0.27	2
C3-V14.....	23.800	26.022	0.155	25.020	0.100	31.222	31.043	30.787	0.39	4
C3-V15.....	13.600	26.540	0.168	25.717	0.123	31.069	30.995	30.891	0.44	4
C3-V16.....	23.800	25.825	0.112	24.822	0.154	31.004	30.822	30.562	0.46	4
C4-V1	28.700	25.339	0.092	24.013	0.199	30.763	30.284	29.600	0.55	4
C4-V2	37.200	25.162	0.096	23.882	0.139	30.896	30.498	29.929	0.42	3
C4-V3	26.900	25.605	0.191	24.600	0.152	30.951	30.785	30.547	0.51	5
C4-V4	54.400	24.881	0.134	23.393	0.234	31.072	30.514	29.718	0.64	4
C4-V5	14.300	26.078	0.149	24.979	0.143	30.666	30.324	29.835	0.46	3
C4-V6	21.600	24.451	0.096	23.339	0.253	29.534	29.232	28.802	0.67	1
C4-V7	19.4	26.65	...	...	...	...	...	...	...	0
C4-V8	17.600	24.995	0.160	23.935	0.257	29.860	29.586	29.195	0.70	1
C4-V9	33.000	25.198	0.126	23.841	0.233	30.789	30.298	29.596	0.63	2
C4-V10.....	14.200	26.353	0.191	25.067	0.132	30.934	30.403	29.644	0.47	5
C4-V11.....	19.0	25.98	...	...	...	...	...	...	...	0
C4-V12.....	40.700	25.207	0.106	24.100	0.185	31.049	30.836	30.531	0.52	2
C4-V13.....	37.200	25.540	0.134	23.996	0.343	31.275	30.612	29.665	0.88	5
C4-V14.....	30.200	25.933	0.119	24.353	0.087	31.418	30.692	29.655	0.35	5
C4-V15.....	22.200	25.837	0.140	24.969	0.145	30.953	30.899	30.822	0.46	3
C4-V16.....	32.400	25.471	0.111	24.098	0.415	31.040	30.530	29.803	1.04	3
C4-V17.....	15.600	25.523	0.125	24.799	0.338	30.216	30.260	30.321	0.87	2
C4-V18.....	29.200	25.954	0.103	24.551	0.113	31.398	30.845	30.055	0.38	3
C4-V19.....	26.500	26.333	0.199	24.785	0.269	31.661	30.950	29.933	0.74	2
C4-V20.....	48.500	25.310	0.091	24.010	0.130	31.363	30.979	30.430	0.41	2
C4-V21.....	26.900	25.628	0.126	24.591	0.181	30.974	30.776	30.493	0.52	4
C4-V22.....	40.700	24.853	0.067	23.782	0.076	30.695	30.517	30.262	0.30	3
C4-V23.....	61.900	25.120	0.052	23.696	0.074	31.524	31.054	30.382	0.29	2
C4-V24.....	18.600	25.526	0.090	24.532	0.080	30.430	30.226	29.935	0.32	2
C4-V25.....	11.600	26.489	0.188	25.258	0.249	30.827	30.325	29.608	0.70	3
C4-V26.....	22.200	26.231	0.149	25.033	0.157	31.347	30.963	30.414	0.49	4

over the cycle) were obtained from the procedure of Labhardt et al. (1997), whereby each F814W magnitude at a randomly sampled phase is converted to a mean value $\langle$F814W$\rangle$ using amplitude and phase information from the more complete F555W light curves. Note that each available observation of F814W can be used independently to derive a mean magnitude. Hence, the scatter of the individual values about the adopted mean F814W value is an *external* measure of the uncertainty in determining $\langle$F814W$\rangle$. It is this external measure of the uncertainty that is retained and propagated in the later calculations. There is one instance (C1-V9) where there is only one available F814W measurement, so only the error estimated by DoPHOT for that observation can be propagated; in this instance the error estimate is very high anyway, and the object plays essentially no role in the final distance estimate.

The prescription given in Paper V for assigning the light-curve quality index, QI (which ranges from 0 to 6), was used. In this scheme, two points (0–1) are given for the quality of the F555W light curves, two points (1–2) for the evenness in phase coverage of the five F814W observation epochs, and three points (1–3) for the amplitude and phase coherence of the F814W observations compared with the F555W light curve. Hence, a quality index of 6 indicates the best possible light curve quality. A quality index of 2 or less indicates near fatal flaws, such as apparent phase incoherence in the two passbands. This is generally an indication that object confusion by crowding and/or contamination by background is likely.

Table 4 lists the characteristics of all 66 objects whose light curves in F555W are consistent with those of Cepheids. For 62 of these, an F814W measurement exists for at least one epoch. The F555W and F814W instrumental magnitudes of Table 3 have been converted to the Johnson V and Cousins (Cape) I standard photometric system by the color equations used in previous papers of this series, as set out in equations (2) and (3) of Paper V, based on the transformations of Holtzman et al. (1995b).

The magnitude scatter $\sigma_{\langle V\rangle}$ in Table 4 is based on the estimated measuring errors in the photometry of the individual epochs. In the case of $\sigma_{\langle I\rangle}$, the *external* uncertainty from the Labhardt et al. (1997) procedure is listed, since it is more robust and realistic. The quality index discussed above is also listed. Other columns of Table 4 are explained later in the text.

4. THE PERIOD-LUMINOSITY RELATION AND THE DISTANCE MODULUS

4.1. *The P-L Diagrams in V and I*

As in the previous papers of this series, we adopt the P-L relation in V from Madore & Freedman (1991) as

$$M_V = -2.76 \log P - 1.40 , \quad (1)$$

whose companion relation in I is

$$M_I = -3.06 \log P - 1.81 . \quad (2)$$

The zero point of equations (1) and (2) is based on an assumed LMC modulus of 18.50.

The P-L relations in V and I for the 62 Cepheids in Table 4 are shown in Figure 6. The filled circles show objects with periods between 20 and 65 days that have a quality index of 3 or higher. The filled circles show smaller scatter, and delineate the P-L relation. The solid lines show the canonical slopes of the P-L relations in V and I with the vertical offset for apparent distance moduli $\mu_V = 31.05$ and $\mu_I = 30.83$, respectively. These values were chosen to be in visual conformity with the points shown by filled circles (they are not intended as a formal derivation of distance). The expected spread in each of the passbands due to the finite width of the instability strip (Sandage & Tammann 1968) is indicated by the flanking dashed lines. The observed scatter of the data outside these envelope lines are due to the combination of (1) measuring and systematic errors due to background and contamination, (2) the random error of photon statistics, (3) the large effects of the variable extinction evident from the dust lanes seen in the images, and (4) objects misidentified as Cepheids.

The period cutoff of 20 days for the filled circles is chosen to prevent a bias at the faint end, because Cepheids at short periods that are at the faint end of the intrinsic scatter about the mean P-L relation and fall below the detection limit in brightness do not populate the P-L relation, which adversely affects the fitting of the P-L relation. A period cut is unbiased, but the value of the shortest included period depends on the magnitude limit of the data. For this reason, it is chosen independently from one galaxy to the next: nearby galaxies can accommodate a shorter period cut, while ones that are farther require a cut at longer periods for the same magnitude detection limit.

4.2. *A Preliminary Analysis of the P-L Relation*

For a first estimate, using $A_V/A_I = 1.7$ (Scheffler 1982) along with the very preliminary apparent moduli in V and I of 31.05 and 30.83, respectively, as estimated above, yields a dereddened modulus $\mu_0 \approx 30.50$ (all values quoted in §§ 4.2–4.4 should have an additional 0.05 mag added for the "long versus short" correction mentioned above to be placed on a par with the final values obtained in previous papers of this series). To explore the presence of differential extinction and to treat the data accordingly, we use the tools developed in Paper V and used again in Papers VII (Sandage et al. 1996), VIII (Saha et al. 1997), and IX (Saha et al. 1999).

For each Cepheid we calculate the apparent distance moduli separately in V and in I from the P-L relations of equations (1) and (2) and the observed $\langle V\rangle$ and $\langle I\rangle$ magnitudes from Table 4. These apparent distance moduli, called U_V and U_I in columns (7) and (8) of Table 4, are calculated by

$$U_V = 2.76 \log P + 1.40 + \langle V\rangle \quad (3)$$

and

$$U_I = 3.06 \log P + 1.81 + \langle I\rangle . \quad (4)$$

They are the same as equations (6) and (7) of Paper V.

If the differences between the V and I moduli are due solely to reddening, and if the dependence of the reddening curve on wavelength is the normal standard dependence as in the Galaxy, then the true modulus, U_T, is given by

$$U_T = U_V - R'_V(U_V - U_I) , \quad (5)$$

where R' is the ratio of total to selective absorption, $A_V/E(V-I)$. This is equation (8) of Paper V. However, equation (5) is valid only if the difference between U_V and U_I is due to extinction, not to correlated measuring errors, in which case the value of R'_V would *not* be given by the normal extinction curve where $A_V/A_I = 1.7$ and the ratio of absorption to reddening is $R'_V = A_V/E(V-I) = 2.43$ (Scheffler 1982). It will be shown that such coupled errors clearly exist, and the derivation of the true distance

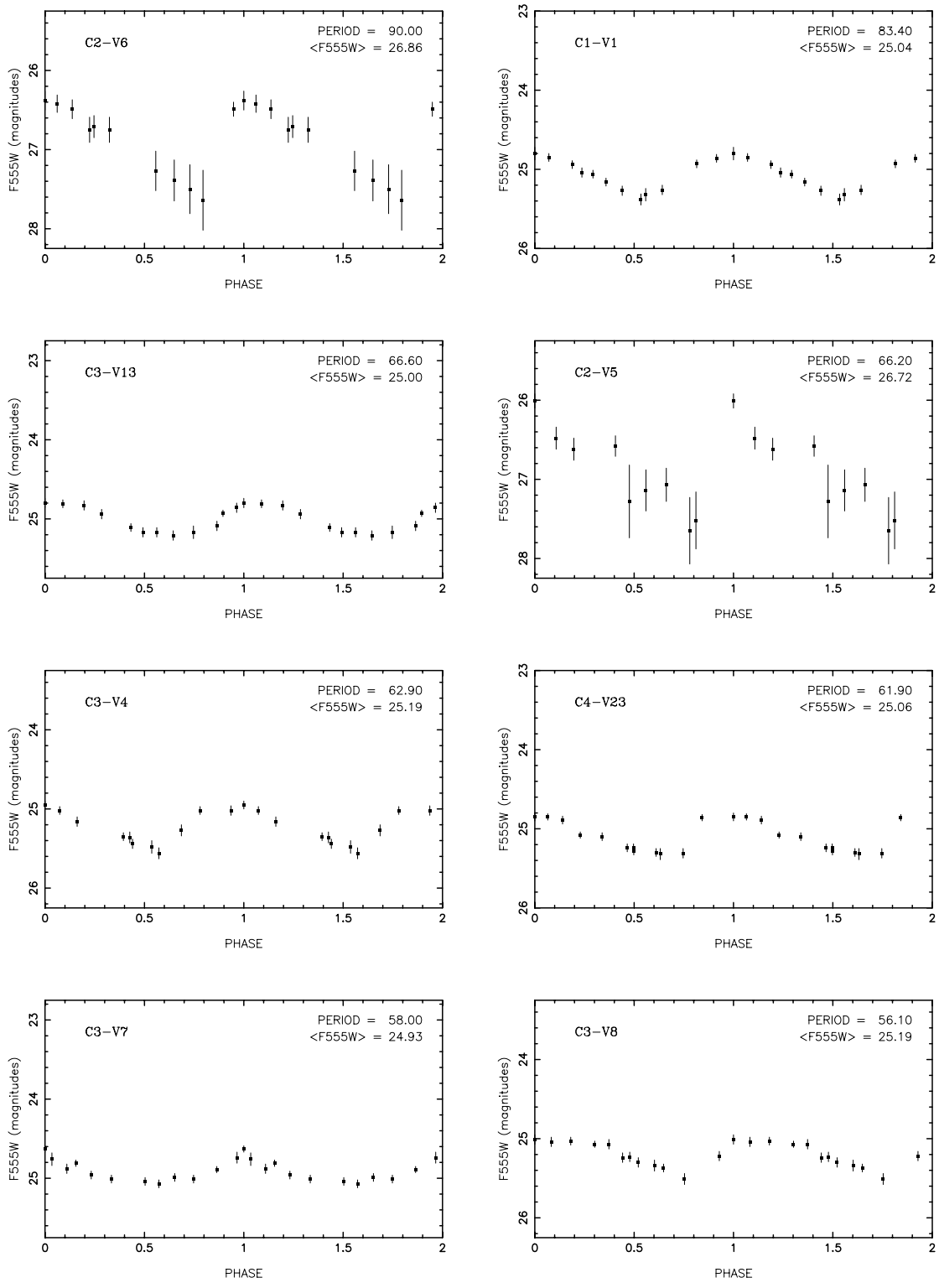

FIG. 4.—Light curves, plotted in order of period, in the F555W band

modulus is considerably more complicated than would be the case in the absence of the correlated systematic measuring errors.

The values of U_T are listed in column (9) of Table 4. These would be the true moduli, as corrected for normal extinction, assuming that there are no systematic measuring errors. The total rms uncertainty for each U_T value is listed in column (10). This uncertainty includes contributions from the estimated random measuring errors in the mean V and I magnitudes (in cols. [4] and [6]), as propagated through the dereddening procedure, as well as the uncertainty associated with the intrinsic width of the P-L relation (i.e., a given Cepheid may not be on the mean ridgeline of the P-L relation), as well as a 10% uncertainty in the esti-

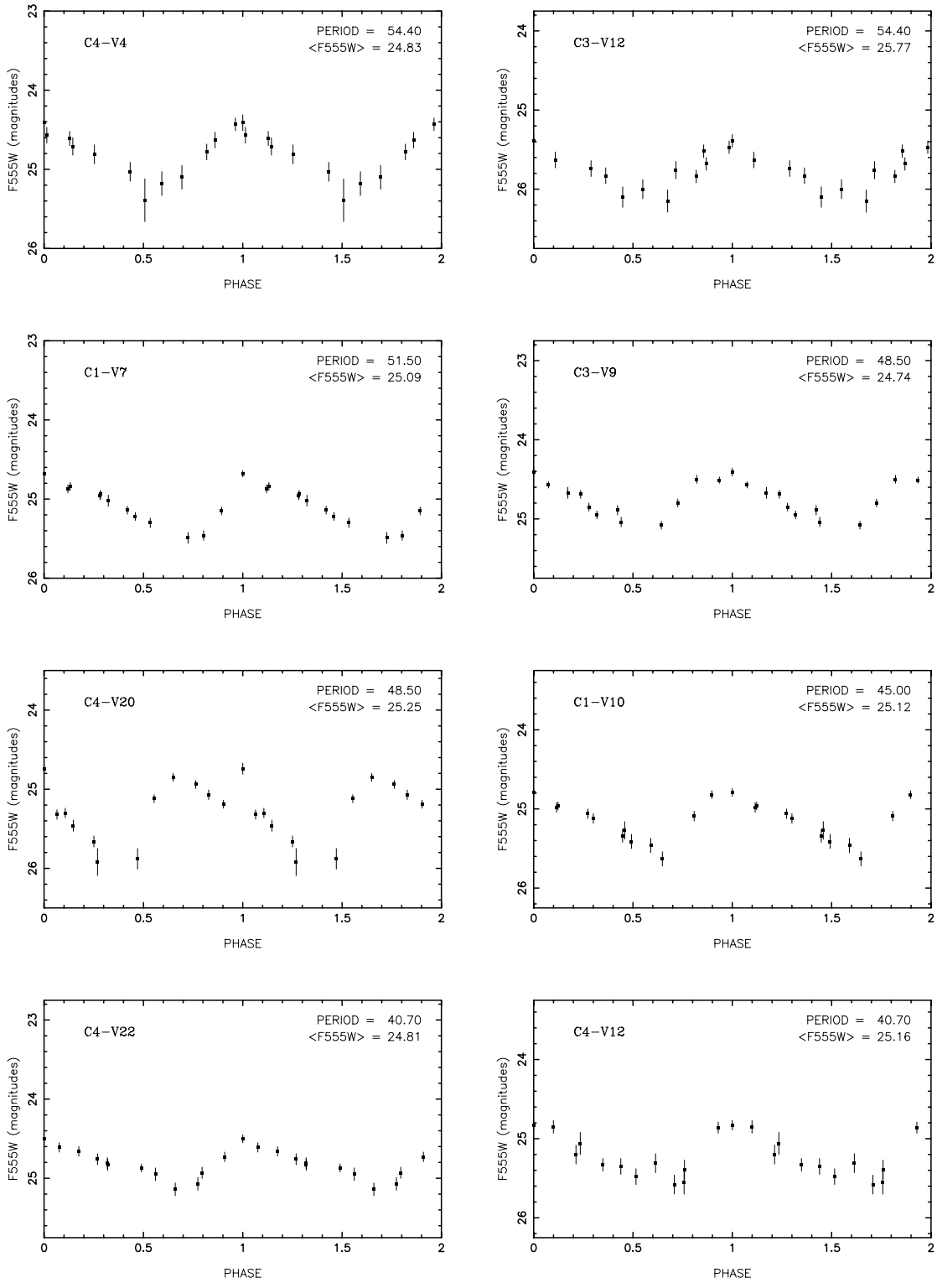

FIG. 4.—*Continued*

mated period. The dereddening procedure amplifies the measuring errors. Therefore, many Cepheids are needed to beat down these large errors (note the very large values in col. [10]) in any final value of the modulus. The values shown in column (10) of Table 4 were calculated using equation (18) of Saha et al. 2000, and also correspond to $\sigma_{\rm tot}$ as defined in Paper V.

It is important to mention that two regrettable chains of error have propagated through our series of papers, concerning the calculation of the uncertainties in U_T. The first is that equation (11) in Paper V for the calculation of $\sigma_{\rm width}$ was incorrectly given, and its correction given in Paper IX was also in error; its use would be tantamount to assuming that the intrinsic width of the P-L relation is uncorrelated in the two passbands. The program that calculates these values was examined, and found to be coded correctly,

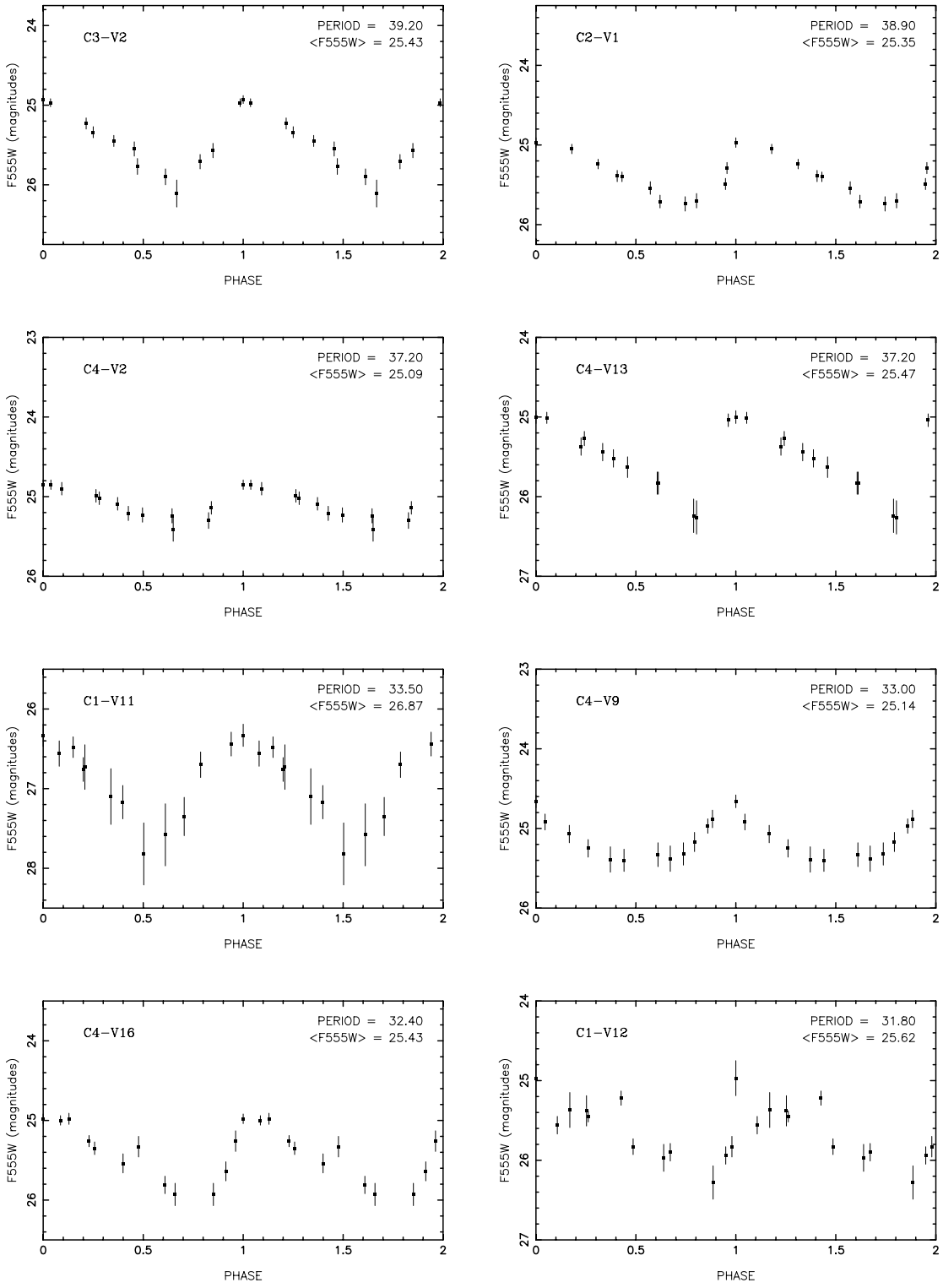

FIG. 4.—*Continued*

according to equation (18) of Saha et al. (2000). However, an error in coding the uncertainty due to the uncertainty in period estimates resulted in *overestimates* of $\sigma_{\rm tot}$ in our previous papers that can be corrected as

$$\sigma^2_{\rm tot}({\rm corrected}) = \sigma^2_{\rm tot}({\rm old}) - 0.34^2 \qquad (6)$$

The values of $\sigma_{\rm tot}$ have been used in Papers V, VIII, and IX for calculating weighted means of U_T, using $1/\sigma^2_{\rm tot}$ as weights. The effect of our prior miscalculations was to "flatten" the weights, an effect that is, however, benign; it makes the weighted averages more like unweighted ones, although the objects with egregious measurement errors were still successfully down-weighted. The final distance moduli using weighted averages are unaffected at the 0.03 mag level, and unweighted averages are completely unchanged.

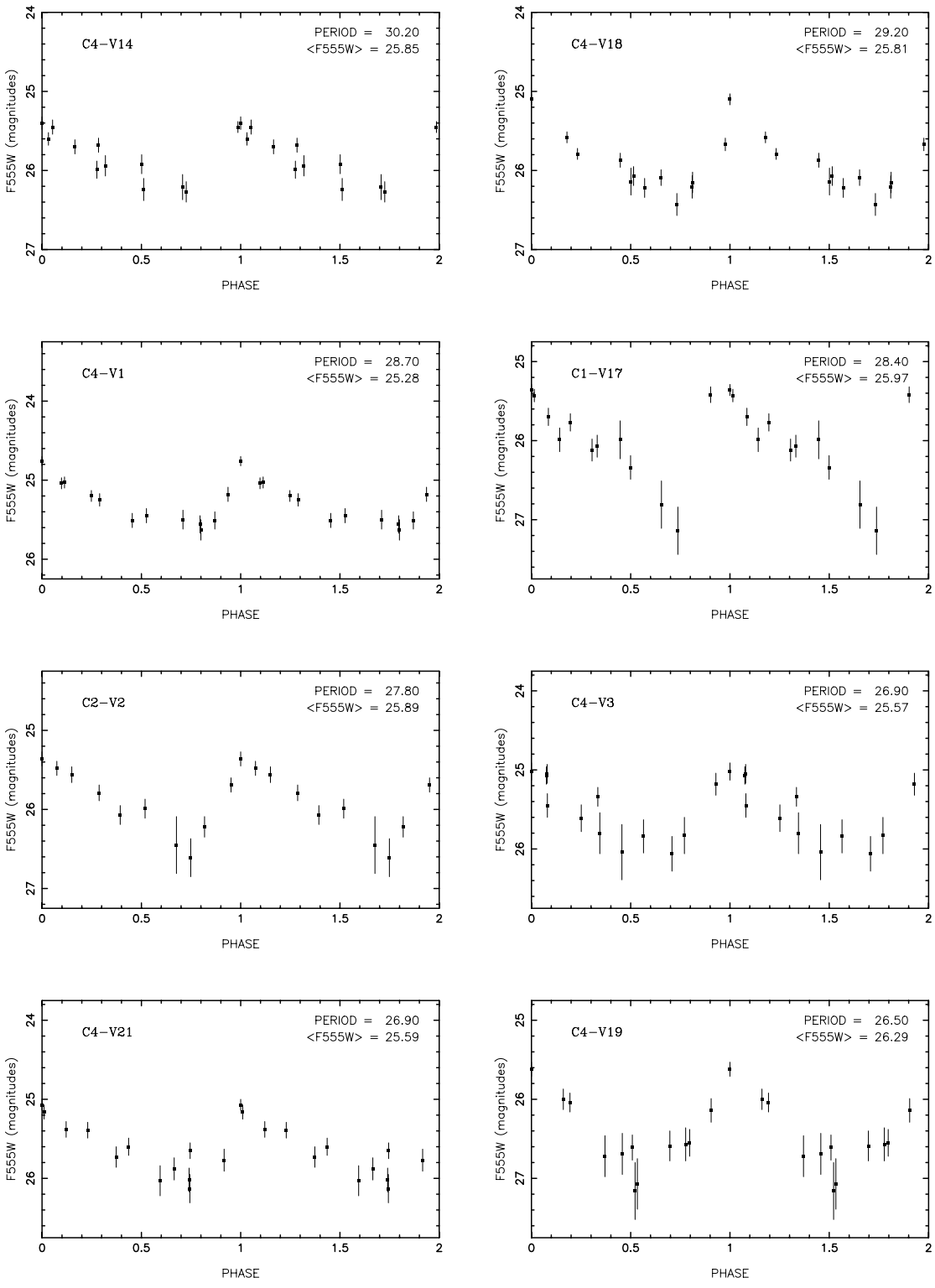

FIG. 4.—*Continued*

From the data in Table 4, the unweighted mean dereddened modulus $\mu_0 = \langle U_0 \rangle$ for all Cepheids with periods from 20 to 65 days with QI ≥ 3 is 30.38 ± 0.10 mag, and the weighted (by $1/\sigma_{\rm tot}^2$) value is 30.43 ± 0.09 mag. Closer examination reveals that the Cepheids in chip 4 systematically give lower distance moduli: the weighted average μ_0 is 30.12 ± 0.13 for the 12 chip 4 Cepheids alone (same period and QI cut), but 30.68 ± 0.12 for the 15 Cepheids in the remaining three chips. The corresponding unweighted averages are 30.08 ± 0.12 and 30.62 ± 0.12, respectively. The average (unweighted) *apparent* moduli μ_V for these two samples are 31.07 ± 0.07 and 31.20 ± 0.08, respectively. The corresponding (unweighted) values for μ_I are 30.65 ± 0.06 and 30.97 ± 0.08 for the apparent modulus. The large discrepancy in the I moduli suggests a possible problem with the chip 4 photometry in I. This is investigated further in

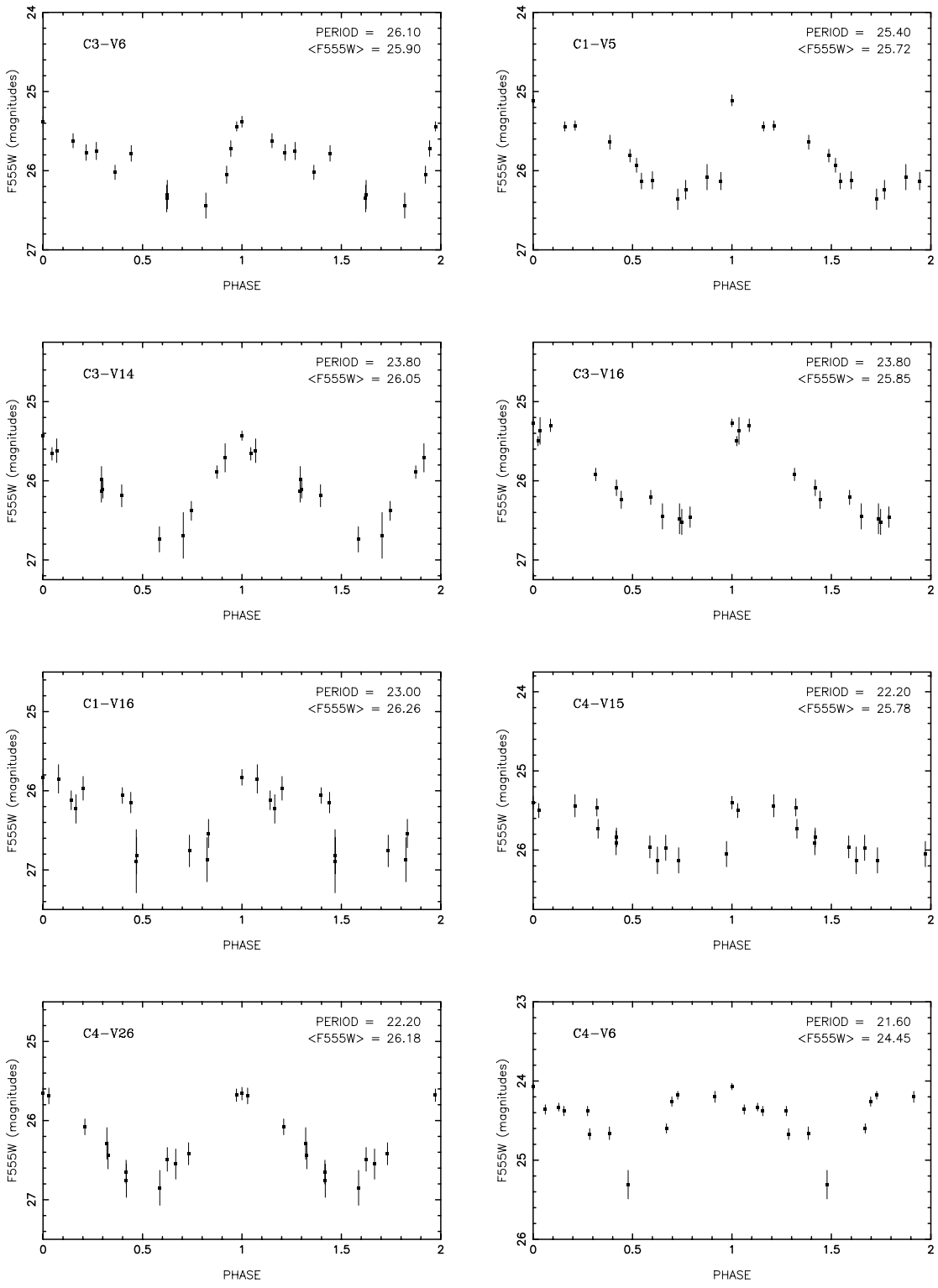

FIG. 4.—*Continued*

§ 4.3. Including Cepheids with QI = 2 typically drops the dereddened modulus by 0.1 mag, while raising the cut to higher QI makes no noticeable difference.

We note again that the derived U_T values depend on the assumption that the differences between U_V and U_I are due to reddening alone, in the absence of appreciable systematic and correlated measuring errors, or when the errors for $U_V - U_I$ *are distributed symmetrically*. If correlated and/or asymmetrical errors in V and I dominate over differential reddening, thereby producing a ratio of the V to I errors that is different from 2.43, the U_T derived via equation (5) *will be systematically in error*.

In particular, several Cepheids that were discovered in V are too faint in I to be measured, as already mentioned. This introduces a selection effect that biases against Cepheids with bluer colors. The effect is most pronounced at short

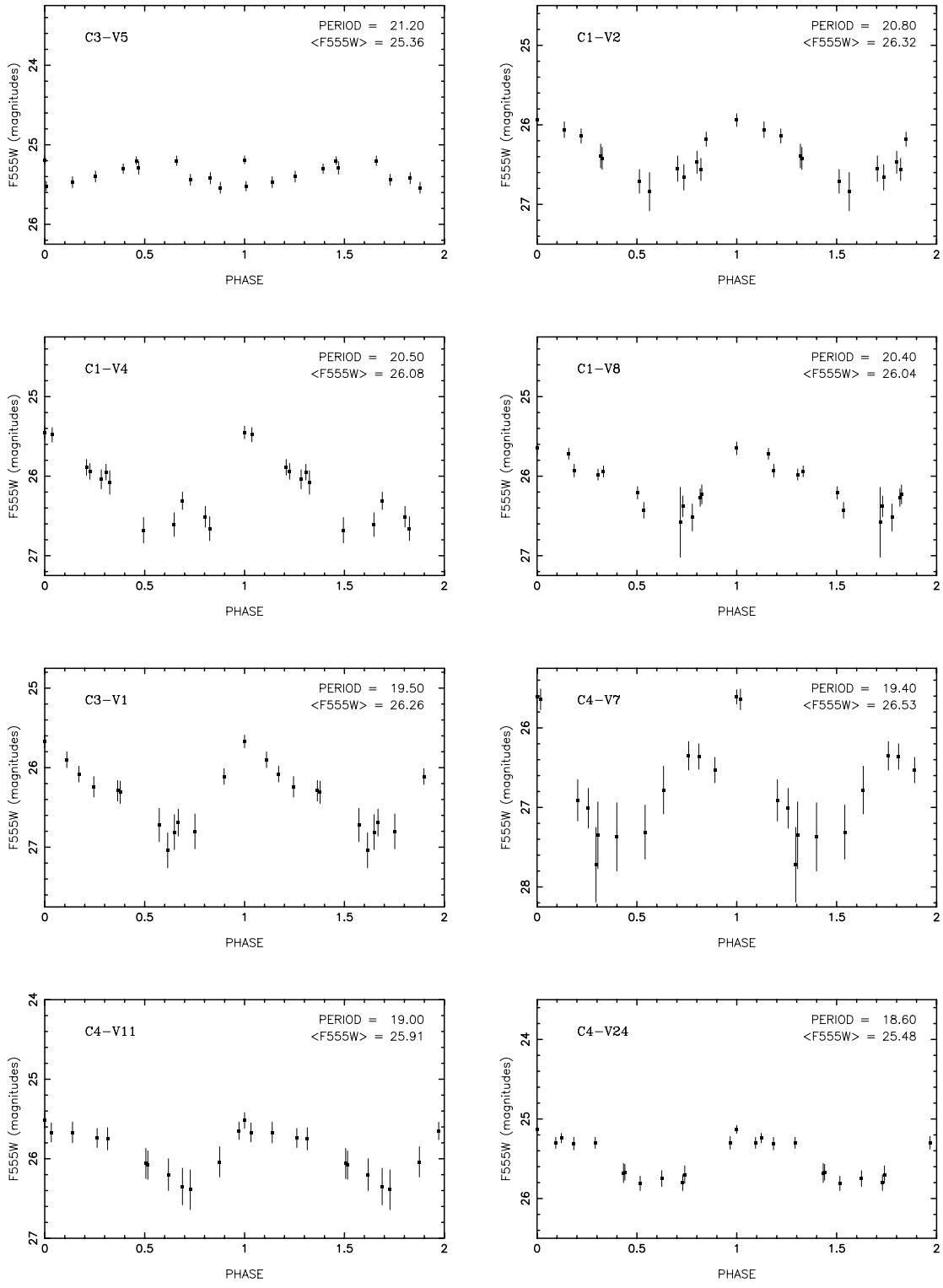

FIG. 4.—*Continued*

periods, where the *intrinsic* colors are bluest. This effect gives an asymmetrical distribution of errors in $U_V - U_I$, in the sense that it makes the dereddened modulus *too small.* This is likely to be more acute for the case of chip 4, where the Cepheids are mostly in regions of extremely high surface brightness and crowding.

In Paper V we devised a method to test for the presence of differential extinction or for the fact that the scatter about the P-L relation is due predominantly to measuring errors, or a combination of both. The method, shown in Figure 11 of Paper V for NGC 4536 and explained in the Appendix there, has also been used in Papers VI, VIII, and IX. The method is to plot the difference in the V and I moduli for any given Cepheid against the V modulus. If there is a systematic trend of the data along a line of slope $dU_V/d(U_V - U_I) = 2.43$, then equation (5) applies and there is

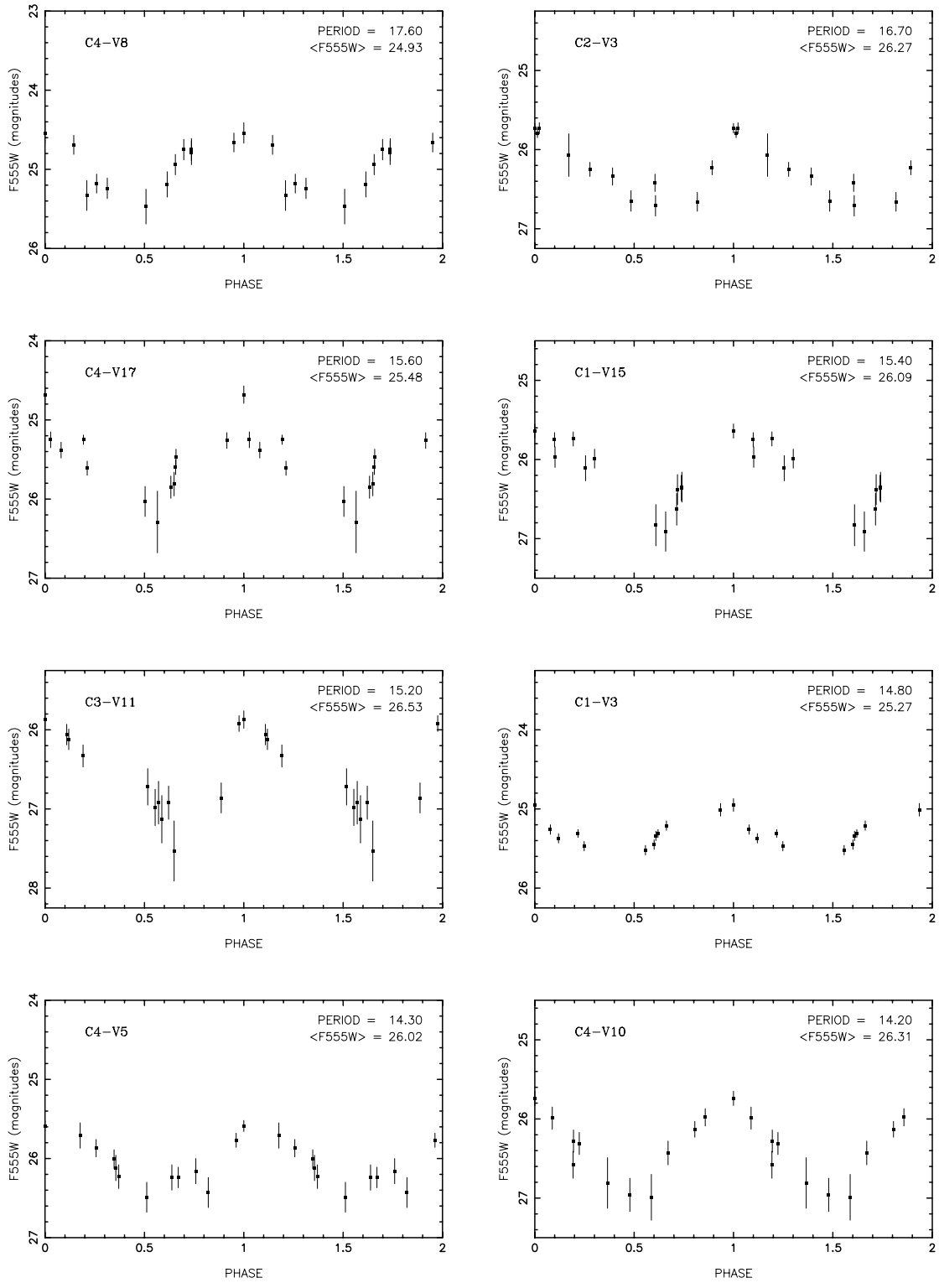

FIG. 4.—*Continued*

clearly differential reddening. If, on the other hand, there is a general scatter with no trend, that scatter is dominated by measuring errors. While in the latter case bona fide differential extinction can be hidden by measuring errors, trying to correct for putative reddening will result in interpreting any asymmetry in the error distribution as specious extinction. In two of the three previous cases, NGC 4536 (Paper V) and NGC 4496A (Paper VI), there is no trend along a differential reddening line. In the third case of NGC 4639 (Paper VIII), there is a slight trend but also large scatter, showing that the spread of points appears to be due to a mixture of measurement errors as well as differential extinction.

The diagnostic diagram just described is shown for the NGC 4527 data from Table 4 in the top panel of Figure 7. The filled circles show Cepheids with periods between 20 and 65 days that have QI $\geq$ 3. The solid line indicates the reddening vector for the P-L ridgeline, if the true (dereddened) distance modulus is 30.50, which was the initial estimate made in this section. The dashed lines show the bounds due to the intrinsic dispersion of the P-L rela-

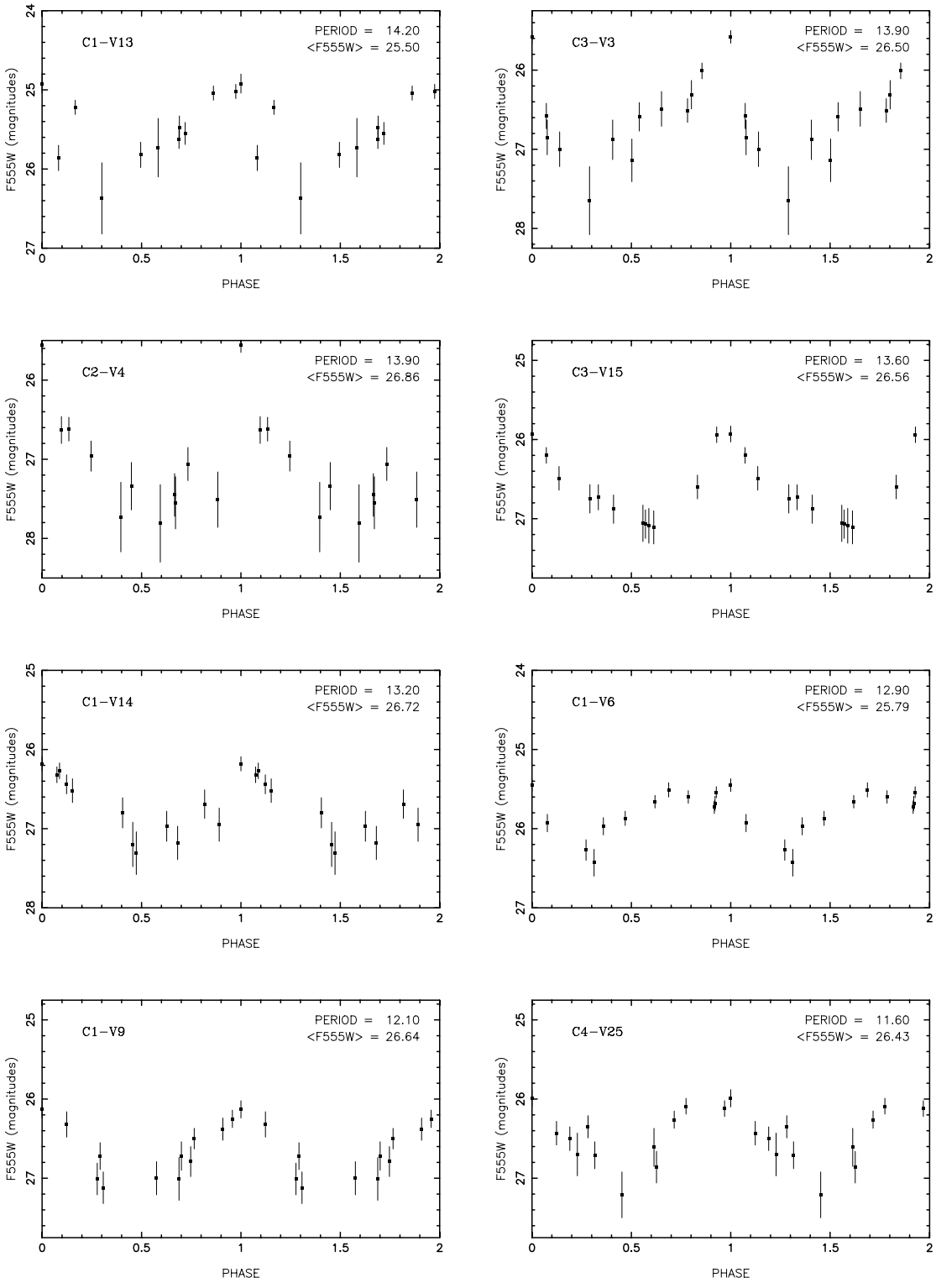

FIG. 4.—*Continued*

tion, as explained in Paper V. The slope of the lines is $A_V/E(V-I) = 2.43$, as explained above.

The scatter in Figure 7 (*top*) is disappointing. In general, the points do not lie within any reddening track; translating the reddening band in this figure would not materially reduce the number of points that would spill out of it. There may be some differential reddening, but the visible trend is that for the "good" Cepheids (*filled circles*) the U_V values do not show any trend with $U_V - U_I$. This is a strong indicator that the range of $U_V - U_I$ is not due to extinction, but rather to measurement errors. The relative constancy of the U_V values in Figure 7 (*top*) suggests that the *differential* extinction is smaller than can be detected, given the errors in the data. The range of values in $U_V - U_I$ must then be due to I-band photometry errors. This prediction can easily be checked by making the I-band analog, shown in the bottom panel of Figure 7, where U_I rather than U_V is shown, and the slope and width of the locus of where the

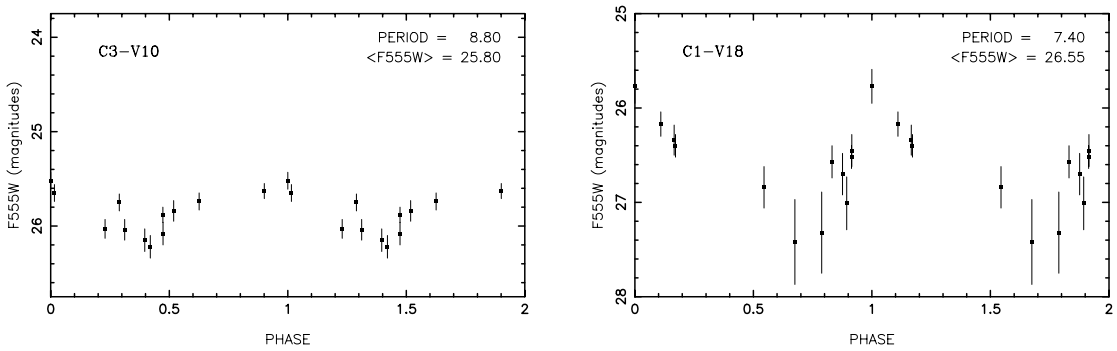

FIG. 4.—*Continued*

reddened Cepheids should lie is appropriately changed. The points shown with concentric outer circles are for Cepheids in chip 4. The "good" Cepheids follow a slope $dU_I/d(U_V - U_I) \approx -1$, which confirms the prediction that the range in $U_V - U_I$ is due to unaccounted-for errors in the I-band photometry (see § 3.2 in Saha et al. 2000). Note also that most of the objects that are overly bright in I are to be found on chip 4, which is the most crowded part of the galaxy.

An alternate perspective is to plot just U_V versus U_I, which is shown in Figure 8. The reddening vector is shown by the solid line, whereas the points seem to stretch along a slope of unity (*dashed line*). In Paper IX we discussed how confusion errors that are correlated in the two passbands can produce arbitrary slopes. The results of simulation experiments performed using an identical photometry procedure on data very similar to those at hand (Saha et al. 2000) show that the slope of the correlated errors is about unity. The extreme points, which are expected to be outliers anyway, seem to follow the results of the simulations, lending credence to the hypothesis that they are the result of confusion errors. It is possible that the remaining points are partially afflicted with confusion noise, in which case the simple use of equation (5) will result in systematic errors. Additional examination of the data by different methods is essential, and is done in §§ 4.3 and 4.4.

This is not to deny the presence of differential reddening, but an acknowledgment that the measurement errors in I dominate the color spread. We proceed by making an additional restriction of the data by color. Note that such a restriction used in conjunction with equation (5) does not introduce a procedural bias in the distance modulus.

4.3. *Inspection of the Color-Magnitude Diagram*

The observed color-magnitude diagrams (CMDs) obtained from DoPHOT photometry on the deep (combining all epochs) images is shown individually in Figure 9 for each of the regions in the four different chips. Two things are worth noting:

1. The general appearance of the CMDs from chips 1, 2, and 3 is not unlike the CMD shown in Figure 14 of Paper V for NGC 4536, with the difference that the blue edge, which is quite sharply defined for NGC 4536, shows some smearing for the NGC 4527 field, and is placed 0.2 mag or more redder than for NGC 4536. This only confirms the general level of reddening that we have already surmised from the Cepheids, and expected, given the appearance of NGC 4527 with its pronounced dust lanes.

2. It is apparent that the CMD obtained from chip 4 is different from the other chips: there are a disproportionate number of stars that are more luminous than in the other chips. It would be nearly absurd to think that this is a real feature, and as we show below, it indicates a problem with the photometry at these high levels of surface brightness, crowding, and dust structure.

The CMD anomaly for chip 4 with respect to the remaining chips is also seen in Figure 10, where the same CMDs are plotted, but with F814W on the ordinate. In Figure 11, the CMD for the chip 4 region alone is shown, but it is broken down by quadrant subregions. The anomaly is clearly visible in the upper left and lower left quadrants, but not noticeable in the two right-hand quadrants. It is immediately clear from Figures 2 and 3 that the anomaly appears in the very bright areas where crowding is most severe, and where dust lanes cut up the background continuity severely.

This anomaly in the photometry is not entirely unexpected. It has been pointed out by Mochejska et al. (2000) and Stanek & Udalski (2000) that photometric blending in overcrowded fields may lead to a systematic underestimate of distances. However, it has also been the subject of thorough empirical investigation by Saha et al. (2000) and Ferrarese et al. (2000). The latter authors, who have run simulation experiments with artificial star frames, find no empirical evidence for such large systematic drifts in photometry with crowding in excess of a few hundredths of a magnitude (which can lead to distance underestimates by 0.1 mag). These studies were done before data were available for NGC 3627 and now NGC 4527, which are by far the data sets most afflicted by high surface brightness, crowding, and dust-lane structure. Of these, NGC 3627 is the closer galaxy, and crowding effects are less likely to have been explicitly noticed. It appears that DoPHOT does not produce reliable photometry in the overly crowded subregions of chip 4 for NGC 4527.

Recall that earlier in this paper, the scatter in the I photometry for the Cepheids was surmised to be worse than for V, while the anomaly in the CMD appears equally bad for V and I. The selection process for Cepheids, which includes not only a consideration for the light amplitude but also a *visual* inspection of each candidate Cepheid on the V (but not I) image, will result in rejecting objects that are likely to be mismeasured in V. However, the same objects may be contaminated seriously in I, and the equivalent checks for object rejection in I were not in place. This may be the explanation for the empirical conclusion made earlier that the color spread is dominated not by differential extinction alone, but by error excursions in the I photometry.

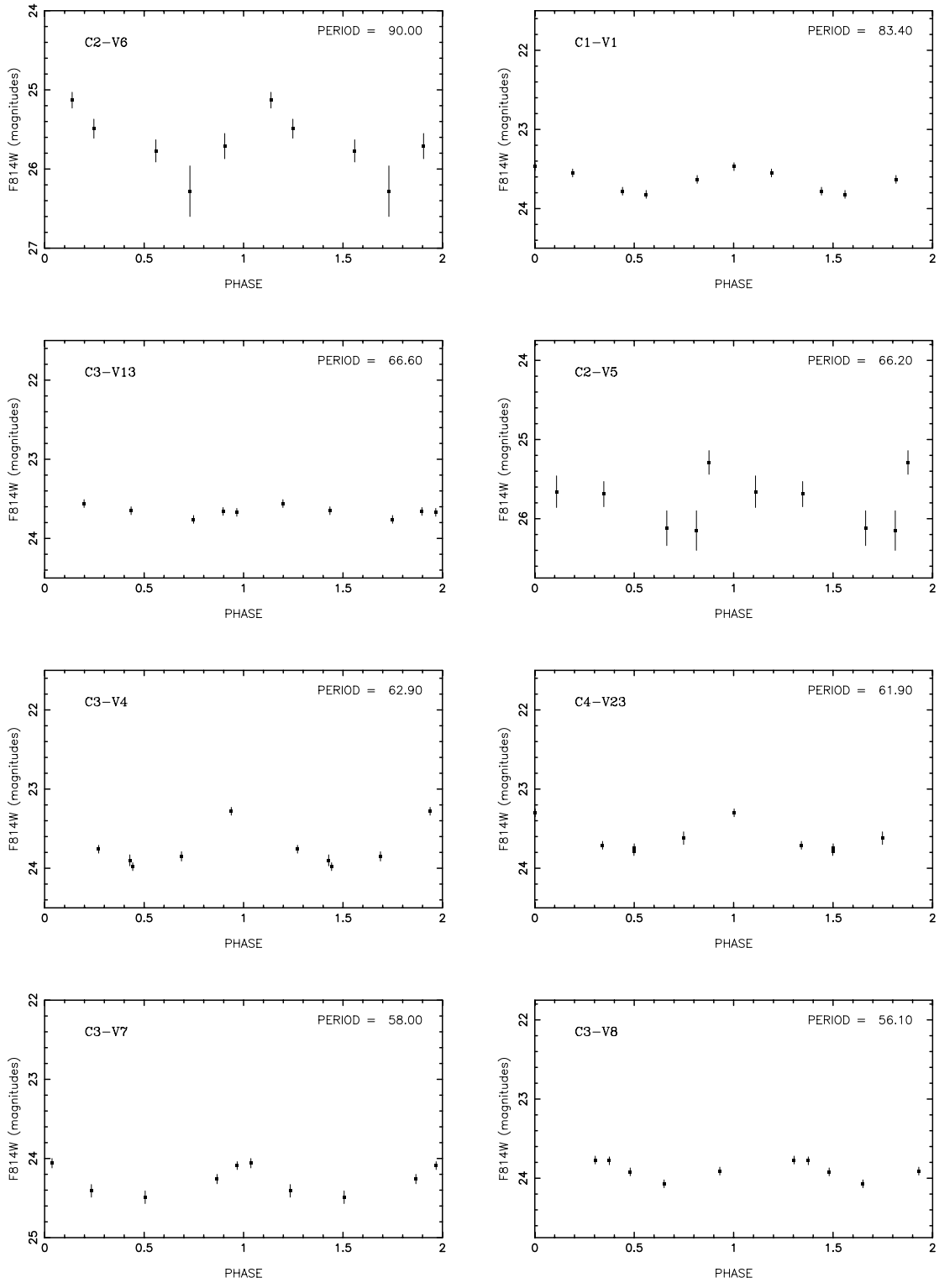

FIG. 5.—Same as Fig. 4, but for the F814W passband, adopting the periods and the phasing used in Fig. 4

Consider now the sample of Cepheids with $20 < P < 65$ days and QI ≥ 3 and including only those objects from chip 4 that lie on the right-hand half, away from the crowded regions ($x > 400$). This sample of 19 Cepheids includes four from chip 4, and yields a true modulus $(m - M)_0 = 30.55 \pm 0.10$ using an unweighted average, and $(m - M)_0 = 30.57 \pm 0.11$ when weighted by the inverse variance. The apparent (unweighted) distance modulus in V for this sample of Cepheids is $(m - M)_V = 31.20 \pm 0.08$, and in I we obtain $(m - M)_I = 30.93 \pm 0.07$. This implies an average characteristic reddening of $E(V - I) = 0.27$.

4.4. *The Distance Modulus by Restricting the Data by Color*

We examine the period-color (P-C) relation to identify Cepheids in our sample that lie close to the intrinsic $(\langle V_0 \rangle - \langle I_0 \rangle)$ period relation for unreddened Cepheids. In

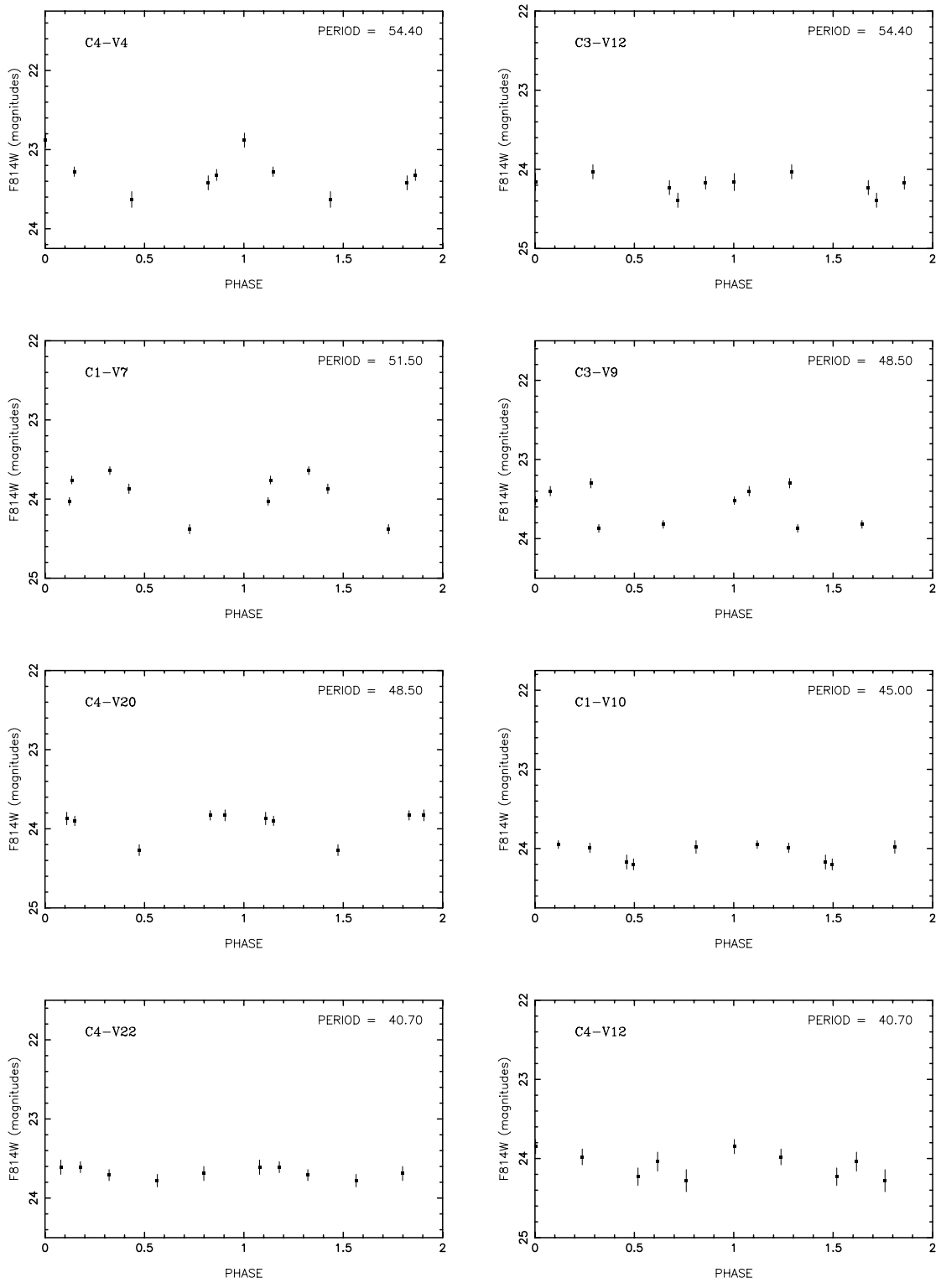

FIG. 5.—*Continued*

Figure 12, the P-C relation for the Cepheids in NGC 4527 are shown. Cepheids with $20 < P < 65$ days and QI ≥ 3 are shown by filled circles. The ridgeline for unreddened Cepheids in the Galaxy, LMC, and SMC as summarized in Sandage, Bell, & Tripicco (1999) from data by Dean, Warren, & Cousins (1978), Caldwell & Coulson (1985), and Fernie (1990) is shown by the dashed line. The P-C relation implied by equations (1) and (2) is shown by the solid line. It is obvious from this figure that hardly any of the Cepheids observed in NGC 4527 are unreddened. The overall trend in the data has a steeper slope with period than the intrinsic P-C relation, since the longest period objects are probably the most strongly reddened, or because they lie in the supercrowded regions of chip 4. Note that selecting by color does *not* introduce an a priori bias in the distance determination (although one must never use such a sample to estimate reddening).

When looking at Cepheids in a disk, we expect to see

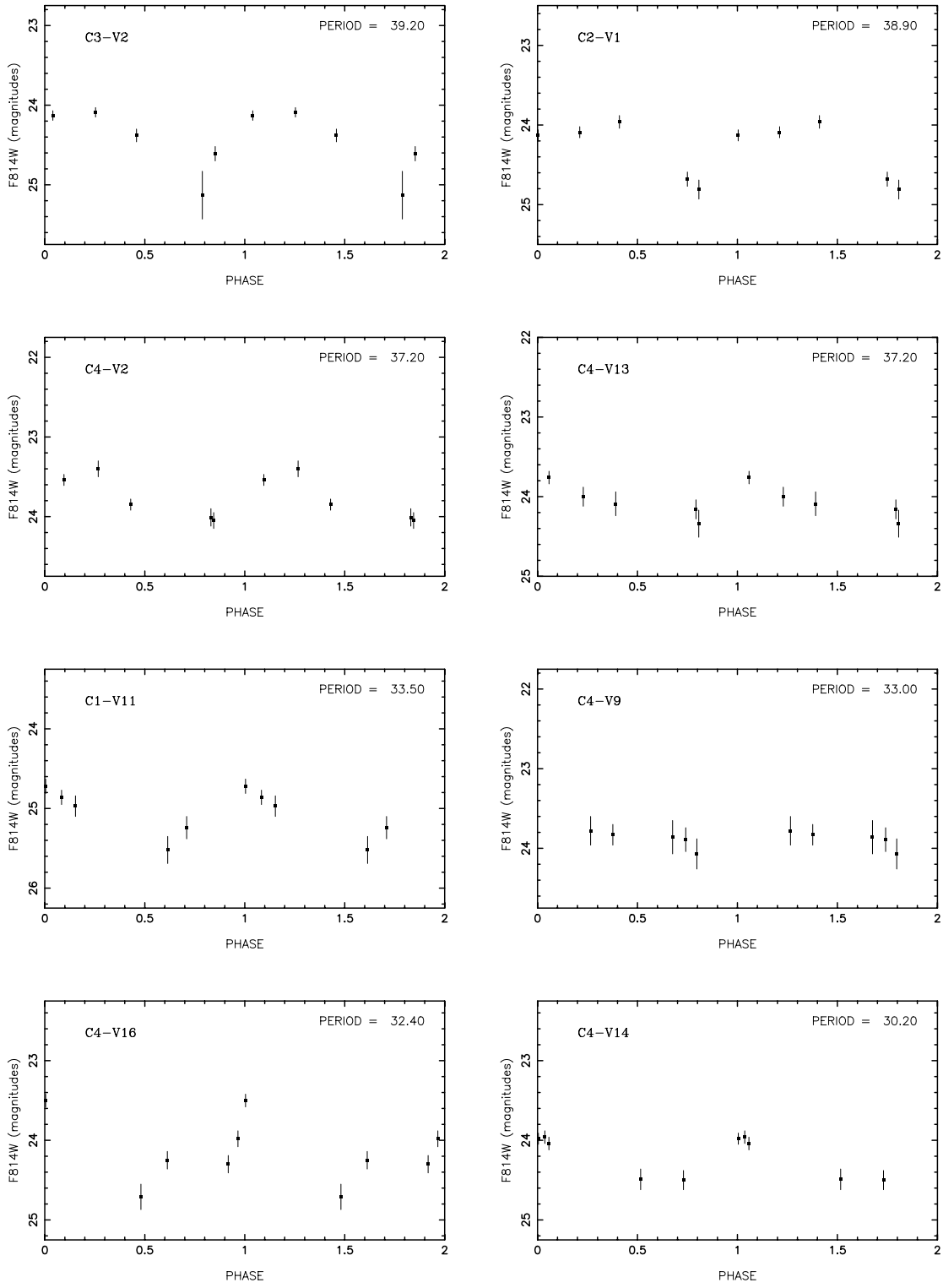

FIG. 5.—*Continued*

ones that are reddened very little because they are on the near side of the dust sheet in the disk, and also those that are reddened substantially, since they are seen through the disk and possibly through dust lanes. The rationale for a color cut is that while bona fide extinction should not affect the dereddened distance modulus irrespective of how the data are cut in color, photometric errors and stars misclassified as Cepheids, which do affect the modulus, can be identified and rejected. A plot of U_T versus apparent color (not shown) for the data at hand easily demonstrates that the derived distance is a strong function of the measured color, showing again that the data are dominated by measurement errors.

One way to proceed is to try various cuts by color, and choose the one(s) that produce the P-L relations with the least scatter in both passbands. Following such a path, we were able to identify two cuts that result in P-L relations without significant outliers:

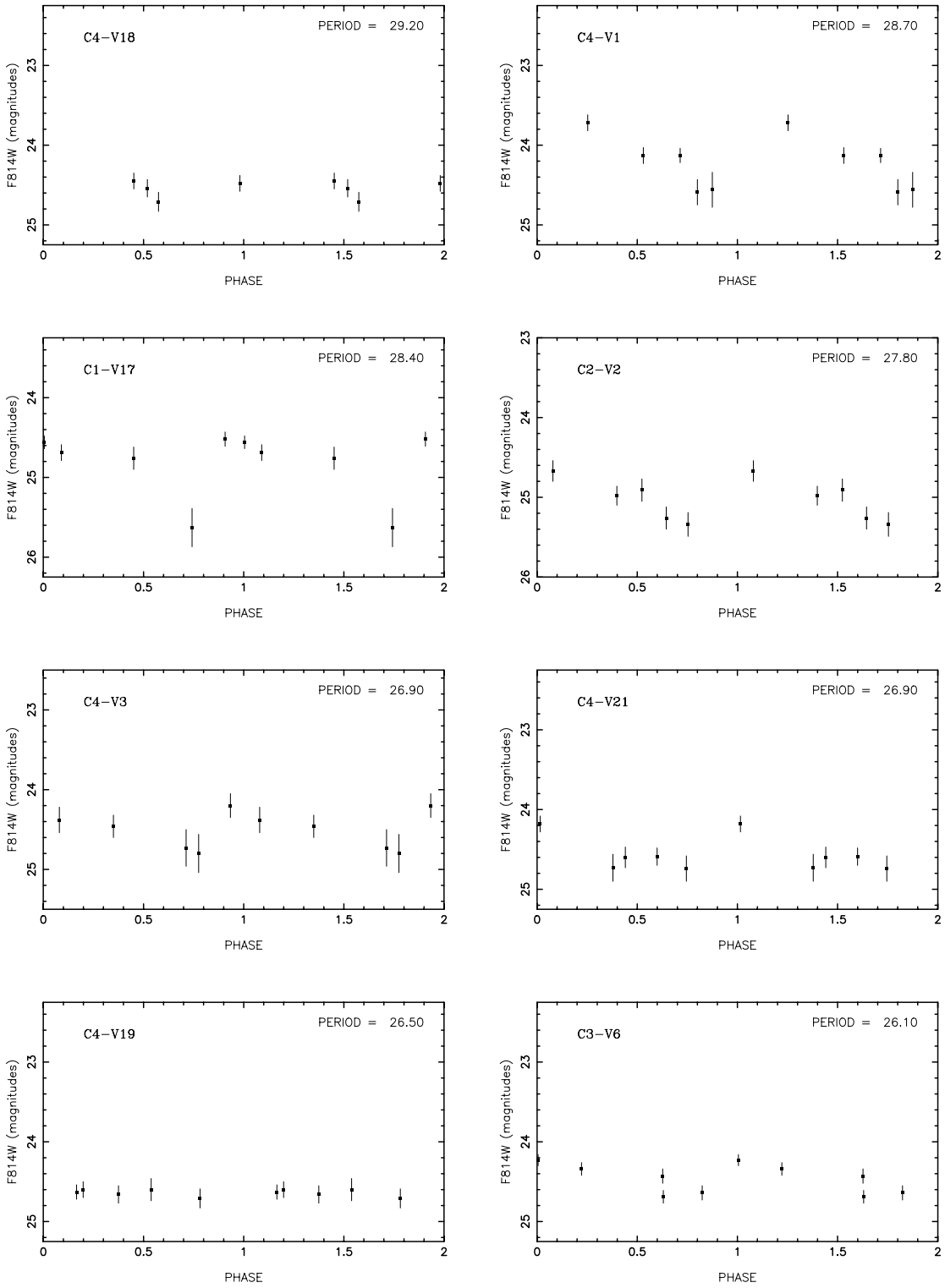

FIG. 5.—*Continued*

1. A cut containing Cepheids bluer than $(V - I) = 1.2$ but also with $(V - I) \geq 0.7$ to remove blue outliers. Objects within the cut appear to follow the slope of the fiducial P-C relation, whereas objects that appear redder follow an anomalously steeper slope. In any case, these are the Cepheids that appear to have minimal reddening. Further restricting the data to include only Cepheids for which $20 < P < 65$ days and QI ≥ 3, to avoid the selection effect at the shortest periods (Sandage 1988), we obtain a weighted average from 16 objects of $\mu_0 = 30.69 \pm 0.11$, and an unweighted average of $\mu_0 = 30.69 \pm 0.09$. The apparent modulus in V from the same sample of Cepheids is $\mu_V = 31.08 \pm 0.05$, which is expected to be biased toward brighter than average because of the color selection.

2. A better cut is one that runs parallel to the fiducial P-C relation, as shown by the dotted lines in Figure 12, drawn 0.2 mag below and 0.3 mag above the mean relation for unreddened Cepheids. The 13 Cepheids included yield

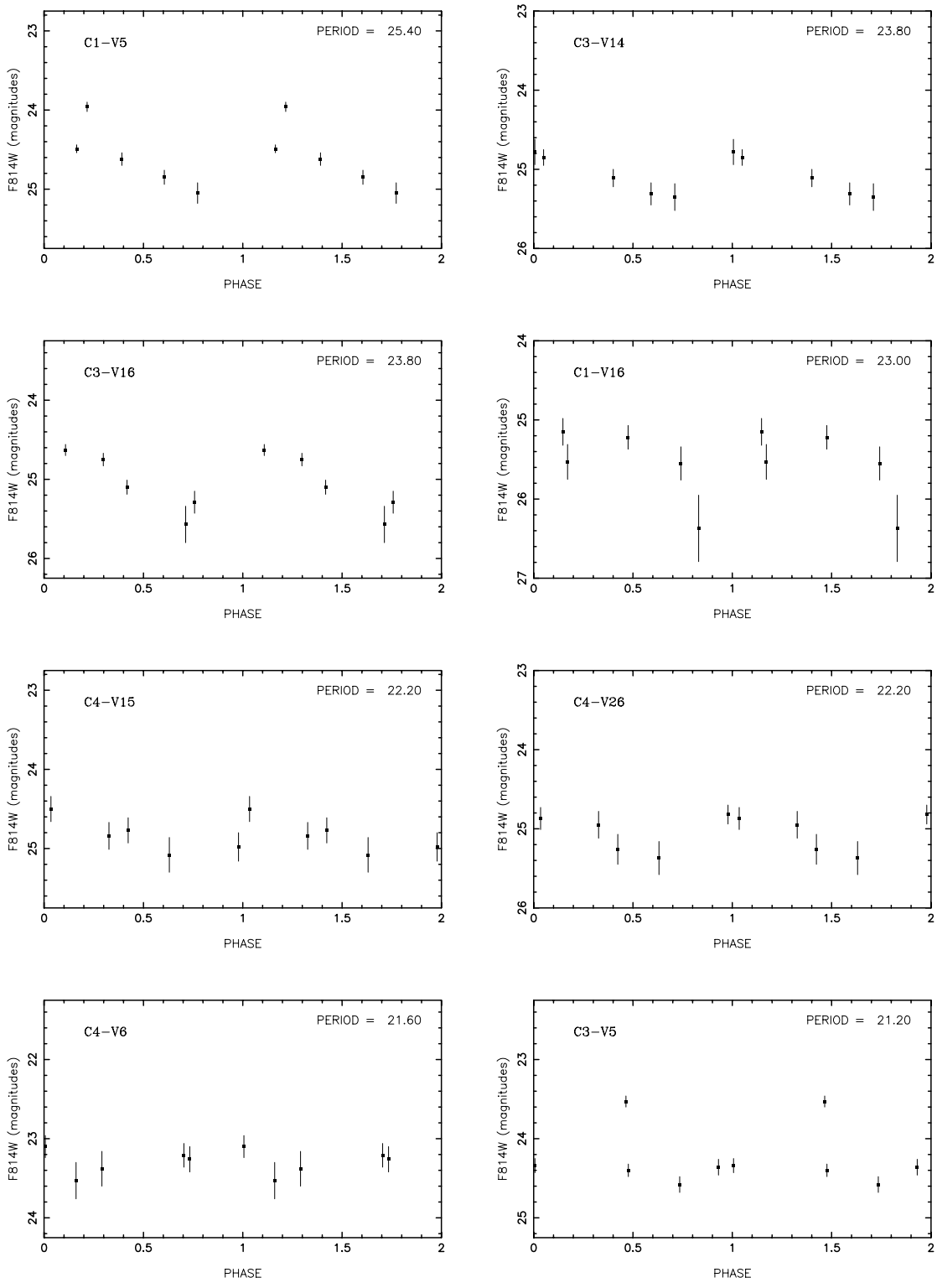

FIG. 5.—*Continued*

$\mu_0 = 30.64 \pm 0.12$ (weighted) and $\mu_0 = 30.66 \pm 0.07$ (unweighted). The V modulus for this sample yields $\mu_V = 31.05 \pm 0.05$, which again is expected to be biased toward brighter than average, since we have selected the least reddened Cepheids.

Moving these cuts redward by even 0.2 mag begins to admit outliers into the resulting P-L relations.

4.5. *The Adopted Distance Modulus*

We have detailed two independent ways of selecting the Cepheids with more reliable photometry, given that there is an obvious difficulty with the magnitudes in the very crowded regions. One method selected objects by spatial position, away from the very crowded and high surface brightness regions, which are also crossed by dust lanes.

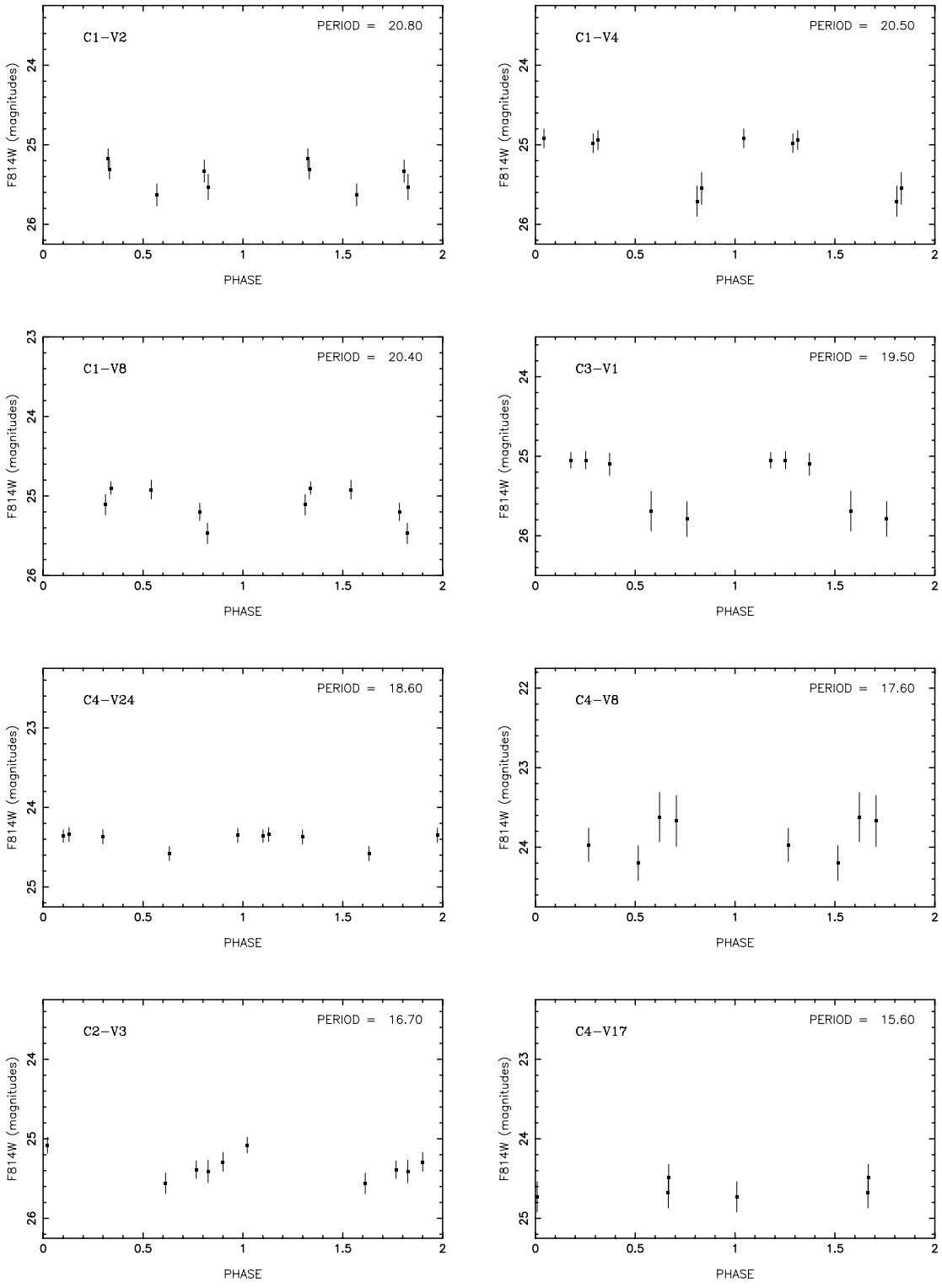

FIG. 5.—*Continued*

The other uses color as a diagnostic, on the premise that while rejecting an otherwise well-measured but very reddened Cepheid does not introduce a systematic bias, objects that have extreme colors often appear so due to noise, and not because they are in fact reddened. These independent approaches yield very similar samples of Cepheids, and the dereddened modulus ranges from 30.55 to 30.68, with characteristic internal rms uncertainties of the order of 0.12 mag, which is comparable to the case-to-case scatter.

Recall that one must add 0.05 mag to bring the values into par with the "long versus short" corrections applied in previous papers of this series; since this applies equally to both passbands, it applies directly to the dereddened modulus also. Including this adjustment, it is reasonable to adopt the central value of the range, and carry forward the case-to-case scatter, which is also the internal rms scatter for each case, as a conservative error estimate:

$$(m - M)_0 = \mu_0 = 30.67 \pm 0.12 \pm 0.12 \, . \qquad (7)$$

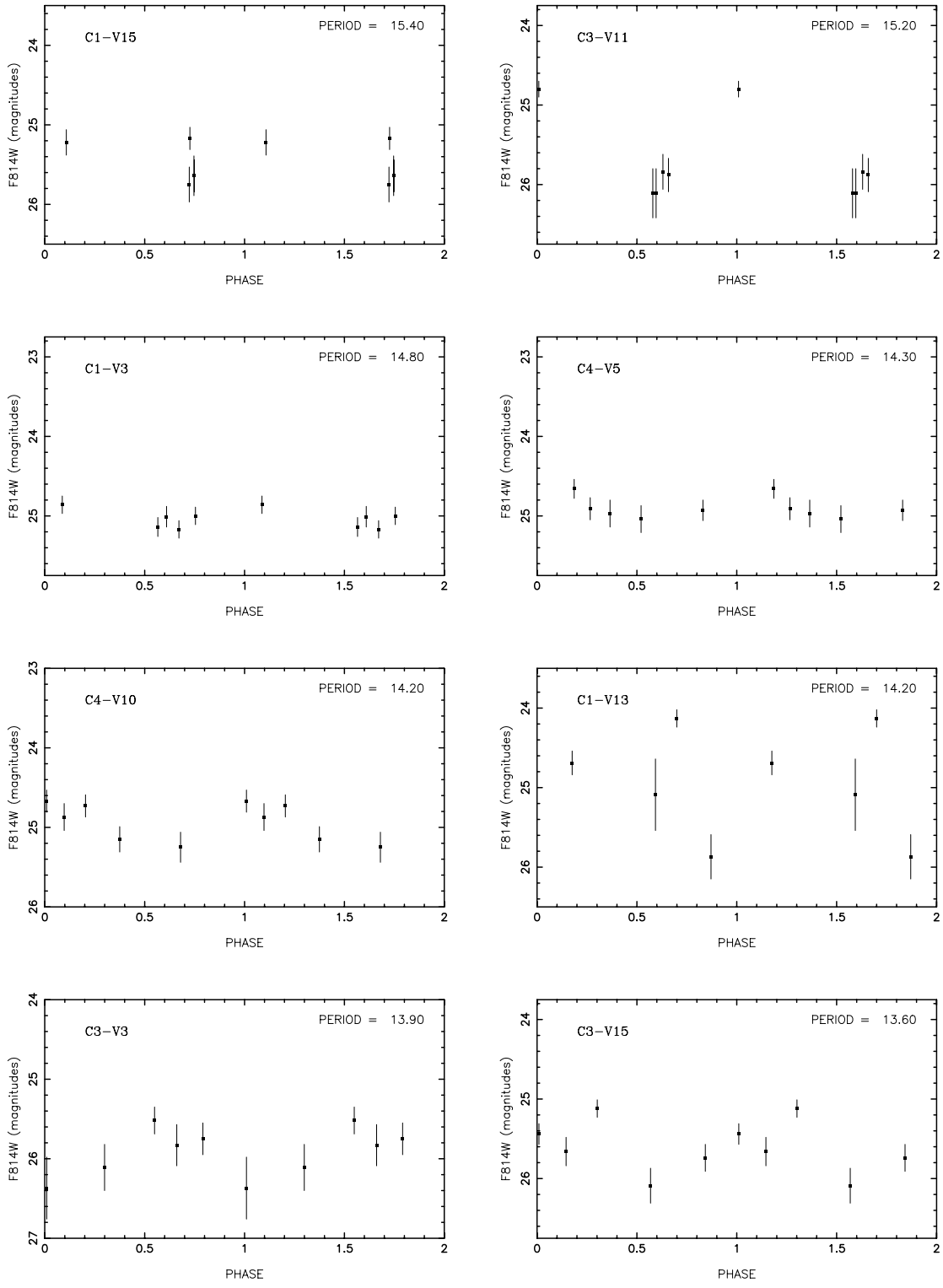

FIG. 5.—*Continued*

From the best case for the V-band apparent modulus, using the unweighted averages of the samples with period and quality cuts only (i.e., no color cut), and propagating the uncertainties from the internal scatter,

$$(m - M)_V = \mu_V = 31.26 \pm 0.08 \, . \tag{8}$$

From a similar consideration of the V- and I-band apparent moduli (but disregarding the case of the color cut which biases the colors), we get a characteristic average reddening for the Cepheids of

$$E(V - I)_{\text{Cepheids}} = \mu_V - \mu_I = 0.26 \pm 0.05 \, , \tag{9}$$

where an additional systematic calibration uncertainty of 0.05 mag should be added in quadrature.

Figure 13 shows the P-L relations in V and I again, but this time with the lines showing the above adopted moduli,

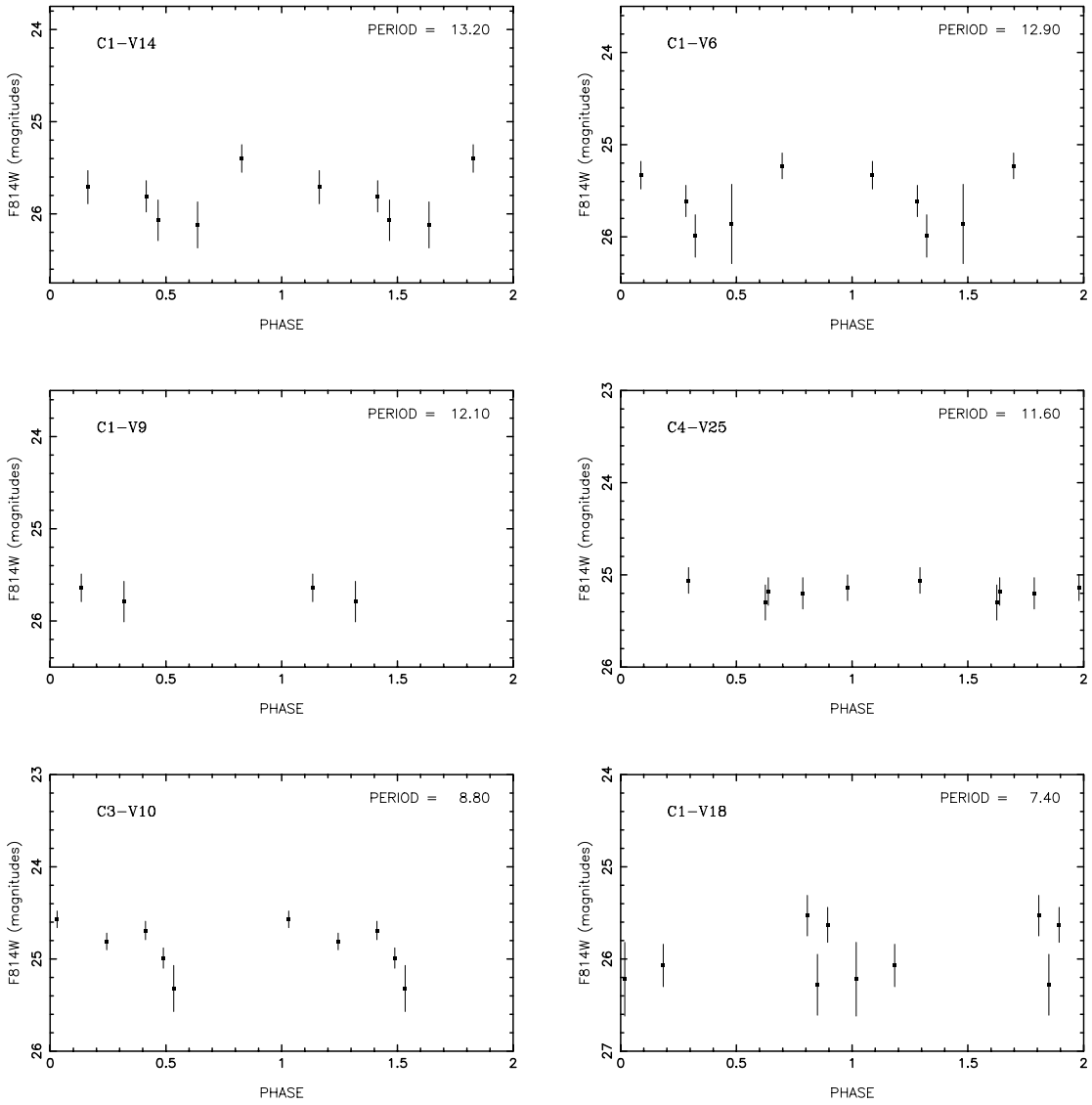

FIG. 5.—*Continued*

and with filled circles showing the sample that has QI ≥ 3, $20 \leq P \leq 65$ days, and where Cepheids in chip 4 are included only if they have positions with $X \geq 400$.

5. ROMAFOT PHOTOMETRY

5.1. *Motivation*

The uncertainty in the photometry of Cepheids from data like those at hand is dominated by both effects of crowding and object confusion, as well as by the difficulty of measuring reliable aperture magnitudes for at least a few stars in the field of view of each CCD chip. Independent determination of aperture magnitudes for a given chip using only the Cepheid data (typically no suitable bright isolated but unsaturated stars exist in these fields) results in aperture corrections with scatter of the order of 0.2 mag. Fortunately, the WFPC2 point-spread functions (PSFs) are stable, and the aperture corrections can be "imported" by different means. The method by which our DoPHOT-based procedure does this was described in Paper V, with an augmentation described in Paper IX. Nevertheless, the possibility of systematic errors in the method cannot be ruled out, particularly as a result of possible long-term drifts in the optics and instrument. Different crowded-field programs, with their different approaches to handling object confusion, will produce somewhat different results. Comparing such results produces a more realistic handle on the true systematics. This was the underlying reason for repeating the data reduction in § 4 using the ROMAFOT (Buonanno et al. 1983) package, which was developed for crowded fields. Because the ROMAFOT path provides an independent evaluation of the photometry, including the aperture correction, we averaged the results of both paths rather than using the ROMAFOT results as a rough confirmation of the DoPHOT results.

Note that because of differences in approach between the two methods, including different sets of Cepheids and quality indices, the postphotometry analysis cannot always be done identically. The methods best suited to the strengths and limitations of ROMAFOT are used; the final comparison, however, should reflect realistic systematic errors, albeit to the extent possible by comparing only two paths.

5.2. *Photometric Reductions with ROMAFOT*

All observations were preprocessed by the standard pipeline as described by Holtzman et al. (1995b). The back-to-

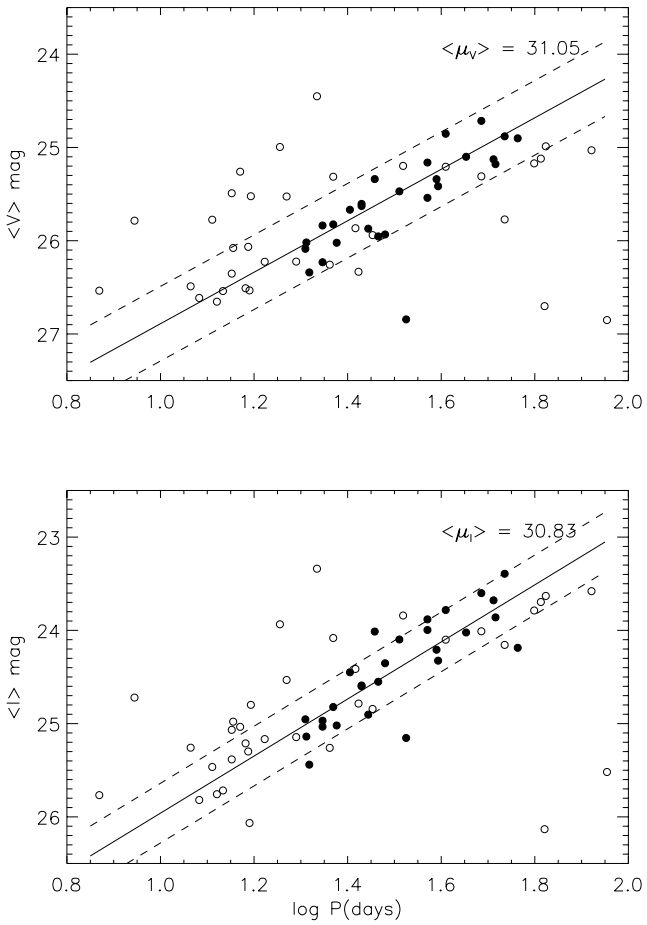

FIG. 6.—Apparent P-L relations V and I, showing all the Cepheid data in Table 4. The filled circles show Cepheids with $65 > P > 20$ days with quality index (QI) of 3 or better. Open circles show the remainder of the variables in Table 4. The solid lines show the adopted P-L relations from Madore & Freedman (1991) in eqs. (1) and (2), used also in the previous papers of this series. The ridgelines have been put arbitrarily at a modulus of $(m - M)_V = 31.05$ and $(m - M)_I = 30.83$ as a first estimate, before analysis of differential extinction. The dashed upper and lower parallel lines indicate the expected projection of the width of the instability strip. The heavy spillage of points outside these bounds indicates the presence of large differential extinction or noise or both.

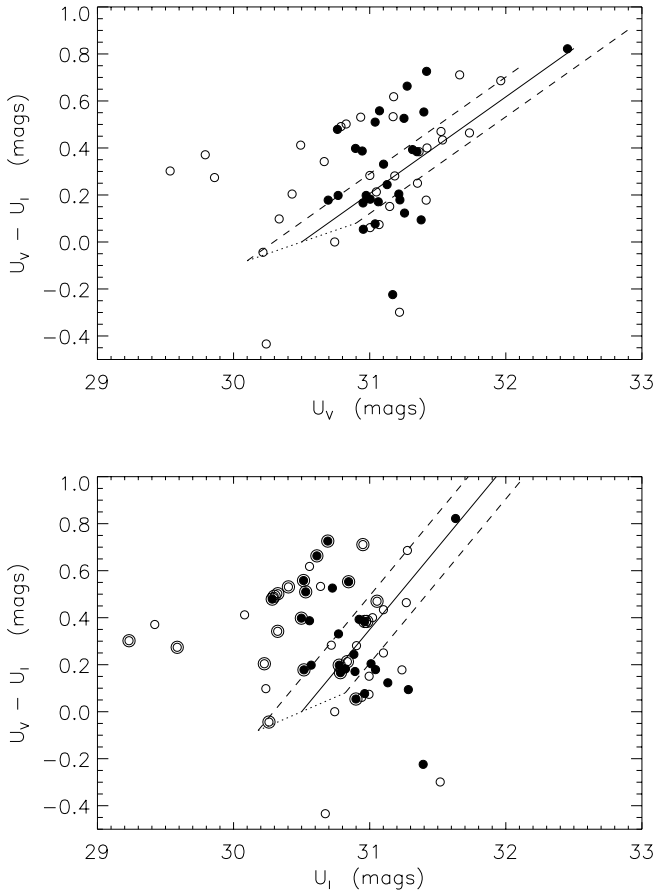

FIG. 7.—Diagnostic diagram for the detection of differential reddening, described in the text. Top panel shows the V-modulus on the abscissa. Bottom panel shows the same figure, but with the I-modulus on the abscissa. In addition, in the bottom panel objects from chip 4 are marked by a concentric outer circle.

back exposures were then coadded by an anticoincidence technique in order to remove cosmic-ray hits (Paper V).

The coadded exposures were aligned to within the nearest whole pixel before the exposures were coadded again to create a deep frame in each color. All 12 epochs in F555W and all five epochs in F814W were used to create the deep images in order to get a better signal-to-noise ratio. The PSFs for each epoch and filter and for the deep frames were determined empirically from the coadded frames; mean PSFs were established with the observed data set, not with external data. This underlying philosophy implies the use of stars that cover the whole chip if possible, in order to account for the spatially varying PSF of WFPC2. Only relatively bright and isolated objects were used to create the different PSFs. For this purpose, ROMAFOT was run in a mode in which the shape parameter of the Moffat function was allowed to vary. Empirical tests have shown that a Moffat function fits the shape of the PSF better than a Gaussian function. ROMAFOT does not discriminate between stars, remaining cosmic rays, and galaxies; therefore, badly fitted objects were deleted from this sample after examination of the observed and the fitted shape of each object.

The appropriate PSF was fitted to the deep frame, separately in V and I. Objects brighter than a certain limit

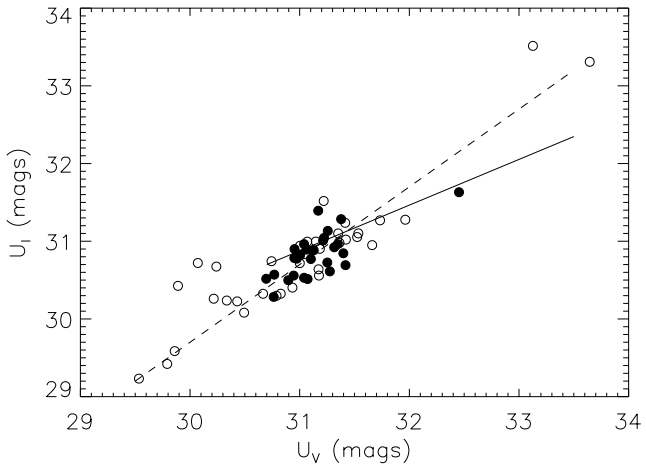

FIG. 8.—Diagram showing the I modulus of individual Cepheids plotted against the V modulus. Filled circles show Cepheids with periods between 20 and 60 days, and QI of 3 or higher. The solid line shows the reddening vector, and the dashed line shows the slope suggested by the data, indicating that the spread in modulus values is not dominated by differential reddening, but is due to additional correlated errors in photometry.

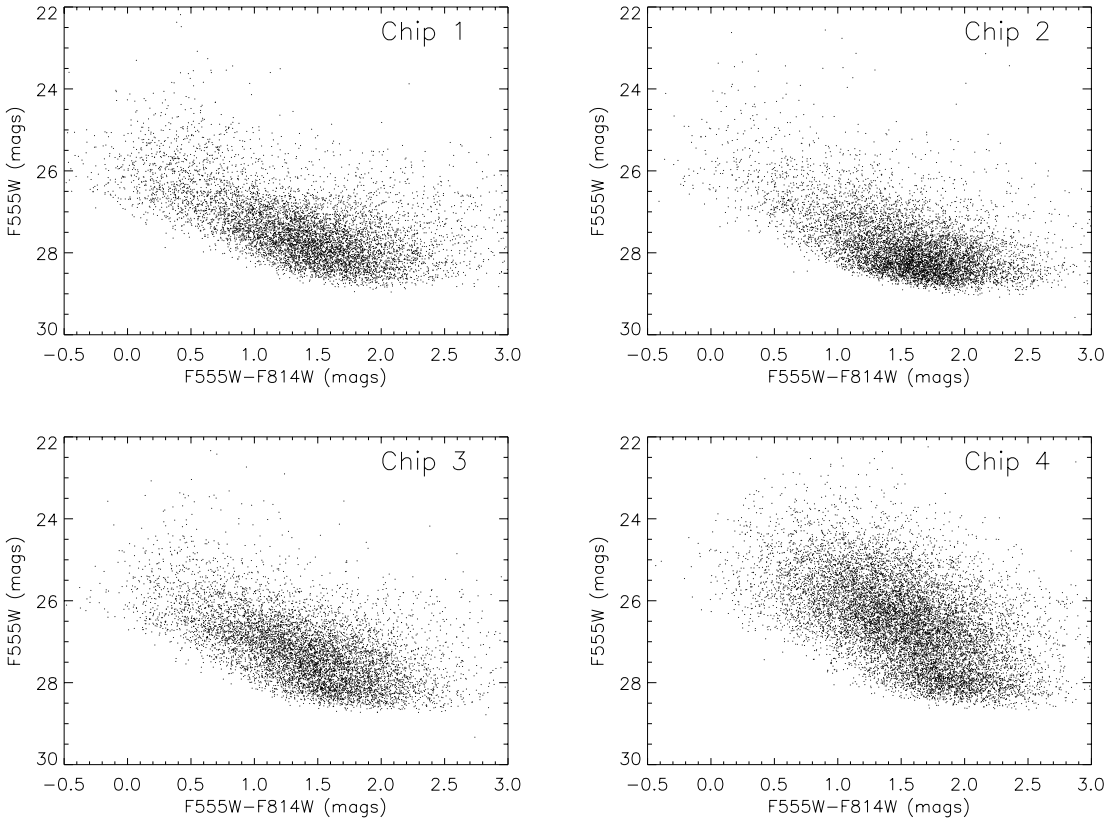

FIG. 9.—Color-magnitude diagrams shown separately for the four different chips. Note the abnormal appearance of the panel from chip 4, indicating problems with the photometry (see text).

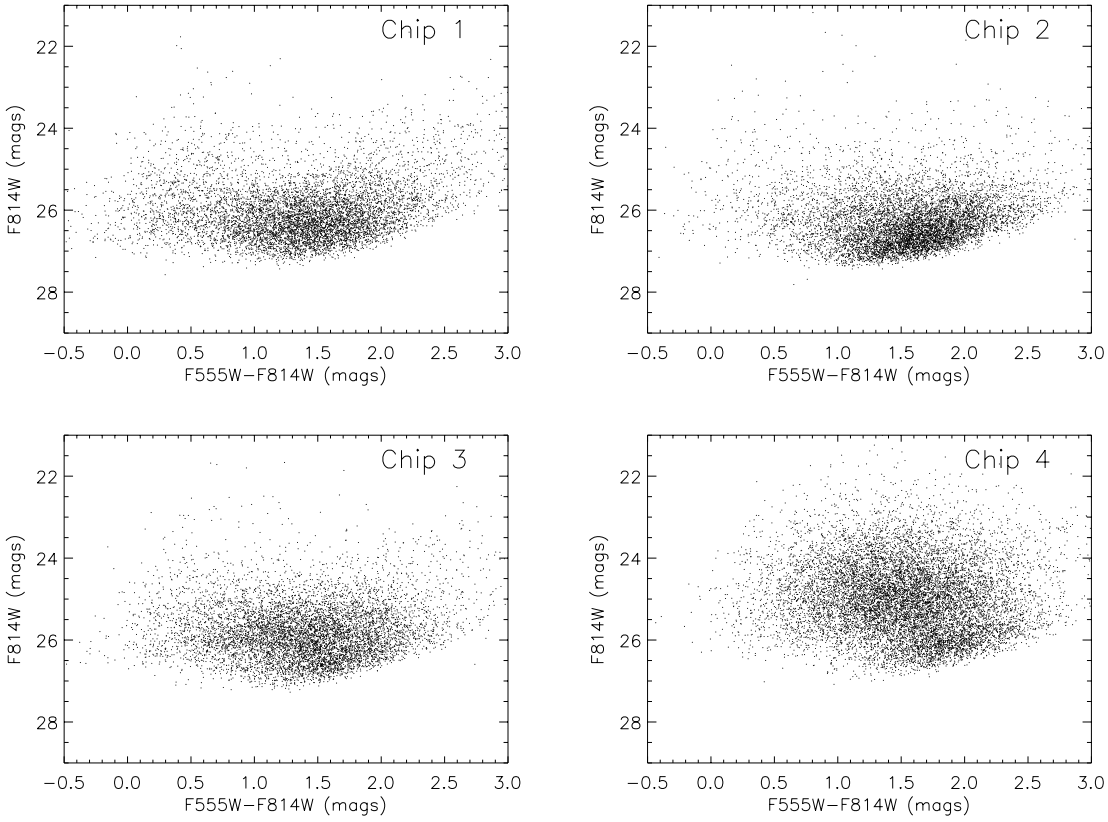

FIG. 10.—Same as Fig. 9, but with F814W magnitudes as the ordinate

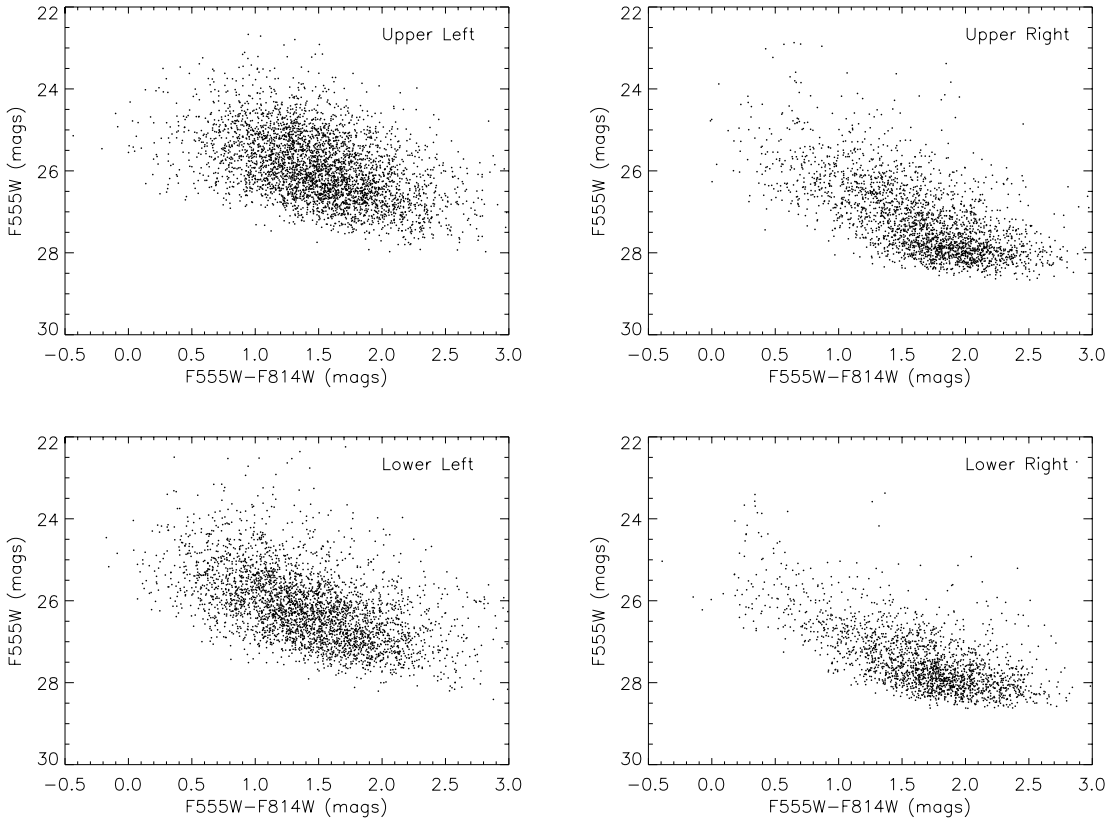

FIG. 11.—Color-magnitude diagram shown for the regions in the different quadrants for the field in chip 4 only. Note that the abnormal appearance is in the two left-hand quadrants, where the surface brightness, dust-lane appearance, and crowding are most pronounced. The CMD from the sparser right-hand section of the chip 4 field shows no abnormality.

were selected and subtracted from the deep frame. These objects are used as a master list for every single epoch. The positions at different epochs are slightly different from those of the deep frame. The corresponding offsets have been calculated using a matching algorithm and are added for every epoch.

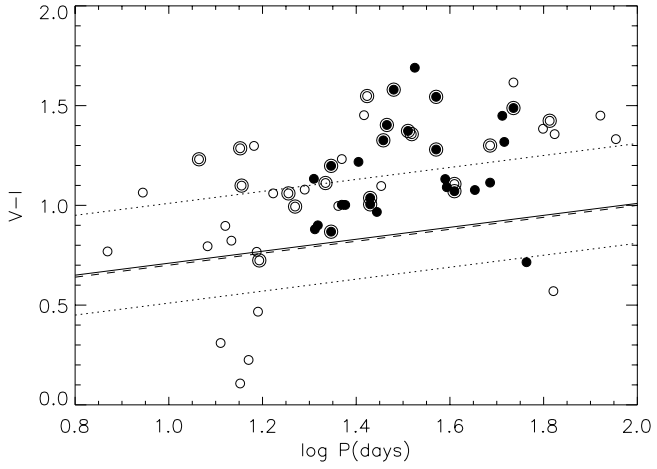

FIG. 12.—Period-color relation for the Cepheids in NGC 4527. The filled circles show Cepheids with $60 > P > 20$ days with quality index QI of 3 or better. Objects on chip 4 are shown with a concentric outer circle. Note again how many of the chip 4 objects show up as outliers. The solid and dashed lines show the fiducial mean P-C relations (from two different sources; see text). Since most of the points are redder than the fiducial relation, there is clearly reddening present. The dotted lines show the color cut made (see text), which runs parallel to the fiducial P-C relation.

The objects were then fitted on the individual frames with the corresponding PSF and subsequently subtracted from them. The procedure was repeated on the residual frames several times in an iterative process cutting at fainter and fainter limits. The results are files giving instrumental magnitudes in V and I for the deep frames and the individual frames, each containing more than 10,000 stars for each chip and filter.

5.3. *Identification of the Variable Stars*

The identification of the variable stars is again based on the method described by Saha & Hoessel (1990). The quantities Θ and the standard deviation σ of the instrumental magnitudes over all epochs in F555W were used to identify the variable candidates. Here we have used $\Theta_{\rm min}$, i.e., the lowest smoothed value, obtained by varying the period between 1 and 90 days. Several hundred stars were suspected to be variable on the basis of ROMAFOT photometry. The light curves of these possible candidates with reasonable values of Θ and σ were individually inspected by eye, and 64 Cepheid candidates were retained that were also selected by DoPHOT. They are listed in Table 5. Column (1) gives the designation of the probable Cepheid, columns (2)–(4) give the DoPHOT mean magnitudes in V and I and the quality class, and columns (5)–(7) give the ROMAFOT mean magnitudes (as derived below) and the quality index (QI) of the Cepheids. The QI's were estimated similarly as in § 3, but independently and based on ROMAFOT alone.

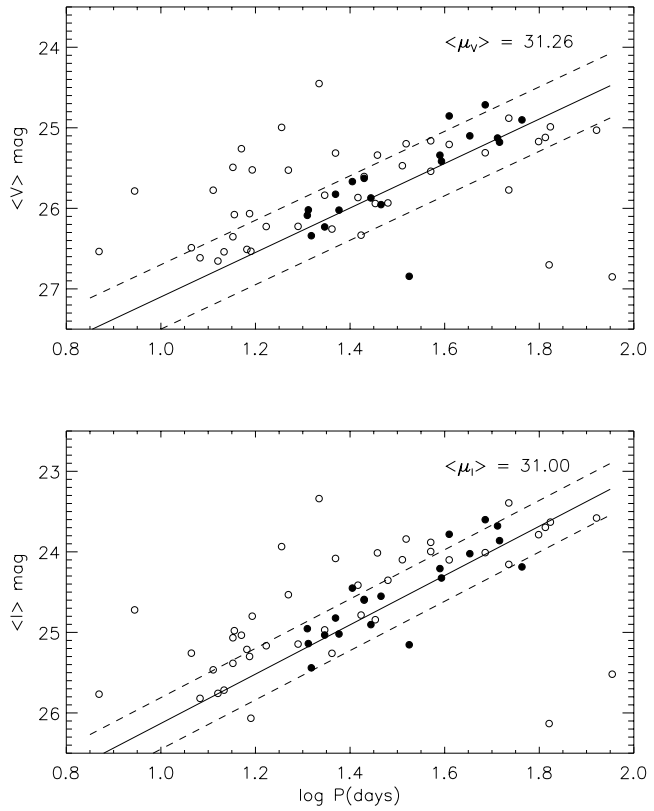

FIG. 13.—P-L relation showing all Cepheids as in Fig. 6, but filled circles now show only those objects with derived periods between 20 and 65 days, quality index 3 or higher, and only those objects on chip 4 that lie on the half of the chip where $X > 400$. The lines show canonical P-L relations corresponding to the final adopted DoPHOT distance moduli.

From the ROMAFOT photometry, 37 Cepheids were judged to be useful (QI $\geq$ 3), 26 of which are among the Cepheids that have been used for the derivation of the distance modulus in § 5.6.

5.4. *Transformation of Instrumental to Standard Magnitudes*

The phase-weighted mean ⟨F555W⟩ and ⟨F814W⟩ magnitudes have been converted to Johnson V and Cousins I using the equations given by Holtzman et al. (1995b). In particular, the ROMAFOT instrumental magnitudes were transformed in a recursive manner. Instead of the unknown standard colors, first the flight colors and then the ground colors were transformed.

The main problem is to tie the fitted magnitudes to the instrumental magnitudes using an aperture of 0.″5 radius, the so-called aperture correction (AC). This is because the transformations given by Holtzman et al. (1995b) refer to a circular aperture of 0.″5 radius. The AC is the correction from the model PSF to the circular aperture, and its value strongly depends on the chosen sky values. The value of the AC should be evaluated in principle from the NGC 4527 frames for each chip, filter, and epoch separately.

Because of the lack of bright isolated stars with constant background on NGC 4527 frames, the values for the aperture correction have also been calculated with the globular clusters Pal 4 (*HST* Archive data, proposal 5672, PI: J. Hesser) and G319 in M31 (*HST* Archive data, proposal 6671, PI: R. M. Rich). The latter was observed in 1999 and lies closest to the date of the present observations. All observations were "long" observations, having exposure times of

TABLE 5

DoPHOT and ROMAFOT Mean Magnitudes in V and I of 66 Cepheid Candidates

	DoPHOT			ROMAFOT		
Variable ID (1)	⟨V⟩ (2)	⟨I⟩ (3)	Quality Index (4)	⟨V⟩ (5)	⟨I⟩ (6)	Quality Index (7)
C1-V1	25.080	23.630	3	25.17	23.69	3
C1-V2	26.390	25.490	3	26.49	25.58	4
C1-V3	25.310	25.085	3	25.44	25.34	1
C1-V4	26.069	25.189	5	26.38	25.42	4
C1-V5	25.718	24.500	5	25.81	24.67	4
C1-V6	25.825	25.515	3	26.05	25.63	2
C1-V7	25.177	23.728	3	25.23	24.14	4
C1-V8	26.137	25.004	4	26.05	25.18	2
C1-V9	26.664	25.869	1	27.19	25.99	2
C1-V10...	25.150	24.073	3	25.23	24.08	4
C1-V11...	26.894	25.204	5	26.76	25.06	5
C1-V12...	25.74	...	...	25.45	24.24	2
C1-V13...	25.541	25.434	3	25.03	24.57	2
C1-V14...	26.704	25.807	4	26.81	25.87	2
C1-V15...	26.116	25.349	3	26.50	25.73	3
C1-V16...	26.307	25.310	2	26.45	25.43	2
C1-V17...	25.990	24.893	2	26.20	25.07	4
C1-V18...	26.586	25.817	3	26.66	26.12	2
C2-V1	25.390	24.258	3	25.47	24.32	4
C2-V2	25.921	24.954	5	26.00	25.15	4
C2-V3	26.276	25.216	3	26.27	25.41	3
C2-V4	26.88	...	...	27.26	...	...
C2-V5	26.752	26.182	4	26.96	25.94	2
C2-V6	26.901	25.569	5	27.03	25.81	5
C3-V1	26.274	25.195	5	26.45	25.58	5
C3-V2	25.466	24.375	5	25.65	24.56	5
C3-V3	26.583	26.116	1	26.77	26.27	1
C3-V4	25.221	23.837	2	25.32	23.76	3
C3-V5	25.364	24.132	1	25.57	24.09	1
C3-V6	25.916	24.464	2	25.97	24.72	3
C3-V7	24.952	24.237	3	25.01	24.51	2
C3-V8	25.229	23.911	3	25.30	24.02	4
C3-V9	24.765	23.651	3	24.80	23.80	4
C3-V10...	25.835	24.771	1	25.78	24.91	1
C3-V11...	26.560	25.262	4	26.50	25.51	2
C3-V12...	25.822	24.206	2	26.06	24.28	3
C3-V13...	25.038	23.681	2	25.16	23.80	3
C3-V14...	26.072	25.070	4	26.17	25.15	4
C3-V15...	26.590	25.767	4	26.77	25.82	4
C3-V16...	25.875	24.872	4	26.03	25.16	5
C4-V1	25.389	24.063	4	25.34	24.11	4
C4-V2	25.212	23.932	3	25.03	23.87	1
C4-V3	25.655	24.650	5	26.17	25.62	2
C4-V4	24.931	23.443	4	...	...	...
C4-V5	26.128	25.029	3	25.97	24.64	2
C4-V6	24.501	23.389	1	24.43	23.20	3
C4-V7	26.70	...	...	...	...	...
C4-V8	25.045	23.985	1	25.43	...	...
C4-V9	25.248	23.891	2	25.49	24.56	3
C4-V10...	26.403	25.117	5	26.07	25.22	1
C4-V11...	26.03	...	...	25.67	23.91	2
C4-V12...	25.257	24.150	2	25.27	24.78	4
C4-V13...	25.590	24.046	5	25.65	25.09	5
C4-V14...	25.983	24.403	5	26.09	24.63	5
C4-V15...	25.887	25.019	3	26.04	24.98	3
C4-V16...	25.521	24.148	3	25.26	23.97	3
C4-V17...	25.573	24.849	2	25.53	...	...
C4-V18...	26.004	24.601	3	25.85	24.52	2
C4-V19...	26.383	24.835	2	26.55	24.88	2
C4-V20...	25.360	24.060	2	25.23	24.09	4
C4-V21...	25.678	24.641	4	25.97	24.87	4
C4-V22...	24.903	23.832	3	24.97	24.11	4
C4-V23...	25.170	23.746	2	25.19	23.73	5
C4-V24...	25.576	24.582	2	25.55	24.71	3
C4-V25...	26.539	25.308	3	26.59	25.55	2
C4-V26...	26.281	25.083	4	26.39	25.67	4

NOTE.—All values are on long exposure scale.

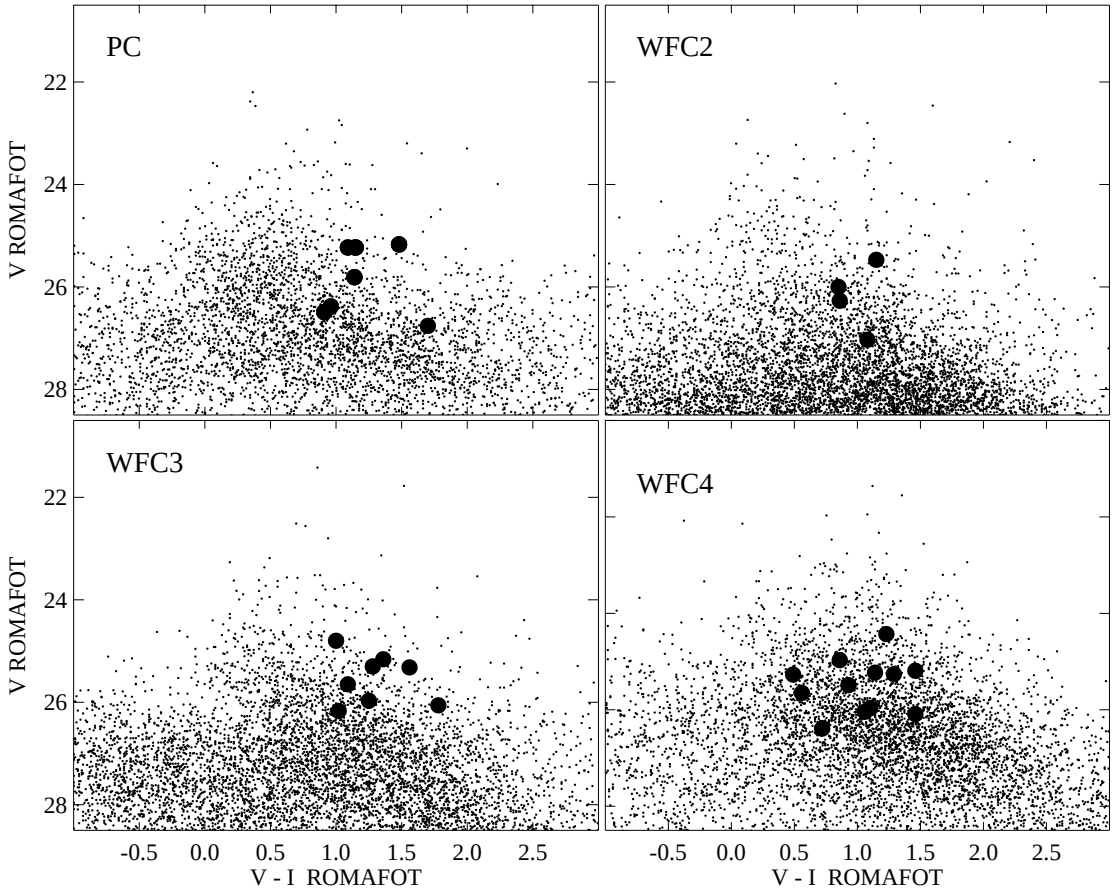

FIG. 14.—Color-magnitude diagram $V-I$ vs. V obtained with ROMAFOT photometry. Cepheids are indicated by filled circles.

more than 1000 s. Because of crowding, blends, and varying background values, proper calculation of the AC is much more difficult than establishing a PSF; furthermore, external archive data were useful in calculating systematic errors. Both globular clusters have many isolated, bright, but not saturated stars with a flat sky. In first approximation, the growth curves of stars in the galaxy frames and the globular cluster frames are expected to be the same, but jitter and focus changes and aging effects of the CCD do affect the inner core of the PSF.

Since the determination of the sky is crucial, the local sky was allowed to vary until the growth curves were flat. Only stars with flat growth curves were considered; stars with rising or falling growth curves up to 3″ radius were rejected. No AC dependence with position on the chip, position within one pixel, or level of background were found. However, there is a weak tendency, yet only on the galaxy frames, for stars with broader FWHM to yield higher ACs. The AC determined for the galaxy frames therefore depends somewhat on the selection of the reference stars. We have selected 20–30 reference stars per frame with moderately small scatter.

To first order, the changes in the intrinsic PSF are radial. If using a constant PSF were to produce systematic position-dependent errors in the photometry, they should show up as differences between stars near the center of a chip versus those on the outside areas of the chip. Since ROMAFOT used a constant PSF, such a trend should show up as a systematic position-dependent variation of the AC. An examination of the typical rms star-by-star scatter for the AC in (say) the Pal 4 data is 0.17 mag. This value does not change by more than 0.01 whether one considers the innermost 400 × 400 pixel region or the whole chip. This is an indication that systematic differences in the AC between inner and outer regions is no more than 0.08 mag. Given this state of affairs, it is not possible to evaluate any reliable AC dependence on position from these data. Nevertheless, since the mean computed AC's reflect the average over the entire chip, unless the Cepheids are distributed extremely nonuniformly, this concern can increase the scatter in the Cepheid-to-Cepheid relative moduli, but should not change the mean results from a sample of Cepheids.

The value of the AC from NGC 4527 is slightly larger than from the globular clusters. The choice of the AC therefore has some effect on the distance modulus, which is discussed in more detail in § 5.6.

Finally, the magnitudes were corrected to the "long-exposure" calibration scale by adding 0.05 mag in V and I, as in § 4.5.

The two master lists in V and I were joined to form a set of about 15,000 stars with $V < 28.0$ mag for which V *and* I are known. Their color-magnitude diagrams $V-I$ versus V and I are shown chip by chip in Figures 14 and 15, respectively. Cepheids are indicated by filled circles.

5.5. *ROMAFOT versus DoPHOT Photometry*

For about 10,000 stars V and I magnitudes are available from DoPHOT as well as from ROMAFOT photometry. Their magnitude differences (all magnitudes in this dis-

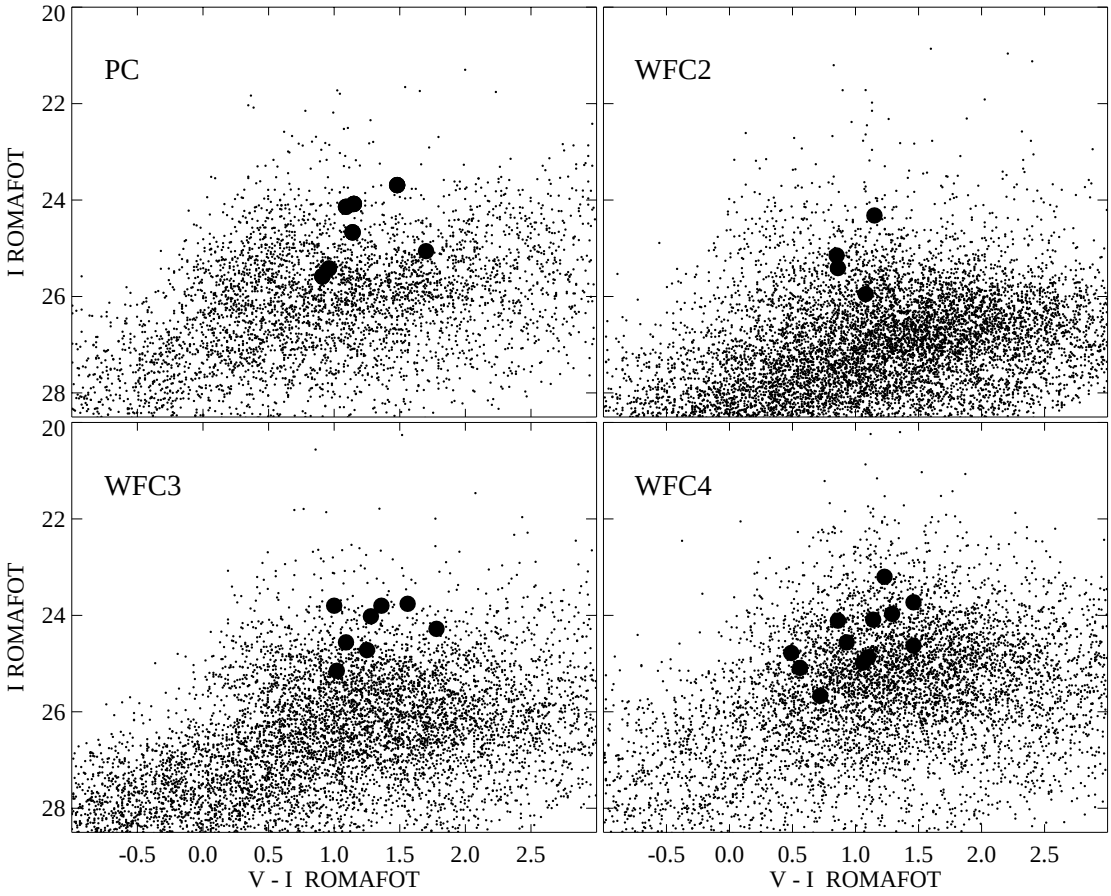

FIG. 15.—Color-magnitude diagram $V-I$ vs. I obtained with ROMAFOT photometry. Cepheids are indicated by filled circles.

cussion, and in Table 5 and later, are on the "long" scale) ΔV and ΔI in the sense ROMAFOT–DoPHOT are plotted versus V(ROMAFOT) and I(ROMAFOT), respectively, in Figure 16. The very strong systematic differences for stars with $V \gtrsim 26$ mag and $I \gtrsim 25$ mag are known also from other comparisons of different photometry programs (Gibson et al. 2000). They are fully explained by mismatches within the matching radius of 0.″5 between objects identified on the V and I frames. As expected, the difficult chip 4 gives the largest scatter. The zero-point offsets as well as the magnitude scatter of the brighter stars are tabulated in Table 6.

For the comparison, ROMAFOT magnitudes have been used that are based on the mean AC of NGC 4527, Pal 4, and G319. The mean differences in Tables 6 and 7, in the sense ROMAPHOT − DoPHOT, would be 0.18 mag more negative in V and 0.14 mag in I if only NGC 4527 had been used for the AC.

A comparison of all 64 F555W and 57 F814W Cepheid candidates in common with differences less than 1 mag in Table 5 is shown in Figure 17. Some magnitude equation is apparent, the brighter Cepheids agreeing better. The mean values for the differences are $\Delta\langle V\rangle$ and $\Delta\langle I\rangle$ of 0.07 ± 0.02 and 0.12 ± 0.03, respectively.

5.6. *The Period-Luminosity Relation and the Distance Modulus*

Out of 66 Cepheid candidates noted by DoPHOT, 64 could also be detected by ROMAFOT and three could not be recovered in F814W. The ROMAFOT candidates, for which both colors could be measured, were assigned quality classes QI similarly as in § 3, but independently and based only on ROMAFOT data. Thirty-seven Cepheids in Table 5 for which both colors could be measured have QI ≥ 3. The diagnostic diagram for the Cepheids from ROMAFOT

TABLE 6

AVERAGE DIFFERENCES BETWEEN THE ROMAFOT AND DoPHOT PHOTOMETRY

	ROMAFOT − DoPHOT			ROMAFOT − DoPHOT		
CHIP	ΔV	σ	NUMBER OF STARS	ΔI	σ	NUMBER OF STARS
1.....	−0.06	0.13	106	−0.06	0.10	143
2.....	−0.03	0.12	73	+0.01	0.12	77
3.....	+0.04	0.11	105	+0.13	0.11	130
4.....	+0.07	0.19	392	+0.13	0.20	428

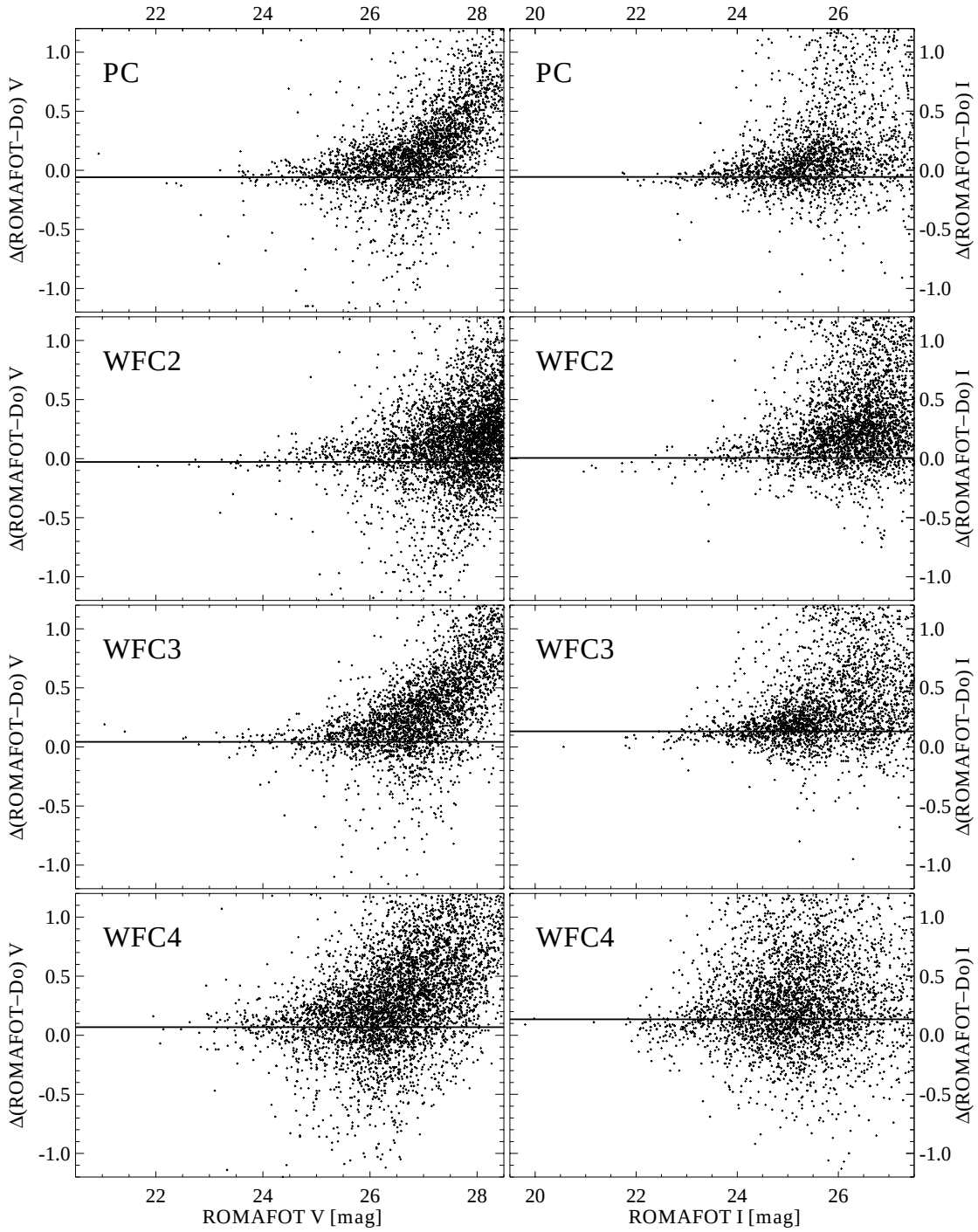

FIG. 16.—Comparison of the ROMAFOT and DoPHOT photometry for all chip and filter combinations. The horizontal line marks the average difference using stars brighter than 25 mag in V and 24 mag in I.

TABLE 7

AVERAGE DIFFERENCES BETWEEN THE ROMAFOT AND DoPHOT CEPHEID CANDIDATES

	ROMAFOT − DoPHOT			ROMAFOT − DoPHOT		
CHIP	ΔV	σ	NUMBER OF STARS	ΔI	σ	NUMBER OF STARS
1.....	+0.08	0.24	18	+0.10	0.28	17
2.....	+0.14	0.13	6	+0.12	0.23	5
3.....	+0.11	0.09	16	+0.15	0.12	16
4.....	+0.02	0.21	24	+0.12	0.28	19

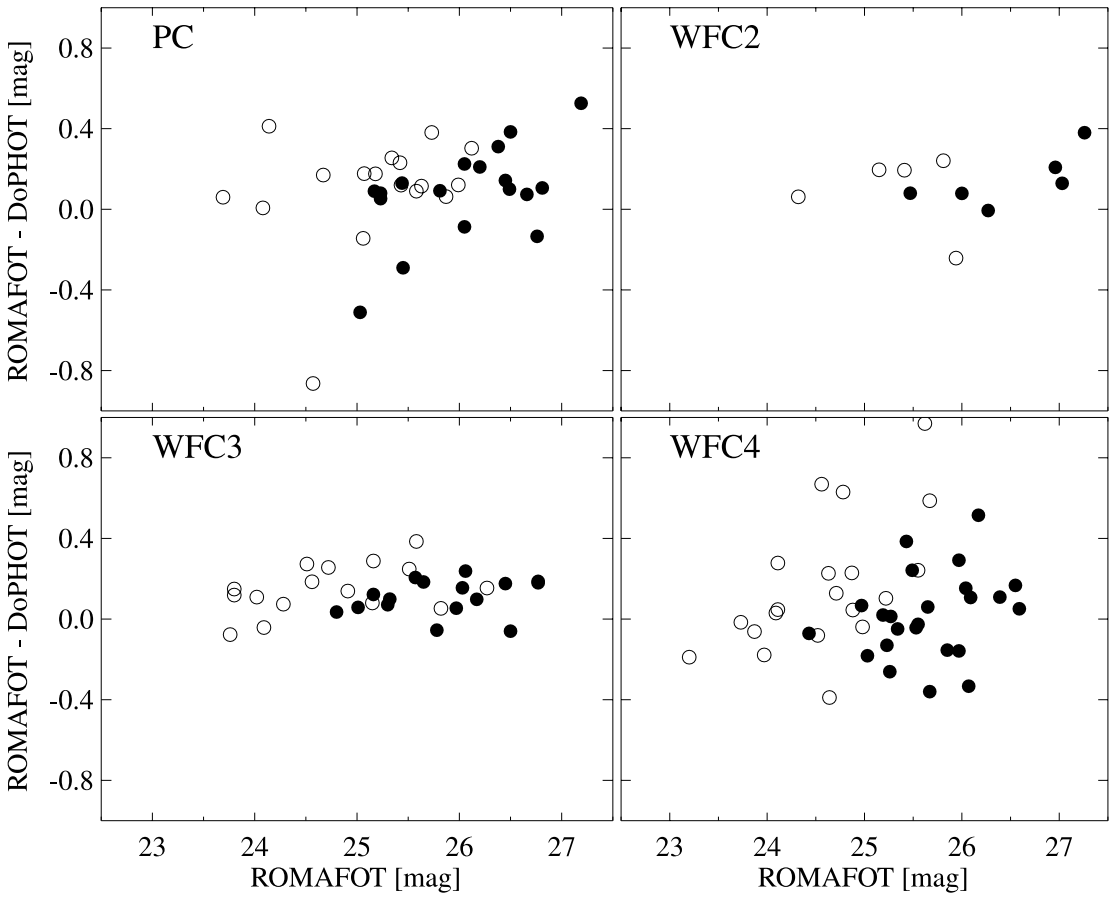

FIG. 17.—Comparison of the ROMAFOT and DoPHOT photometry for all Cepheid candidates given in Table 5 for V and I. Open symbols represents I and filled circles V measurements.

photometry is shown in Figure 18, and their P-L diagrams in V and I in Figure 19.

As before, the diagnostic diagram shows little differential reddening along the reddening line, except for C1-V11 and C3-V12, which seem to have more than average reddening. C2-V6 is very faint for its long period and is probably a W Vir star (Population II Cepheid). These three variables, as well as the outlying C4-V6, are not considered for the distance determination.

Again, a period cut from 20 to 65 days has been applied to these 33 good Cepheids in order to avoid a possible bias. These 26 Cepheids with ROMAFOT photometry are shown in Figure 19 (*filled circles*). Since the distance moduli depend somewhat on the aperture correction (AC) adopted, different solutions are given in Table 8, i.e., with the AC from NGC 4527 proper, or from the globular clusters Pal 4, G319, Pal 4 and G319, or from the mean AC of NGC 4527, Pal 4, and G319 (cf. § 5.4). Also shown is a solution for only the Cepheids in chips 1–3 and those in chip 4. The result from applying a color cut exactly as for case 2 in § 4.4 is also shown for comparison.

The star-by-star fitting errors reported by ROMAFOT appear to underestimate (at least in these overcrowded fields) errors in the fitted magnitude when compared with the scatter in the values obtained for the same stars on repeated images. Without reliable star-by-star error estimates from the fitting errors, no meaningful weighting scheme can be applied. All averages calculated from the ROMAFOT data are unweighted. The quoted uncertainties in μ_V and μ_I reflect the random error in measurement for each category considered. The uncertainty in μ_0 was calculated with the rms scatter of the dereddened distance moduli of the individual Cepheids. The variation from case to case as a function of adopted aperture correction and chip grouping is a rough indication of the systematic errors: estimates of 0.13 for μ_V and 0.08 for μ_I (in the mean) are indicated. The systematic error in μ_0 appears to be small, as gleaned by the case-to-case scatter, since the changes in the aperture corrections for V and I appear to change from case to case in a way that attenuates the variation in μ_0. If we assume this to be chance coincidence, and that systematic errors in measuring the aperture corrections in V and I are uncorrelated, the systematic error in μ_0 ought to be the one from propagating the systematic errors from μ_V and μ_I, thus giving ± 0.27 mag per case. However, such an estimate disregards the correlated color variation due to differential extinction, and is likely to be an overestimate.

The best compromise solution is apparently the one with the AC taken from NGC 4527, Pal 4, and G319. The moduli in V and I lead [with $A_V = 2.43E(V-I)$] to the true moduli in the last column of Table 8. The indicated errors of the true moduli are dominated by the error in $E(V-I)$. This compromise solution is estimated to have a systematic error of approximately ± 0.07 mag in μ_0.

We have presented the preferred distance estimates from DoPHOT (§ 4.5) and ROMAFOT (above) values of dis-

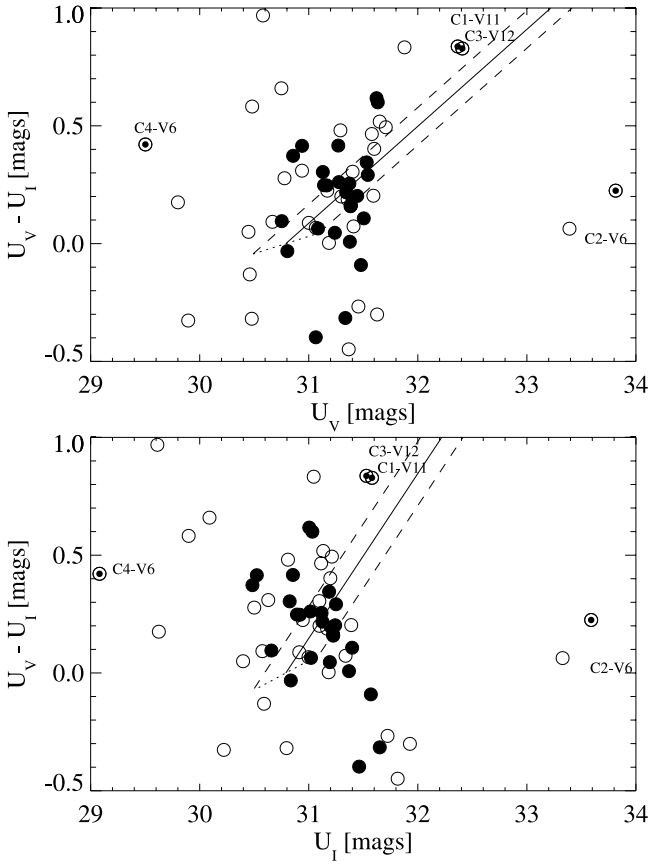

FIG. 18.—Diagnostic diagram to detect the presence of differential absorption. Filled circles indicate Cepheids with $20 \leq P \leq 65$ days and quality index 3 or better; open circles show the remaining candidates. The candidates C1-V11, C2-V6, C3-V12, and C4-V6 are labeled.

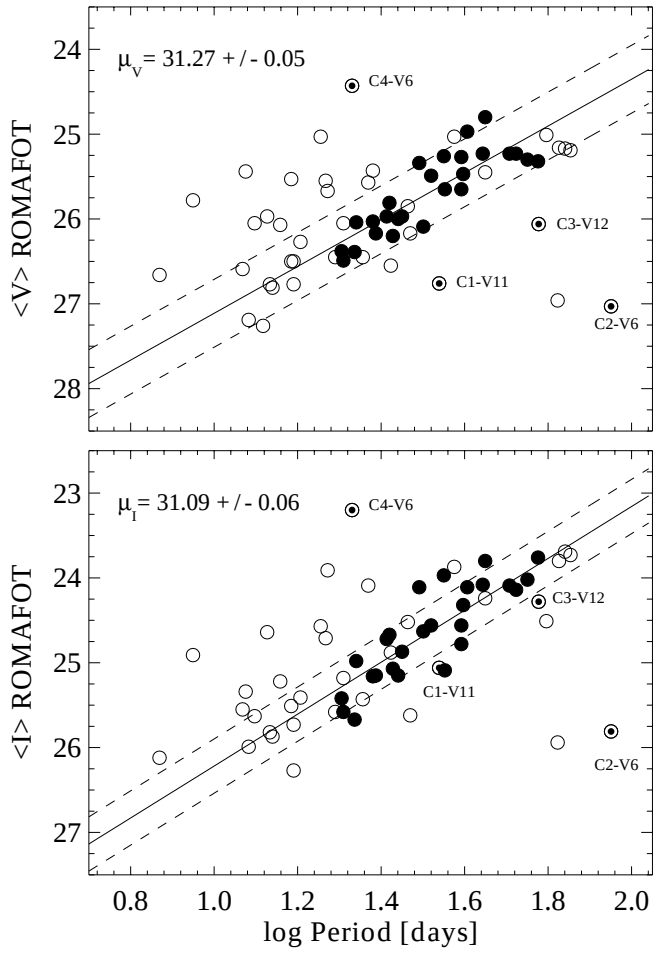

FIG. 19.—Period-luminosity relation in V (*top*) and I (*bottom*) based on the ROMAFOT photometry. Filled circles indicate Cepheids with $20 \leq P \leq 65$ days and quality index 3 or better; open circles show the remaining candidates. The candidates C1-V11, C2-V6, C3-V12, and C4-V6 are labeled.

tance modulus for NGC 4527. The various cases discussed for both sets of reduction/analysis are presented in Table 8. For the ROMAFOT reductions, we calculate (for the preferred aperture correction) the results for the cuts made for the DoPHOT data analysis, which are also given in Table 8. The slightly larger moduli from ROMAFOT are consistent with the fact that this photometry package in combination with the adopted AC generally yields magnitudes roughly 0.1 mag fainter than DoPHOT. Work to address this zero-point offset is in progress, along with more complete simulations of ROMAFOT's performance.

An inspection of Table 8 shows that the preferred estimates of the two methods, as well as estimates from cuts that eliminate suspect data from *both* methods, differ by 0.11–0.21 mag, in the sense that ROMAFOT gives the larger moduli. Averaging the unweighted preferred estimates from each approach gives $\mu_0 = 30.74$, which is well within the uncertainty estimates of each method (even within the *weighted* uncertainty for the DoPHOT estimates). For an overall uncertainty, we could statistically combine the individual uncertainties from the two methods, but we prefer to be conservative and carry over the value common to each of the two methods, thus obtaining

$$(m - M)_0 = 30.74 \pm 0.12 \pm 0.12 , \qquad (10)$$

which corresponds to $14.1 \pm 0.8 \pm 0.8$ Mpc. The systematic error is estimated from the scatter in derived dereddened moduli for the various "method/selection" cases for both DoPHOT- and ROMAFOT-based reductions listed in Table 8. Note that the distance moduli from the acceptable (i.e., no obvious problems identified) subsamples listed in Table 8 range from 30.60 to 30.93, with favored values between 30.60 and 30.88. These numbers demonstrate the degree to which the distance determination is robust.

The best estimates from DoPHOT and the best compromise solution from ROMAFOT for μ_V are in remarkable agreement, even though the samples are formally different. We average them and retain the larger of the two uncertainties to reflect the real dispersion among the Cepheids. The adopted values for μ_I for the two methods differ by 0.09 mag. Again, we average the moduli and keep the larger uncertainty. The final numbers are shown in the last row of Table 8. The systematic variations in μ_V and μ_I as seen from case to case within DoPHOT and ROMAFOT are not inconsistent with these adopted uncertainties. In particular, note that for the selected samples without a color cut, μ_V values range from 31.12 to 31.27 from DoPHOT, and from 31.09 to 31.42 from ROMAFOT, since a direct V-band comparison to SN 1991T is made later in § 6.1.

The distance Höflich & Khokhlov (1996) derived for SN 1991T from modeling its light curve and spectrum is

TABLE 8

DISTANCES OF NGC 4527 FROM DoPHOT AND ROMAFOT PHOTOMETRY

Method/Selection	n	$(m-M)_V$ (mag)	$(m-M)_I$ (mag)	$(m-M)_0$ (mag)
DoPHOT[a]				
Weighted Averages				
$20 \le P \le 65$; $QI \ge 3$	27			30.48 ± 0.09
$20 \le P \le 65$; $QI \ge 3$; chip 4	12			30.17 ± 0.13
$20 \le P \le 65$; $QI \ge 3$; chips1, 2, 3	15			30.73 ± 0.12
$20 \le P \le 65$; $QI \ge 3$; chips1, 2, 3, 4 ($X > 400$)	19			30.62 ± 0.10
Color cut (see § 4.4)	13			30.69 ± 0.12
Combine (.AND.) above 2 lines	11			30.63 ± 0.13
Unweighted Averages				
$20 \le P \le 65$; $QI \ge 3$	27	31.20 ± 0.06	30.88 ± 0.06	30.43 ± 0.10
$20 \le P \le 65$; $QI \ge 3$; chip 4	12	31.12 ± 0.07	30.70 ± 0.06	30.13 ± 0.12
$20 \le P \le 65$; $QI \ge 3$; chips 1, 2, 3	15	31.27 ± 0.10	31.02 ± 0.08	30.67 ± 0.12
$20 \le P \le 65$; $QI \ge 3$; chips 1, 2, 3, 4 ($X > 400$)	19	31.25 ± 0.08	30.98 ± 0.07	30.60 ± 0.10
Color cut (see § 4.4)	13			30.71 ± 0.07
Combine (.AND.) above 2 lines	11			30.66 ± 0.08
Adopted DoPHOT estimate:		31.26 ± 0.08	31.00 ± 0.07	30.67 ± 0.12
ROMAFOT[a]				
Unweighted Averages				
$QI \ge 3$[b,c]	33	31.28 ± 0.05	31.08 ± 0.05	30.79 ± 0.09
$QI \ge 3$; chips 1, 2, 3[b,c]	20	31.35 ± 0.05	31.11 ± 0.05	30.77 ± 0.08
$QI \ge 3$; chip 4[b,c]	13	31.17 ± 0.10	31.03 ± 0.11	30.82 ± 0.20
$20 \le P \le 65$; $QI \ge 3$; all chips[b]	29	31.29 ± 0.09	31.05 ± 0.09	30.71 ± 0.13
$20 \le P \le 65$; $QI \ge 3$; all chips[b,c]	26	31.27 ± 0.05	31.09 ± 0.06	30.82 ± 0.11
$20 \le P \le 65$; $QI \ge 3$; chips 1, 2, 3, 4 ($X > 400$)[b]	20	31.42 ± 0.09	31.16 ± 0.06	30.78 ± 0.09
$20 \le P \le 65$; $QI \ge 3$; Color cut (see § 4.4)[b]	16	31.26 ± 0.06	31.13 ± 0.06	30.93 ± 0.08
$20 \le P \le 65$; $QI \ge 3$; AC with N4527[c]	26	31.09 ± 0.05	30.95 ± 0.06	30.75 ± 0.11
$20 \le P \le 65$; $QI \ge 3$; AC with Pal 4, G319[c]	26	31.36 ± 0.05	31.14 ± 0.06	30.83 ± 0.11
$20 \le P \le 65$; $QI \ge 3$; AC with Pal 4[c]	26	31.33 ± 0.05	31.15 ± 0.06	30.88 ± 0.11
$20 \le P \le 65$; $QI \ge 3$; AC with G319[c]	26	31.39 ± 0.05	31.14 ± 0.06	30.78 ± 0.11
Adopted ROMAFOT estimate:	26	31.27 ± 0.05	31.09 ± 0.06	30.82 ± 0.11
Final adopted:		31.27 ± 0.08	31.05 ± 0.07	30.74 ± 0.12

[a] All values are on a long exposure scale.
[b] The mean AC from NGC 4527, Pal 4, and G319 is used.
[c] The Cepheid candidates C1-V11, C2-V6, C3-V12, C4-V6 are excluded.

$(m-M)_0 = 30.4 \pm 0.3$. Sparks et al. (1999) estimated an upper limit of 15 Mpc [$(m-M)_0 = 30.9$] for SN 1991T by modeling the polarized emission from its light echo.

6. THE PEAK BRIGHTNESS OF SN 1991T

6.1. *The Observed Brightness at Maximum*

The most comprehensive photometry for SN 1991T, which was discovered 12 days before maximum light, is presented in Lira et al. (1998). The maximum brightness in B and V is seen to be

$$B_{\max} = 11.70 \pm 0.02\ , \quad V_{\max} = 11.51 \pm 0.02\ ,$$
$$\text{and hence} \quad B_{\max} - V_{\max} = 0.19 \pm 0.03\ . \qquad (11)$$

Combining the V maximum with the adopted modulus $(m-M)_V = 31.27$ in Table 8 gives

$$M_V^0(\max) = -19.76 \pm 0.12\ . \qquad (12)$$

This value holds only under the assumption that SN 1991T suffers the same absorption as the Cepheids in NGC 4527. The uncertainty reflects the realistic error in the *average* μ_V for a Cepheid; the random error estimates for $(m-M)_V$ given in Table 8 are convolved with the statistical errors gleaned from the different acceptable cases shown in the same table. An individual object can be quite different, depending on where it is located with respect to the dust, and so it is quite likely that the absorption of the SN is different. Therefore, we attempt to estimate its reddening independently in the following subsection.

6.2. *Estimating Reddening and Extinction*

The Galactic absorption to NGC 4527 is given by Schlegel, Finkbeiner, & Davis (1998) to be $A_B = 0.09$ and $A_V = 0.07$. The total absorption must be larger and is estimated in the following ways.

A first approximation is obtained by assuming that SN 1991T has the same reddening as the Cepheids on average, i.e., $E(V-I) = 0.22$ (mean of DoPHOT and ROMAFOT), and hence $E(B-V) = 0.18$.

If it is assumed that SN 1991T has the same intrinsic color as blue, Branch-normal SNe Ia, i.e., $(B_{\max} - V_{\max}) = -0.01 \pm 0.01$ with an intrinsic scatter of $\sigma_{B-V} = 0.05$ (Parodi et al. 2000), one obtains $E(B-V) = 0.20 \pm 0.06$ with equation (11). [An estimate of $E(V-I)$ is not attempt-

ed, because standard SNe Ia have a wider color scatter of $\sigma_{V-I} = 0.08$.]

If, instead, it is argued that the spectroscopically peculiar SN 1991T cannot be compared with the colors of standard SNe Ia, it can be compared with its spectroscopic twin SN 1995ac (Garnavich et al. 1996). The latter has (after correction for Galactic reddening following Schlegel et al. 1998) $(B_{\max} - V_{\max}) = -0.06$. This yields for SN 1991T $E(B-V) = 0.25 \pm 0.06$ (estimated error).

Phillips et al. (1999) have suggested that all SNe Ia evolve similarly in color at late phases in their light curves, i.e., 50 days past maximum. They argue that since this is based on the nebular phase of SNe, it is expected to be more robust than the color at maximum. Accordingly, they obtain a total reddening of SN 1991T corresponding to $E(B-V) = 0.16 \pm 0.05$. This value may have to be reduced to $E(B-V) = 0.12 \pm 0.05$, because their adopted mean color of all SNe Ia is 0.04 bluer on average than found by Parodi et al. (2000).

From the strong Ca and Na interstellar absorption lines in the spectrum of SN 1991T at the radial velocity of NGC 4527, Ruiz-Lapuente et al. (1992) and Filippenko et al. (1992) have concluded that $E(B-V) = 0.34$ and $E(B-V) = 0.13$–0.23, respectively.

The various reddening estimates are consistent with an adopted value of $E(B-V) = 0.21 \pm 0.08$ (i.e., the mean and standard deviation of the various estimates listed above), which was also favored by Fisher et al. (1999), who adopted $E(B-V) = 0.2 \pm 0.1$. This value is not significantly different from the mean reddening of the Cepheids in NGC 4527. With $R_B = 4.1$, $R_V = 3.1$, and $R_I = 1.9$, one then obtains a total absorption of $A_B = 0.82 \pm 0.33$, $A_V = 0.62 \pm 0.25$, and $A_I = 0.38 \pm 0.15$, leading to the true magnitudes of SN 1991T of

$$B^0_{\max} = 10.88 \pm 0.33\,, \quad V^0_{\max} = 10.89 \pm 0.25\,,$$
$$\text{and } I^0_{\max} = 11.29 \pm 0.16\,. \tag{13}$$

Together with the true modulus of NGC 4527 from Table 8, this yields absolute magnitudes of

$$M^0_B(\max) = -19.86 \pm 0.36\,, \quad M^0_V(\max) = -19.85 \pm 0.29\,,$$
$$\text{and } M^0_I(\max) = -19.45 \pm 0.21\,. \tag{14}$$

When these magnitudes are compared with the mean absolute magnitude of eight blue standard SNe Ia, whose luminosities are calibrated through Cepheids (Paper IX), one finds an overluminosity of SN 1991T of

$$\Delta M_B = 0.37 \pm 0.37\,, \quad \Delta M_V = 0.37 \pm 0.30\,,$$
$$\text{and } \Delta M_I = 0.20 \pm 0.22\,. \tag{15}$$

These differences are further reduced by ~ 0.05 if one compares SN 1991T with standard SNe Ia of equally slow light-curve decline of $\Delta m_{15} = 0.95$ (cf. Parodi et al. 2000, eqs. [3]–[5]). Yet the comparison remains inconclusive because of the large errors of the absolute magnitudes of SN 1991T, which are dominated by the uncertainty in $E(B-V)$. Within the errors it is possible that $M_B(\max)$ and $M_V(\max)$ are up to ~ 0.6 mag brighter than for normal SNe Ia. However, a high value would cause difficulties with $M_I(\max)$. From equation (14) SN 1991T is, with $(V-I) = -0.40$, the bluest SN Ia known, and any increase of $E(B-V)$ above the adopted value can only make it bluer.

It might be argued that SN 1991T, as a peculiar SN Ia, may be as blue in $V-I$ as it wants. However, its spectroscopic twin SN 1995ac (see below) has $(V-I) = -0.24 \pm 0.08$, after correction for Galactic absorption, which is close to the mean value of normal SNe Ia of $\langle V-I \rangle = -0.29 \pm 0.02$ (Parodi et al. 2000).

Of course, it is more telling to compare the bolometric luminosities instead of the absolute magnitudes in different passbands. Standard SNe Ia with $\langle M_V \rangle = -19.48 \pm 0.07$ (Paper IX) and a bolometric correction of 0.1 ± 0.1 (Höflich 1995; Mazzali, Danziger, & Turatto 1995; Nugent et al. 1995; Branch, Nugent, & Fisher 1997) have $M_{\rm bol} = -19.38 \pm 0.12$. SN 1991T had a larger fraction of its energy in the near-ultraviolet near maximum, and its bolometric correction is therefore -0.1 ± 0.1 (Fisher et al. 1999), and hence with equation (14) $M_{\rm bol}(\text{SN } 1991T) = -19.95 \pm 0.31$, which is brighter by 0.57 ± 0.33 than standard SNe Ia. It lies outside the scope of this paper to decide whether the (poorly determined) excess luminosity of SNe Ia can be fuelled by a Chandrasekhar mass or not (see, e.g., Fisher et al. 1999).

7. CONCLUSIONS

7.1. *The Surprisingly Small Distance of NGC 4527*

NGC 4527 lies in de Vaucouleurs' X-cloud, which is part of the W-cloud (Binggeli, Popescu, & Tammann 1993) southwest of the Virgo cluster and outside the isophlets and X-ray contour of the cluster.

The W-cloud is known to have a considerable depth (Federspiel, Tamman, & Sandage 1998). It is therefore not too surprising that the distance of NGC 4527 of $(m-M)_0 = 30.74 \pm 0.12 \pm 0.12$ ($14.1 \pm 0.8 \pm 0.8$ Mpc) is even somewhat smaller by 0.3–0.4 mag than the Cepheid distances of the two neighboring galaxies NGC 4536 and NGC 4496A (Papers V and VI). The three galaxies have (with observed velocities near 1750 km s^{-1}; Sandage & Tammann 1987) large peculiar velocities. They apparently lie on the near side of the Virgo cluster, probably infalling for the first time (Tully & Shaya 1984).

7.2. *The SN 1991T Class of SNe Ia*

The consequence of the small Cepheid distance of NGC 4527 is that the suspected overluminosity (Fisher et al. 1999 and references therein) of SN 1991T becomes marginal. The excess luminosity in M_B, M_V, and M_I depends entirely on the adopted internal extinction, $E(B-V)$. However, because of its negative bolometric correction SN 1991T seems to have a higher bolometric luminosity by $\Delta M_{\rm bol} = 0.57 \pm 0.33$ than standard SNe Ia, a difference still barely at the $2\,\sigma$ level.

A few other SNe Ia are known that have similar spectra, i.e., SN 1997cw (Garnavich et al. 1997), SN 1998ab (Garnavich, Jha, & Kirshner 1998), SN 1998es (Jha et al. 1998), and SN 1999cw (Rizzi et al. 1999), as well as SN 1995bd and SN 1995ac (Garnavich et al. 1996), and SN 1997br (Qiao et al. 1997), for which additional photometry is available. Some photometric parameters of the three latter are compared with SN 1991T in Table 9.

It is a curious fact that SN 1991T received much attention because of its seemingly high luminosity, which is now marginal at best in the light of the new Cepheid distance, while its spectroscopic twin SN 1995ac, which was discovered later, appears to be considerably overluminous

TABLE 9

PHOTOMETRIC PARAMETERS OF SN 1991T–LIKE SNe Ia

SN	log v	Δm_{15}	M_B^0	M_V^0	M_I^0	$(B-V)_0$	$(V-I)_0$
1991T[a]	...	0.95	−19.86	−19.85	−19.45	−0.01	−0.40
1995ac[b]	4.166	0.96[d]	−20.04	−19.98	−19.74	−0.06	−0.24
1995bd[c]	3.681	0.89[d]	−19.39	−19.68	...	+0.29	...
			(−20.62)	(−20.61)	...	(−0.01)	...
1997br[e]	3.342	1.00	−19.25	−19.46	−19.54	+0.21	+0.08
			(−20.36)	(−20.28)	(−20.12)	(−0.08)	(−0.16)

[a] Luminosities repeated from equation (14).

[b] Apparent magnitudes from Riess et al. 1999. Corrected for Galactic absorption (Schlegel et al. 1998). $H_0 = 60$ adopted.

[c] Apparent magnitudes from Riess et al. 1999. First entry: Corrected only for Galactic absorption (Schlegel et al. 1998). Second entry: Assuming normal color $(B-V) = -0.01$ and correcting for additional internal absorption. $H_0 = 60$ adopted.

[d] Mean of Riess et al. 1999 and Phillips et al. 1999.

[e] Photometric parameters from Li et al. 1999. First entry: Corrected for Galactic absorption (Schlegel et al. 1998). Second entry: Corrected for total absorption assuming $E(B-V) = 0.40$ (see text). $H_0 = 60$ adopted.

indeed. It should be noted that the overluminosity of SN 1995ac is independent of any adopted value of H_0, because it lies 0.5 mag above the Hubble line of standard SNe Ia and its recession velocity of 14,700 km s^{-1} cannot be significantly altered by peculiar motions.

SN 1995bd does not shed additional light on the discrepancy between SN 1991T and SN 1995ac. It is strongly absorbed by Galactic dust, i.e., $A_V = 1.65$ according to Schlegel et al. (1998), but remains somewhat underluminous and very red in $B-V$ after a corresponding correction. If it is assumed that it suffers additional internal absorption and that its $B-V$ color is that of standard SNe Ia and similar to its two counterparts, it becomes extremely overluminous. The latter conclusion holds for any reasonable value of H_0. Even adopting an extreme value of $H_0 = 80$ makes it have $M_B(\max) = -20.0$. For $H_0 = 60$, the absolute magnitude becomes $M_B(\max) = -20.62$, again using the large absorption correction.

Unfortunately, the case of SN 1997br is even more ambiguous. Li et al. (1999) find this object to be more reddened than SN 1991T by $\Delta E(B-V) = 0.21$, which with the color excess adopted for the latter gives $E(B-V) = 0.41$ for SN 1997br, in good agreement with $E(B-V) = 0.39$ from the Na absorption line (Li et al. 1999). With $E(B-V) \approx 0.41$, SN 1997br becomes clearly overluminous. However, we have adopted the individual recession velocity of ESO 576-G40, host of SN 1997br, namely $v_0 = 2070 \pm 20$ km s^{-1} (Li et al. 1999), which becomes $v_{220} = 2199$ km s^{-1} after correction for Virgocentric infall. Li et al. (1999) have instead adopted the mean velocity of 1583 km s^{-1} of the NGC 5084/87 group, of which ESO 576-G40 may be a member. In addition, they assume only $E(B-V) = 0.35$. With these different precepts, SN 1997br becomes 0.90 mag fainter than listed in Table 9 and the SN takes roughly the luminosities and colors of standard SNe Ia.

In spite of all uncertainties, it seems unavoidable that SN 1991T–like objects form a very heterogeneous class. Even if one treats the extinction as a free parameter, they differ significantly either in luminosity or in color or both. Some may require more than the Chandrasekhar mass (like SN 1995ac), others not. It is remarkable that three out of four SNe Ia in Table 9 have an internal extinction of probably $E(B-V) > 0.20$, which is quite unusual among known standard SNe Ia.

We thank the many individuals at STScI who worked hard behind the scenes to make these observations possible. We also thank an insightful referee whose comments have improved this paper. A. S. and A. S. acknowledge support from NASA through grant GO-5427.02-93A from the Space Telescope Science Institute, which is operated by the Association of Universities for Research in Astronomy. L. L. and G. A. T. thank the Swiss National Science Foundation for continued support.

REFERENCES

Baade, W. 1938, ApJ, 88, 285
Baade, W., & Zwicky, F. 1938, ApJ, 88, 411
Barbon, R., Ciatti, F., & Rosino, L. 1973, A&A, 25, 241
Bertola, F. 1964, Ann d'Astrophys., 27, 319
Bertola, F., Mammano, A. S., & Perinotto, M. 1965, Contrib. Asiago Obs. No. 174
Bertola, F., & Sussi, M. G. 1965, Contrib. Oss. Astron. Univ. Padua No. 176
Binggeli, B., Popescu, C. C., & Tammann, G. A. 1993, A&AS, 98, 275
Branch, D. 1981, ApJ, 248, 1076
———. 1982, ApJ, 258, 35
———. 1986, ApJ, 300, L51
Branch, D., Fisher A., & Nugent, P. 1993, AJ, 106, 2383
Branch, D., Nugent, P., & Fisher A. 1997, in Thermonuclear Supernovae, ed. P. Ruiz-Lapuente, R. Canal, & J. Isern (Dordrecht: Kluwer), 715
Branch, D., & Tammann, G. A. 1992, ARA&A, 30, 359
Buonanno, R., Buscema, G., Corsi, C. E., Ferraro, I., & Iannicola, G. 1983, A&A, 126, 278
Caldwell, J. A. R., & Coulson, I. M. 1985, MNRAS, 212, 879
Dean, J. F., Warren, P. R., & Cousins, A. W. J. 1978, MNRAS, 183, 569
de Vaucouleurs, G. 1975, in Galaxies and the Universe, ed. A. Sandage, M. Sandage, & J. Kristian (Chicago: Univ. Chicago Press), 557
Elias, J. H., Mathews, K., Neugebauer, G., & Persson, S. E. 1985, ApJ, 296, 378
Federspiel, M., Tammann, G. A., & Sandage, A. 1998, ApJ, 495, 115
Fernie, J. D. 1990, ApJ, 354, 295
Ferrarese, L., et al. 2000, PASP, 112, 177
Filippenko, A. V., et al. 1992, ApJ, 384, L15
Fisher, A., Branch, D., Hatano, K., & Baron, E. 1999, MNRAS, 304, 67
Garnavich, P., Jha, S., & Kirshner, R. 1998, IAU Circ. 6857
Garnavich, P., Jha, S., Kirshner, R., & Challis, P. 1997, IAU Circ. 6699
Garnavich, P. M., Riess, A. G., Kirshner, R. P., Challis, P., & Wagner, R. M. 1996, BAAS, 28, 1331
Gibson, B. K., et al. 2000, ApJ, 529, 723
Hamuy, M., Phillips, M. M., Schommer, R. A., Suntzeff, N. B., Maza, J., & Aviles, R. 1996, AJ, 112, 2391
Harkness, R. P., & Wheeler, J. C. 1990, in Supernovae, ed. A. G. Petschek (Berlin: Springer), 1

Harkness, R. P., et al. 1987, ApJ, 317, 355
Höflich, P. A. 1995, ApJ, 443, 89
Höflich, P., & Khokhlov, A. 1996, ApJ, 457, 500
Holtzman, J. A., et al. 1995a, PASP, 107, 156
———. 1995b, PASP, 107, 1065
Jha, S., Garnavich, P., Challis, P., & Kirshner, R. 1998, IAU Circ. 7054
Kowal, C. T. 1968, AJ, 73, 1021
Labhardt, L., Sandage, A., & Tammann, G. A. 1997, A&A, 322, 751
Lafler, J., & Kinman, T. D. 1965, ApJS, 11, 216
Li, W. D., et al. 1999, AJ, 117, 2709
Lira, P., et al. 1998, AJ, 115, 234
Livio, M., Panagia, N., & Sahu, K., eds. 2000, The Greatest Explosions Since the Big Bang: Supernovae and Gamma-Ray Bursts (Cambridge: Cambridge Univ. Press)
Madore, B. F., & Freedman, W. L. 1991, PASP, 103, 933
Mazzali, P. A., Danziger, I. J., & Turatto, M. 1995, A&A, 297, 509
Minkowski, R. 1939, ApJ, 89, 156
———. 1941, PASP, 53, 224
———. 1964, ARA&A, 2, 247
Mochejska, B. J., Macri, L. M., Sasselov, D. D., & Stanek, K. Z. 2000, AJ, 120, 810
Nugent, P., Phillips, M., Baron, E., Branch, D., & Hauschildt, P. 1995, ApJ, 455, L147
Panagia, N. 1985, in Supernovae as Distance Indicators, ed. N. Bartel (New York: Springer), 14
Parodi, B. R., Saha, A., Sandage, A., & Tammann, G. A. 2000, ApJ, 540, 634
Phillips, M. M. 1993, ApJ, 413, L105
Phillips, M. M., et al. 1992, AJ, 103, 1632
———. 1999, AJ, 118, 1766
Porter, A. C., & Filippenko, A. C. 1987, AJ, 93, 1372
Pskovskii, Yu. P. 1967, Soviet Astron., 11, 63
———. 1971, Soviet Astron., 14, 798
———. 1984, Soviet Astron., 28, 658
Qiao, Q. Y., Wu, H., Wei, J. Y., & Li, W. D. 1997, IAU Circ. 6623
Riess, A. G., et al. 1999, AJ, 117, 707
Rizzi, L., Patat, F., Benetti, S., Cappellaro, E., & Turatto, M. 1999, IAU Circ. 7215
Ruiz-Lapuente, P., et al. 1992, ApJ, 387, L33
Saha, A., & Hoessel, J. G. 1990, AJ, 99, 97
Saha, A., Labhardt, L., & Prosser, C. 2000, PASP, 112, 163
Saha, A., Sandage, A., Labhardt, L., Tammann, G. A., Macchetto, F. D., & Panagia, N. 1996a, ApJ, 466, 55 (Paper V)
———. 1996b, ApJS, 107, 693 (Paper VI)
———. 1997, ApJ, 486, 1 (Paper VIII)
Saha, A., Sandage, A., Tammann, G. A., Labhardt, L., Macchetto, F. D., & Panagia, N. 1999, ApJ, 522, 802 (Paper IX)
Sandage, A. 1988, PASP, 100, 935
Sandage, A., Bell, R. A., & Tripicco, M. J. 1999, ApJ, 522, 250
Sandage, A., Saha, A., Tammann, G. A., Labhardt, L., Panagia, N., & Macchetto, F. D. 1996, ApJ, 460, L15 (Paper VII)
Sandage, A., & Tammann, G. A. 1968, ApJ, 151, 531
———. 1982, ApJ, 256, 339 (Steps VII)
———. 1987, Revised Shapley-Ames Catalog of Bright Galaxies (2d ed.; Washington: Carnegie Inst.), 47
———. 1993, ApJ, 415, 1
———. 1997, in Critical Dialogues in Cosmology, ed. N. Turok (Singapore: World Scientific), 130
Sandage, A., Tammann, G. A., & Saha, A. 2000, in The Greatest Explosions Since the Big Bang: Supernovae and Gamma-Ray Bursts, ed. M. Livio, N. Panagia, & K. Sahu (Cambridge: Cambridge Univ. Press), in press
Schechter, P. L., Mateo, M. L., & Saha, A. 1993, PASP, 105, 1342
Scheffler, H. 1982, in Landolt-Börnstein Astronomy and Astrophysics, Vol. 2c, ed. K. Schaifers & H. H. Voigt (Berlin: Springer), 46
Schlegel, D. J., Finkbeiner, D. P., & Davis, M. 1998, ApJ, 500, 525
Sparks, W. B., Macchetto, F., Panagia, N., Boffi, F. R., Branch, D., Hazen, M. L., & della Valle, M. 1999, ApJ, 523, 585
Stanek, K. Z., & Udalski, A. 2000, ApJL, submitted (preprint astro-ph/9909346)
Tammann, G. A., & Sandage, A. 1995, ApJ, 452, 16
Tripp, R. 1998, A&A, 331, 815
Tripp, R., & Branch, D. 1999, ApJ, 525, 209
Tully, R. B. 1988, Nearby Galaxy Catalog (Cambridge: Cambridge Univ. Press)
Tully, R. B., & Shaya, E. J. 1984, ApJ, 281, 31
Uomoto, A., & Kirshner, R. P. 1985, A&A, 149, L7
Wheeler, J. C., & Levreault, R. 1985, ApJ, 294, L17